MODELING THE INTERACTION BETWEEN HYDRAULIC AND NATURAL FRACTURES USING THREE DIMENSIONAL FINITE ELEMENT ANALYSIS

By

Aditya Balasaheb Nikam

A Thesis Submitted in Partial Fulfillment of the Requirements

for the Degree of

Master of Science

in

Petroleum Engineering

University of Alaska Fairbanks

August 2016

APPROVED:

Dr. Obadare Awoleke, Committee Chair

Dr. Mohabbat Ahmadi, Committee Co-chair

Dr. Abhijit Dandekar, Committee Member

Dr. Gang Chen, Committee Member

Dr. Il Sang Ahn, Committee Member

Dr. Abhijit Dandekar, Chair

Department of Petroleum Engineering

Dr. Douglas Goering, Dean

College of Engineering and Mines

Dr. Michael Castellini, *Dean of the Graduate School*

Abstract

Natural fractures are present in almost every formation and their size and density definitely affect the hydraulic fracturing job. Some of the analysis done in the past shed light on hydraulic fracture (HF) and natural fracture (NF) geometries. The interaction of the HF with existing NF in a formation results in a denser fracture network. The volume of rock covering this fracture network is called the stimulated reservoir volume (SRV). This SRV governs the hydrocarbon production and the ultimate revenue generation. Moreover, past studies show that a microseismic interpreted SRV can be different than the actual SRV. Additionally, there is always limited subsurface access, which makes it imperative to understand the HF – NF interaction to plan and execute a successful hydraulic fracturing job.

A three layered, three dimensional complex geomechanical model is built using commercially available finite element analysis (FEA) software. A propagating HF approaching mainly orthogonal NF is studied and analyzed. Cohesive pore pressure elements in FEA software capable of modeling fluid continuity at HF – NF intersection are used to model the HF – NF interaction. Furthermore, a detailed sensitivity analysis considering the effect of stress contrast, job design parameters, NF properties, and properties of the formation is conducted.

The sensitivity analysis of properties such as principal horizontal stress contrast, job design parameters, NF properties and properties of target formation reveals a broad variation in the impact of the sensitivity parameters on the HF, NF, and HF-NF geometry and interaction. The observations and the corresponding conclusions were based on broadly classified sensitivity parameters. The most important parameters solely for HF resultant geometry are observed to be a high stress contrast with stress reversal, highest injection rate, and farther NF distance from the injection point. The least important parameter is observed to be the scenario with almost equal horizontal stresses. However, the most important parameter solely for resulting NF geometry is only the high stress contrast with stress reversal. Conversely, for the considered sensitivity cases, the least important parameters are the injection rate, lower injection viscosity (10 cP), higher NF leak-off coefficient, target formation thickness, Young's modulus, and lowest value of target formation Poisson's ratio. Collective conclusions for considering HF-NF are also obtained.

Dedication

I dedicate this work to my beloved parents, my brother, and my family for their infinite love, support and inspiration; to my grandfather, the late Pai. Shri. Sahadeo Haribhau Nikam; and to my dearest teacher, the late Dr. Prof. Hoshang D. Moogat.

Table of Contents

Page

List of Figures

Page

List of Tables

Page

Acknowledgements

I would like to take this opportunity to thank my committee chair, Dr. Obadare Awoleke and committee co-chair Dr. Mohabbat Ahmadi, for being a constant source of advice, support, and guidance. I also thank my committee members Dr. Abhijit Dandekar, Dr. Gang Chen, and Dr. Il Sang Ahn for their valuable tips and suggestions for completing the thesis work. I express my warm thanks to Dr. Shirish Patil for his valuable guidance and support in all aspects since I first met him.

The financial support provided by the Department of Petroleum Engineering is gratefully acknowledged. I am indebted to the Department of Residence Life and Conference Services for always being supportive to help fund myself through on-campus student jobs for appreciable amount of my student tenure.

I remain grateful to my parents, Mr. Balasaheb Sahadeo Nikam and Mrs. Shubhangi Balasaheb Nikam, and my sibling, Hrishikesh, for their endless love, support, and encouragement that I relied on throughout my tenure at the University of Alaska Fairbanks. I would definitely like to thank my friends, Mr. Saurav Bhowmick, who has always been supportive and caring like an elder brother through the tough and difficult times, and Bakul Mathur for being very supportive and helpful during the critical times. Finally, I would like to thank all my friends and the Faculty at the University of Alaska Fairbanks and UAF LIVE office who made my stay at Fairbanks one of the most memorable and enjoyable experiences of a lifetime.

CHAPTER 1 INTRODUCTION

Hydraulic fracturing is a vital and principal stimulation technology, especially applied to tight porous media. Hence it is considered as a primary means of improving recovery and maintaining the productivity of a well. Hydraulic fracturing was introduced in the early 1940s. Today, almost around 2.5 million hydraulic fracturing jobs are conducted with nearly 60% of the drilled wells being fractured (Smith and Montgomery 2015). Recent studies done by the U.S. Energy Information Administration (2016), determined that nearly 50% of the U.S. oil production comes from hydraulically fractured wells. **Figure 1-1** shows that though the hydraulic fracturing technology developed over the last six decades, it has been implemented considerably in the past few years. This accounts for the increased fracturing activities in the lower 48, as observed in **Figure 1-2**. **Figure 1-3** clearly complements this fact by showing increased water usage for fracturing jobs in the United States from 2011 to 2014 (U.S. Geological Survey, 2015)

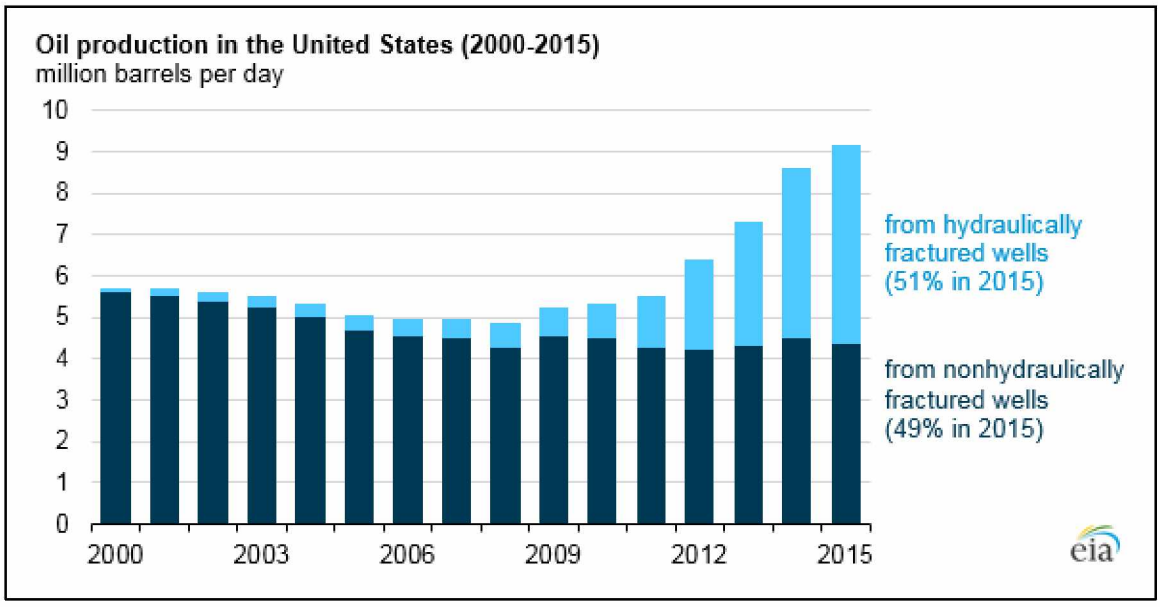

Figure 1-1 Oil production in the United States (U.S. Energy Information Administration, 2016).

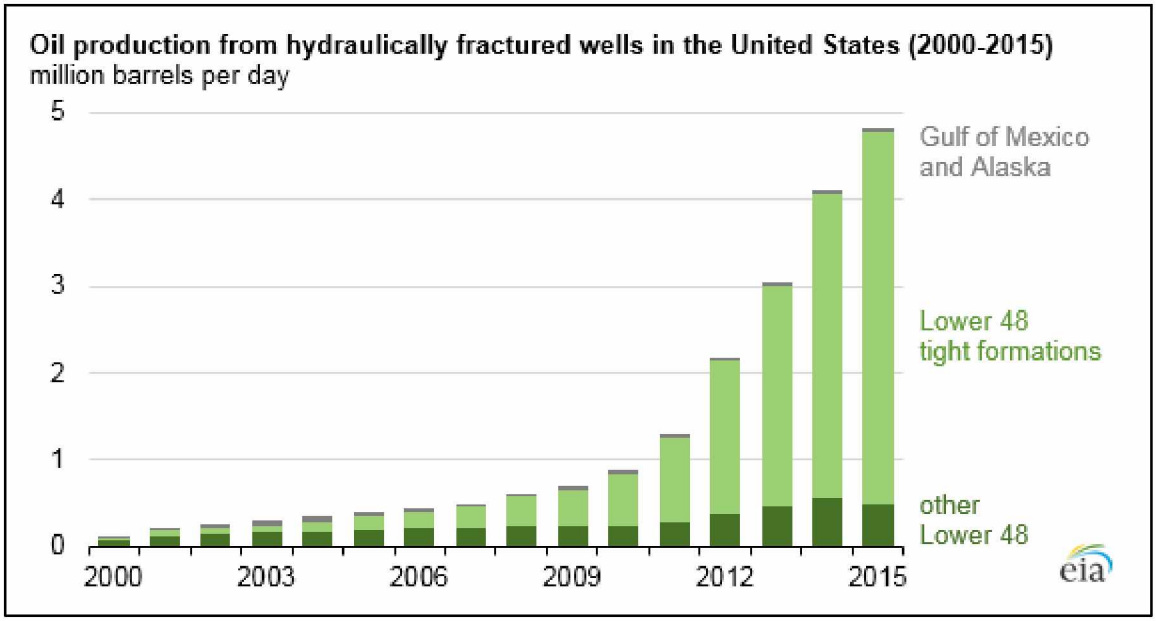

Figure 1-2 Oil production from hydraulically fractured wells in the United States (U.S. Energy Information Administration, 2016).

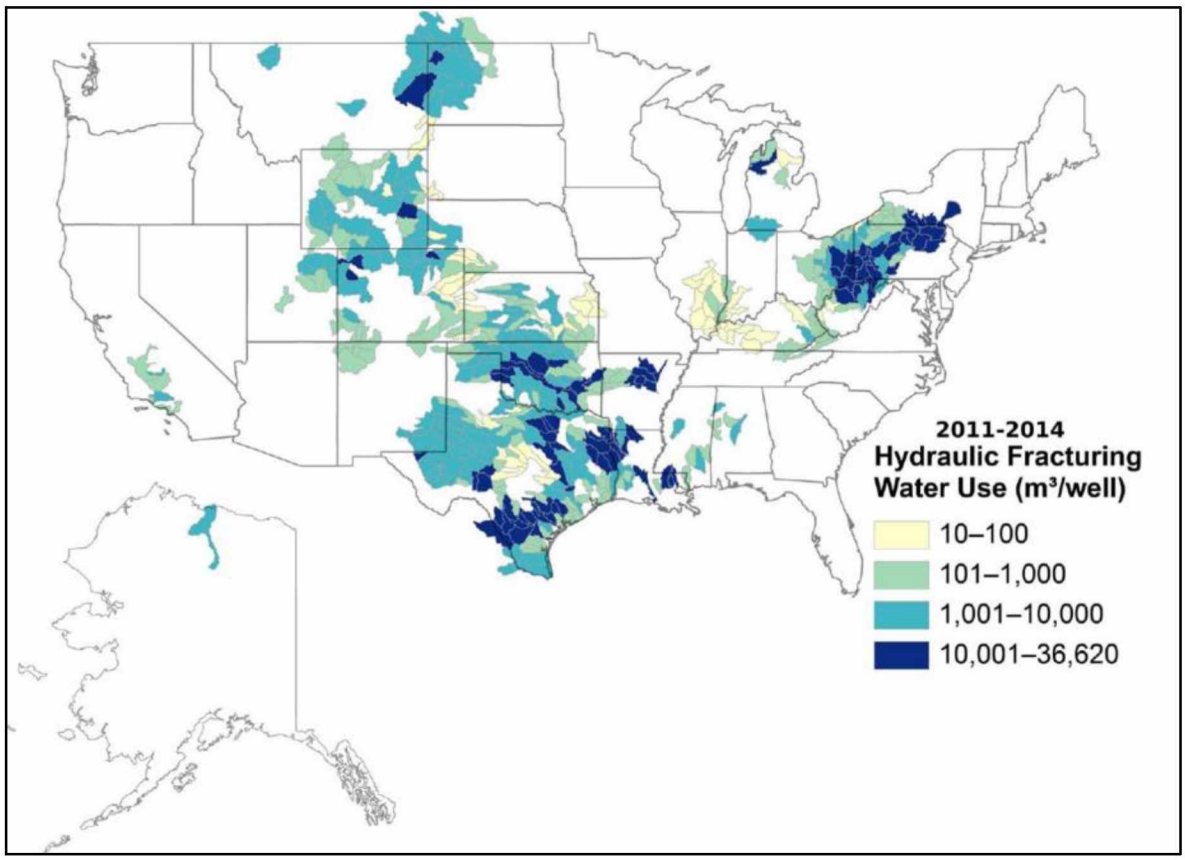

Figure 1-3 Hydraulic fracturing water usage and lower 48 shale plays (U.S. Geological Survey, 2015).

1.1 Alaska's Unconventional Oil and Gas Potential

As per a U.S. Geological Survey (2012), Alaska is supposed to have more conventional oil than other countries in the Arctic. Alaska also has world-class unconventional reserves. The unconventional resources of oil and gas in Alaska mainly include shale oil, heavy oil, viscous oil, shale gas, tight gas, and gas hydrates. The unconventional oil is projected to be on a scale of tens of billions of barrels and the unconventional gas around trillions of cubic feet. As compared to most of the basins worldwide, Alaska seems to be the most underexplored area. To gauge it, there are around 500 exploratory wells on the North Slope as compared to 19,000 in Wyoming. Hence, Alaska has a significant unexplored unconventional oil and gas potential, with shale gas and oil, tight gas, and gas hydrates being the most significant in the pool (Alaska Department of Revenue, 2015). **Figure 1-4** and **Figure 1-5** show the comparison between proved reserves and undiscovered hydrocarbons for Alaska and other North American peers. It is clear that Alaska lags behind in exploring the undiscovered reserves.

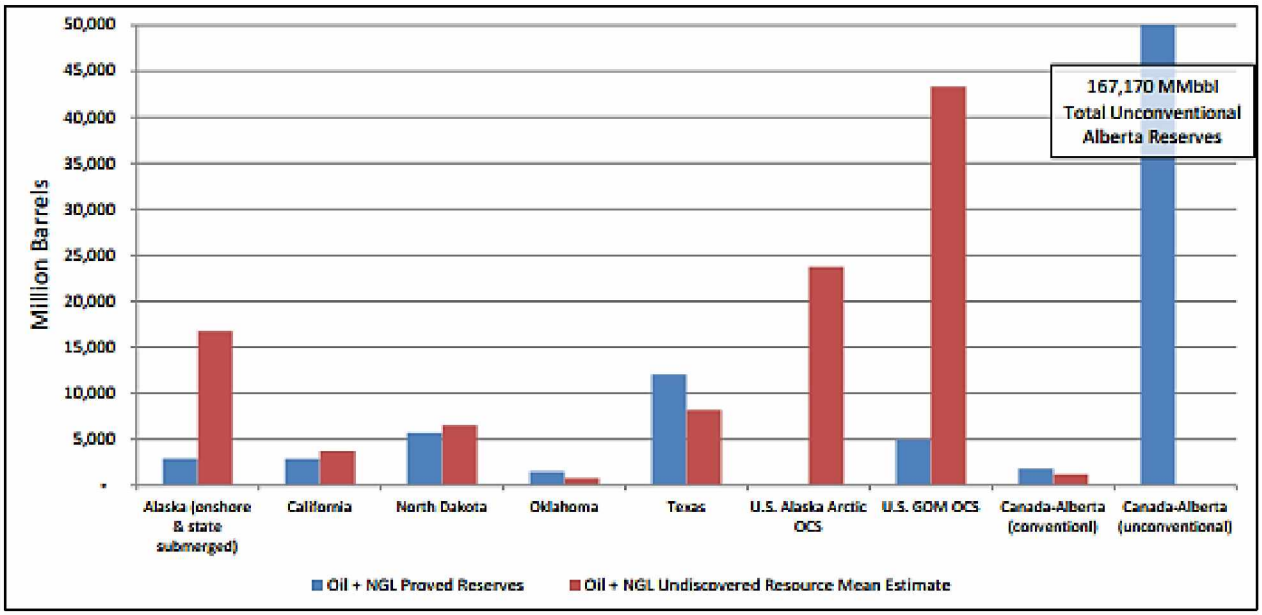

Figure 1-4 Comparison of proved reserves and undiscovered liquid hydrocarbons (Alaska Department of Revenue, 2015).

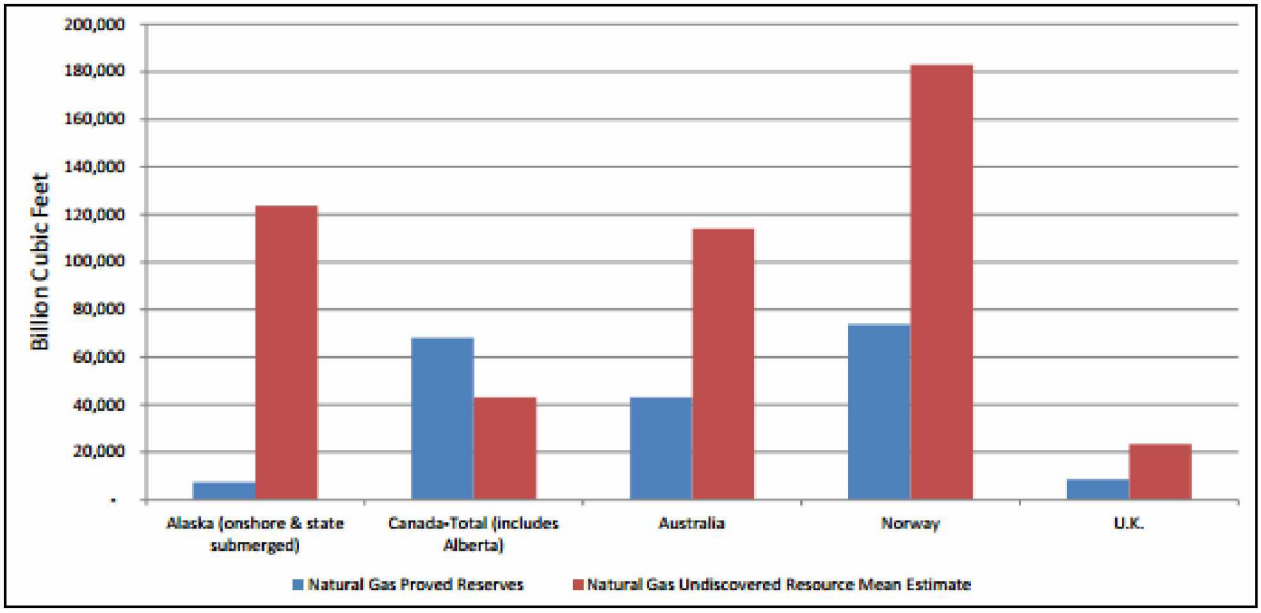

Figure 1-5 Comparison of proved reserves and undiscovered liquid hydrocarbons (Alaska Department of Revenue, 2015).

Apart from unconventional resources, it was also documented that almost 20% of the conventional wells in Alaska were also hydraulically fractured (E and E Publishing, LLC, 2013). As per the U.S. Geological Survey (2012), the estimates of undiscovered shale oil and shale gas for the North Slope come close to those for the Eagle Ford Shale. This proves the North Slope's shale potential, impact, and worth. **Figure 1-6** and **Figure 1-7** show the data from a report provided by the U.S. Geological Survey (2012).

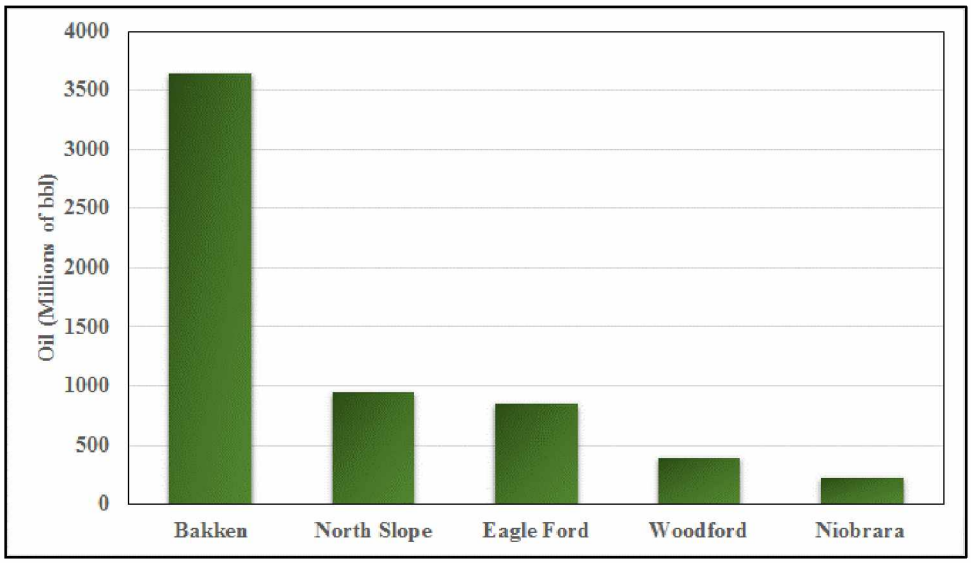

Figure 1-6 Mean estimates of undiscovered oil (U.S. Geological Survey, 2012).

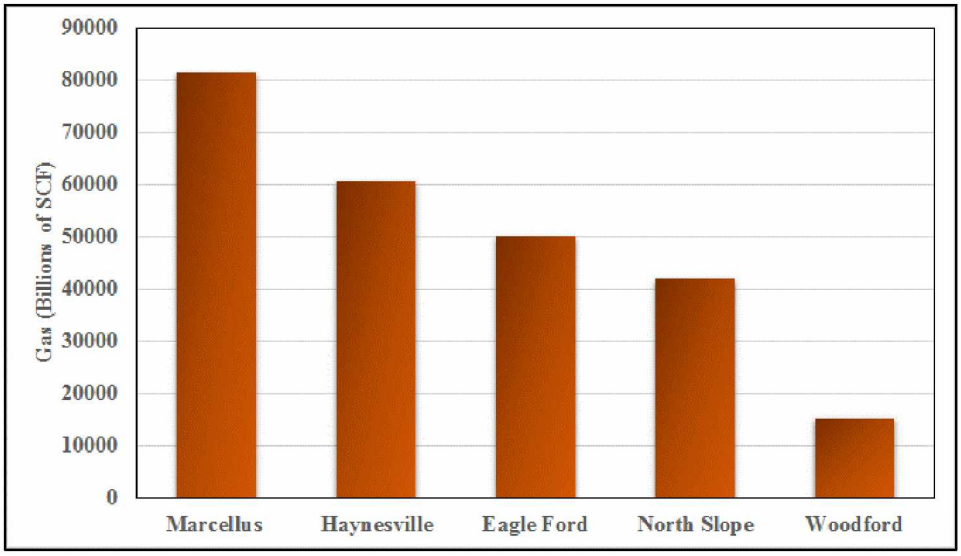

Figure 1-7 Mean estimates of undiscovered gas (U.S. Geological Survey, 2012).

The important and high potential shale plays in Alaska with theoretically recoverable hydrocarbons include the Shublik Shale, the Brookian Shale (Pebble Shale + Hue Shale), and the Kingak Shale. **Figure 1-8** (U.S. Geological Survey, 2012) shows the mean prediction for oil, gas and NGL for the three important shale gas plays on the North Slope. Clearly, the Shublik shale has the highest potential, while Kingak has the lowest in the group.

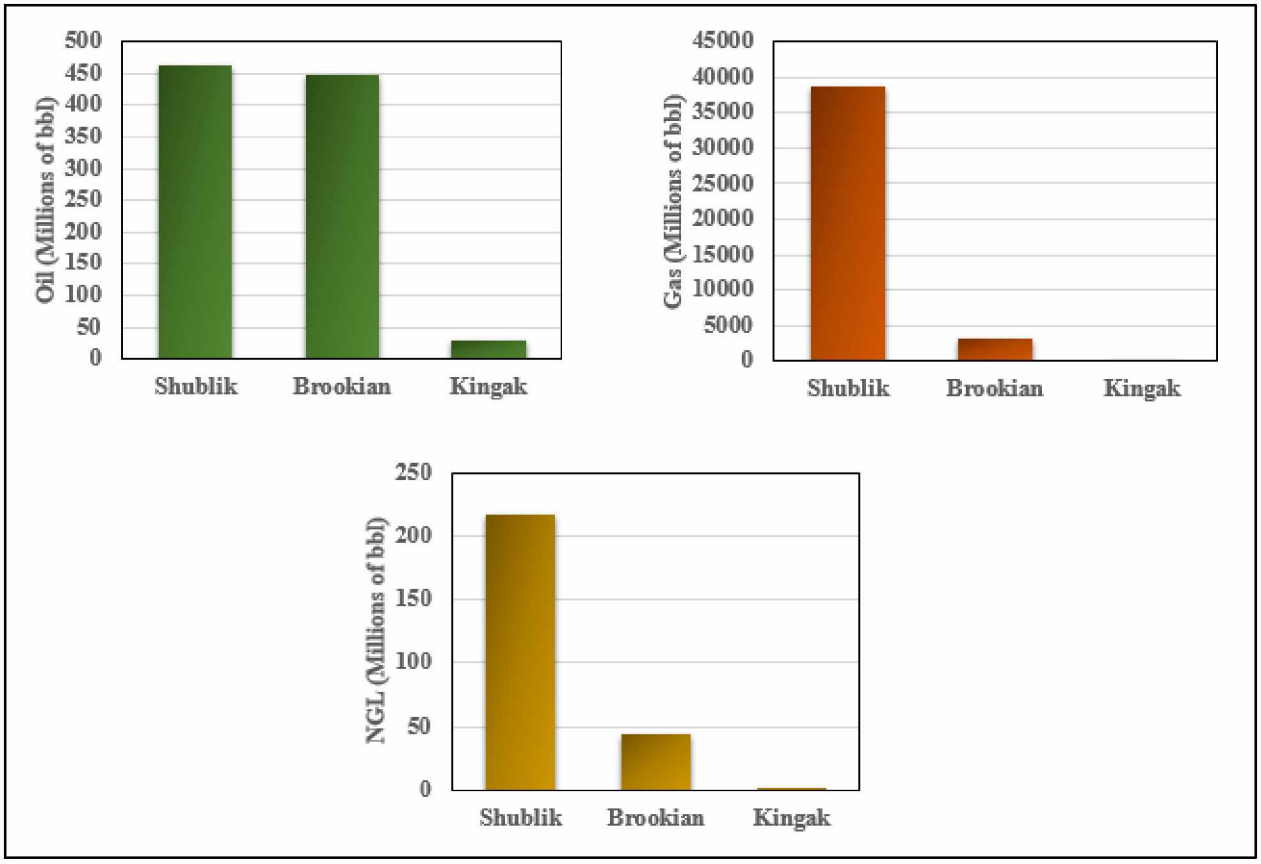

Figure 1-8 North Slope shale oil and gas assessment results (U.S. Geological Survey, 2012).

1.2 Need for HF – NF Interaction Research

The previous section show cased the importance of shale reserves in Alaska. Hydraulic fracturing is one of the primary approaches to deal with such unconventional reserves. Hence, it becomes important to study the complexities like the HF-NF interaction associated with it. Moreover, a detailed literature survey of the topic gave several insights and reiterated the prominence of HF and NF modeling. Several discussions in the literature shed considerable light on the HF-NF impact and the need for this study. A few of the important ones are mentioned in this section.

It was observed that NF are present in almost every formation (Narr et al., 2006). The size and density of NF were seen to affect the hydraulic fracturing job to a greater extent (Gonzalez-Chavez et al., 2015). This calls for carefully studying, planning, and designing a fracturing job, considering HF – NF interaction.

There are several possible HF – NF interaction scenarios: 1) HF crossing the NF; 2) HF being diverted into the NF; and 3) HF being arrested at the NF (Taleghani and Olson, 2014). This

interaction governs the fracture network created. The volume or the portion of the formation rock containing this fracture network is called the stimulated reservoir volume (SRV). The SRV, in turn, governs hydrocarbon production and revenue generation. Hence, it is necessary to carry out this type of research to understand and plan an optimum fracking job targeting a denser HF – NF network and bigger SRV.

Studies done by Aimene and Nairn (2014) showed that the Microseismic SRV (MSRV) was different from the Actual SRV (ASRV) due to unknown and unusual interaction and behavior of HF and NF. Hence, it becomes important to understand and estimate the HF – NF interaction not only before a fracturing job, but also once the job is completed.

Fu and others (2015) also suggested that some of the modes of HF - NF interaction, such as the crossing of NF by HF, cannot be completely or correctly studied or represented in two dimensions. This is because the progressing HF tip will not be constant while it crosses the NF and will change with other parameters. Hence, a detailed and complex three dimensional study of HF - NF interaction is required for precise and accurate studies and prediction. Moreover, there is always limited subsurface access, which demands understanding and pre-study of HF and NF interaction (Taleghani et al., 2014).

1.3 Outline of Present Research

The main objective of this research was to study the interaction between HF and NF using a three dimensional Finite Element Analysis (FEA). The HF path and the existing NF were modeled using advanced cohesive and pore pressure elements in the FEA software. These elements have the capability to model fluid continuity at the HF – NF intersection. Moreover, these elements were for the first time used in the technical literature to model this HF – NF interaction. Thus the key objectives of this research work can be stated sequentially as follows:

- To study the interaction between a single HF and a single NF using Finite Element Analysis (FEA).
- To conduct a detailed sensitivity analysis to observe the effects of in-situ stress contrast, job design parameters, NF mechanical properties, and rock mechanical properties on the resulting HF – NF geometry.

- To scrutinize the least and the most important sensitivity parameters in the context of resultant HF, NF, and HF – NF geometry.

1.4 Summary of Subsequent Chapters

This thesis is divided into four chapters. Chapter 2 consists mainly of a detailed literature review. The literature review covers the beginning of hydraulic fracture modeling. It mainly talks about past work and findings in the HF-NF modeling research area. It further sheds light on the different approaches and tools used for modeling HF – NF interaction.

Chapter 3 forms the main body of the thesis. It covers the model description and construction along with the assumptions made to simplify the complex problem and still provide logical results. It also covers the laws, governing equations, and theory behind the model construction, properties, and computation approach. It mainly covers the theory related to fluid flow modeling and deformation modeling. It further talks about the model validation and construction of the base case. It then covers the studies individually and discusses detailed observations of several sensitivity parameters considered for HF - NF interaction. The sensitivity parameters are broadly classified as the effect of stress contrast, job design parameters, NF properties, and formation properties for logical and sequential representation. Ultimately, all the observations are summarized to give a quick look at the results and observations for the different cases considered. As a final point, Chapter 3 sheds some light on the valuable findings and provides detailed and sequential conclusions of the conducted studies and acquired results. Finally, the recommendations on the conducted work are provided to gather more knowledge related to the research topic.

CHAPTER 2 LITERATURE REVIEW

Hydraulic fracturing is a process where highly viscous fluids containing suspended solids are pumped down a well at a high enough pressure and rate to fracture the formation rock. The highly viscous fluid is called the fracturing fluid/carrier fluid and the suspended solids are called proppants. The proppants help keep the fracture open against the in-situ stresses trying to close the created fracture. Hydraulic fracturing is mainly done in four important stages: 1) the pad stage; 2) the slurry stage; 3) the post flush stage; and finally 4) the flow back stage. However, prior to a new fracturing job, a mini-frac is conducted to have an idea about the formation breakdown parameters. It involves pumping the base fluid to fracture the formation and record the parameters. The first step in a hydraulic fracturing job is a pad stage, where the base fracturing fluid without proppant is pumped to widen the fracture enough to accept the proppants. Then the second step is pumping single or multiple slurry stages containing proppants, as per job design. The third stage, the post flush stage, involves pumping one wellbore volume to flush all the fracturing fluid with proppants in the formation. The fourth and final step is flowing back the well to remove the fracturing fluids, leaving the proppants inside the fractures to keep them open. Hence, the created fracture follows the laws of fracture mechanics and opens in the direction of minimum principal horizontal stress and propagates in the direction of maximum principal horizontal stress.

Due to heterogeneities in the "n" number of oil and gas reservoirs all over the world, hydraulic fracturing will always be a research area to be fine-tuned based on past findings and present scenarios. This can be understood easily from the evolution in research related to hydraulic fractures. This research actually started with the study of cracks and then was applied to the petroleum industry to stimulate the reservoir to increase its productivity and make prospects economical.

2.1 Hydraulic Fracture Modeling

The hydraulic fracturing models were developed from the study of cracks in the early 1920s. They were developed by linking the work of fracturing experts in the past and further applying and developing the results for specific conditions in the petroleum industry. Most of the evolutionary work was an extension of thoughts or existing work. The main aim of the researchers was to actually study the factors affecting fracture geometry and to derive relationships among the factors

and/or the fracture length and width. The hydraulic fracturing job parameters like the viscosity of fracturing fluids, fluid efficiency, and pumping pressure were discussed in accordance with fracture geometry. Several researchers also discussed the propagation of fractures with respect to surrounding stresses and rock properties. Some also studied the effect of geology on fracture nature and characteristics.

The modeling of hydraulic fractures can be 2D, 3D or Pseudo 3D. For 2D models, one of the fracture dimensions, e.g., height, is fixed, while the other two dimensions, length and width, are determined. These dimensions are guidelines for designing a first fracture job for a particular formation. However, the design is fine-tuned as more precise and practical field data becomes available. The most common 2D models that were used in the past include Perkin's-Kern-Nordgren (PKN) (Perkins and Kern, 1961) and Khristianovic and Zeltov- Geertsma- De Klerk (KGD) (Geertsma and De Klerk, 1969). PKN can be used when the length of the fracture is very large compared to its height and KGD can be used when the height of the fracture is very large compared to its length. On the other hand, for 3D or pseudo 3D models, the fracture length, width, and height are simultaneously determined when all the geological and reservoir information or data related to the pay zone and the surrounding layers is known. 3D models are similar to PKN and KGD models that depend on the length/height ratio that is related to stress contrast. The length/height ratio is high when the confining stress is high, which results in less height. The model behaves like the PKN model. Conversely, when the length/height is low, which happens when the confining pressure is low, there is less restriction on height. The model behaves like the KGD model. Also, when there is no stress or modulus contrast, the fracture propagates radially developing a penny-shaped structure.

3D models can also be further categorized as 1) general, 2) planar and 3) pseudo 3D. In general 3D models, there are no assumptions about the orientation of the fractures. They calculate fracture geometry based on a finite element grid system. As the grid changes, the shape changes, as governed by fracture growth. It requires a good amount of input data in the form of rock properties and in situ stresses, and the results are time-consuming. Therefore, these models are most often handled by researchers. The planar 3D models are considered to be perpendicular to the far field in situ minimum stress. These are computationally demanding and are used for routine design. The pseudo 3D models are planar 3D models with reduced/no computational complexities. They can

be further classified as 1) lumped and 2) cell-based pseudo 3D models. In lumped pseudo 3D models, the vertical cut section of the fracture is in a form of two half ellipses joined in the center. In these models, the horizontal length and width of the fracture at the wellbore are calculated at every time step. The assumptions of the fluid flow streamlines from the perforation to the edges of the ellipse are based on analytical solutions. In cell-based pseudo 3D models, the fracture is divided into a series of cells, assuming plane strain and each cell acting independently. **Figure 2-1** summarizes the discussed fracture models.

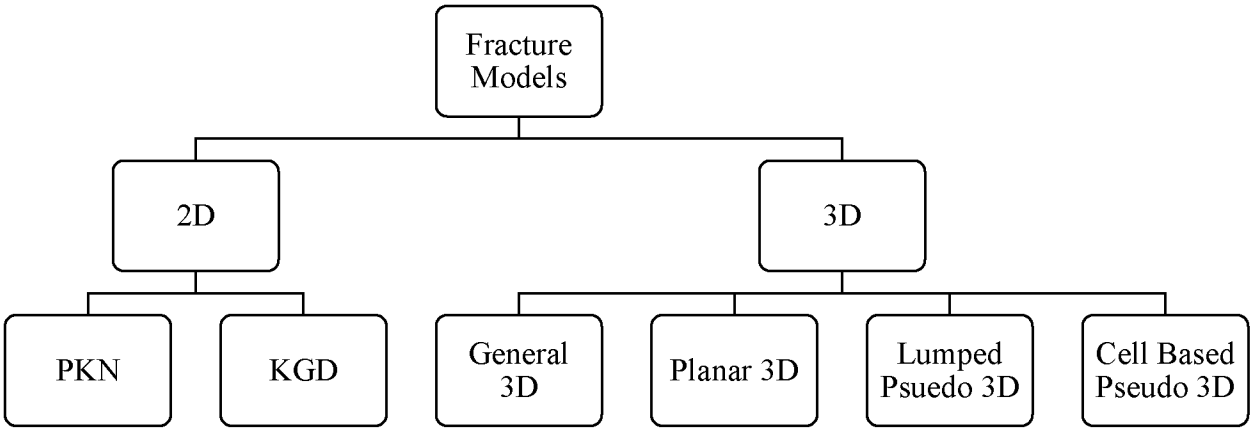

Figure 2-1 Hydraulic fracture models.

In the past, 2D models like PKN and KGD were used to design fractures excessively, but now the more realistic 3D and pseudo 3D models are being used, which deliver remarkable precision and less or no computational complexity.

2.1.1 2D Models

The most widely used, followed, and studied 2D models in hydraulic fracturing are PKN and KGD. However, there is much associated research, studies, modifications, and additions to these stated models. Some research is also altogether different based on new thoughts for designing and interpreting hydraulic fractures.

Griffith (1920) actually stated a characteristic of rock similar to surface tension in liquids, called surface energy. He said that whenever there are cracks in the rock that are horizontally stressed without any external force, the decrease in strain energy is due to the balancing of the elastic strain

in the vicinity of the crack with the increase in surface energy. Perkins and Kern, 1961 used the same principle to study the fracture geometry.

Sneddon and Elliott (1946) introduced the concept of the fracture being a penny-shaped structure showing elastic inflation when the pressure inside increases. They further developed a relationship for crack shape and pressure inside the crack. They derived a relationship between crack volume and fracture radius. They also derived an expression for the width of fractures that expanded radially. They further proved that the minimum pressure to open a fracture is inversely proportional to the fifth root of the volume pumped. Furthermore, the formula for calculating fracture width was derived from the mentioned relationship. Zeltov (1955) used the derivations to develop the KGD model.

Using the concept of the elastic nature of fractures from Sneddon and Elliott (1946), Sack (1946) derived an equation and showed that the minimum fracture pressure is proportional to the radius of the fracture. Considering a penny-shaped crack, the minimum pressure to open the fracture was obtained by equating the work done to open fracture to the energy stored in the fracture system. He further concluded from the equation that the minimum fracture pressure is inversely proportional to the fracture radius. This was an extension of the work of Griffith (1920). It was said that the pressure at the tip of the fracture equals the tensile strength of the rock. This concept was further studied and clarified by Barenblatt (1946).

Hubbert and Willis (1957) deduced the state of stress for various types of geologic deformation. The results were proved experimentally and expressions for normal stress and shear stress were obtained. The angle of internal friction was also studied theoretically. The same was studied through experiments on various rock samples and nitrogen fluid in it. Hubbert and Willis (1957) used these results directly in a theoretical study applying Mohr's diagram to a realistic reservoir scenario.

Howard and Fast (1957) derived a relationship for the area of extending fractures having constant width, created at constant injection rate, with a fluid loss to the formation. The equation, called Carter's equation, considered one of the most important influential parameters for fracture geometry: fluid loss. However, the fluid loss in the equation was represented as a function of time. This led to several complications in computing fracture geometry and the equation was not used

by most of the researchers. Furthermore, Pattillo, 1975 saw that the equation also contained another constant parameter that could be varied to see the applicability of the equation. The parameter was the constant width of the fracture considered in Carter's Equation.

Hubbert and Willis (1957) considered the failure of rocks under shear conditions and the concept of elasticity of the rocks. Perkins and Kern (1961) assumed rocks to be brittle and elastic materials. Using energy balance, minimum fracture pressure was estimated, from which the width of the crack resulting from extending the fracture length was estimated. The fracturing width estimated was found to be greater than minimum widths of extending fractures. It was also shown that the crack width was controlled by the pressure drop in the fracture. Then the relationship for the minimum fracture pressure and for the corresponding fracture width was studied. The different conditions considered were vertical fractures with Newtonian fluid and laminar and turbulent flows. The non-Newtonian laminar flow was also considered. The relationship of fracture width to flow restriction due to sand in the fracture was also discussed. According to Perkins and Kern, 1961, these conditions covered most of the cases and hence were a generalized representation.

Using Griffith's (1920) work explained above, Perkins and Kern (1961) studied the fracture widths resulting from an external injection of fracturing fluid under static conditions. They combined Sneddon and Elliott's (1946) equation and Sack's (1946) equation and further developed a relationship between minimum fracture pressure and crack volume. Also, Sneddon and Elliott's (1946) equation for fracture width was represented graphically using some constant physical properties of rocks.

The above work focused mainly on the static nature of fractures. Perkins and Kern (1961) also studied fracture geometry in dynamic conditions. It was stated that the fluid pressure drop controlled the width of the fracture. Also, it was said that the opposing force, i.e., Earth's stress, was equal to the pressure in the fracture at the tip. As stated earlier, the fracture geometry was studied for two generalized conditions: crack widths from Newtonian fluids in laminar and turbulent flows and crack widths for laminar flow of non-Newtonian fluids. They also studied the fracture geometry of horizontal fractures separately. They stated that the shallow fractures have widths influenced by overburden lifting, while deeper ones' widths are due to compression of rocks. They derived an equation to compute fracture width. They characterized fractures as shallow or deep depending on the ratio of fracture radius to depth. They also made an argument that in the

case of horizontal fractures, the flow near the wellbore is turbulent and does not extend far into the fractures, and hence can be considered only laminar. They developed a relationship for laminar flow that was approximately correct for most cases. Finally, they reviewed all the factors affecting fracture width. The factors mainly included pay zone thickness, depth of pay zone, rock properties, viscosity of the fracturing fluid slurry, pumping rate, radius of fracture, and proppant concentration in the slurry.

Nordgren (1972) considered the fluid loss effect and fracture volume on fracture geometry, which was not studied by Perkins and Kern (1961). He derived an expression for linearly expanding fractures. It mainly related fracture width and length. The developers of the KGD model used his equation to develop linear and radial models.

Geertsma and De Klerk (1969) provided simple approximate formulae for fracture width and length for quick calculations. They considered the formation to be homogeneous, the elastic stress-strain relations linear, the fracturing fluid purely viscous, the flow in the fracture to be dynamic, and the nature of the fracture to be a point source or rectilinear. The viscosity theory of Poiseuille and the linearly and radially expanding fractures equations given by England-Green and Sneddon were used along with the boundary conditions stated by Zheltov (1955). An equation for the width of the fracture for the stated assumptions or conditions was obtained. Linear fractures were considered to be wedge-shaped at the tip and approximately elliptical in shape. They proved that the fracture pressure is directly proportional to the root of the fracture length, hence, the pressure decreases with increasing fracture length. Using an equation, they also proved that the fracture pressure approaches the tectonic stress for larger values of fracture length, which is in agreement with the field data. In the case of radially propagating fractures, the shape of the fracture was stated to be parabolic except at its tip. In a similar manner, an equation for radial flow and for fracture pressure was developed. It was seen that the fracture pressure decreases with increasing fracture radius and was equal to the tectonic stress of the formation for very high fracture radius values. They also studied the effect of formation permeability on fracture dimensions. They introduced a concept of fracture charts. In fracture charts, the aforementioned equations were expressed in terms of dimensionless groups for the linear and radial cases. The concept of dimensionless spurt loss was derived.

Carter's equation (Howard and Fast, 1957), which was not used by most of the researchers due to the functional term of fluid loss involved, was further studied by Pattillo (1975). He observed that the constant width throughout considered in the equation can be varied along the length and the effect can be studied. He extended or conducted sensitivity analysis on Carter's equation to see the effect of varying width of fracture.

Simonson and others (1978) studied linear elastic fracture mechanics. They studied the effect of material properties, varying stresses, and hydrostatic gradients on containment of fractures. If we look into previous research, we can clearly observe that the parameters affecting fractures considered by Simonson and others (1978) were not considered in previous models and were assumed not to affect the fracture geometry. Some of the models, like PKN, considered the material properties to be constant and generalized the same for the different few categories of reservoir rocks. In a nutshell, Simonson and others (1978) actually considered the effect of three parameters on the containment of massive hydraulic fractures. So their theory was more related to the nature of fracture advancement of than fracture geometry. In comparison to the previous work on hydraulic fracturing, he provided a good method to have an idea about some important parameters that influenced the fracture containment. Also, Simonson and others (1978) relationship for height migration can be used to calculate the critical net pressure to avoid the opening of fractures in surrounding layers.

Irwin (1957) studied the effect of the stiffness of the surrounding zone and pay zone using the stress intensity factor. It was observed that when the stiffness of the surrounding formation is greater than the stiffness of the pay zone, the crack is restricted and controlled within the pay zone. On the other hand, when the stiffness of the surrounding formation is less than that of the pay zone, the fracture will not be restricted as it advances and will not be contained in the pay zone. Therefore, it was suggested that the formation with greater stiffness compared to the surrounding formation would tend to have a contained fracture. The second effect discussed was that of varying stress in the fractured zone. He considered an example of stress zones in which the fracture had propagated. He then developed a relation between the fracture extension pressure and the extended fractional length of fractures in the high stress zone and critical stress intensity where fractures initiate. It was observed from the equation that if the difference in the stresses of the pay zone and surrounding zone was significantly high, then fracture pressure was a good indicator of fracture

propagation in the surrounding zone. This will help in studying and programming the containment of fractures in the pay zone. He also derived a relationship between stress intensity factors and pressure gradients for formation matrix and formation fluids.

The fracture models studied are based on several assumptions and specific constant and variable parameters to simplify the problem mathematically. This helps in developing a logical relationship to obtain some idea of the fracture geometry for varying scenarios. Mostly the work done by Howard and Fast (1957) and Hubbert and Willis (1957) was used as a basis for new or extended research done by most of the authors. The parameters considered to affect fracture geometry were not only restricted to the fracture job parameters and reservoir rock properties, but were also extended to the properties of the surrounding lithology and included tectonic stresses. Researchers were inclined towards doing a sensitivity analysis on the basis of the old work to face present challenges and to come out with altogether different results and/or modified conclusions. Considering fracturing today, the stated models can form a fair general basis to design and plan hydraulic fracturing jobs. Different authors have considered different parameters to obtain more precise fracture geometry for specific scenarios. A critical review of the assumptions and constant and variable parameters of existing models will guide selection of the appropriate model to be used for initial design. However, as mentioned before, the availability of practical data will further fine-tune the model to represent more realistic scenarios.

2.1.2 3D Models

Due to the availability of advanced computers, different numerical methods are used to design or develop pseudo 3D models. These numerical methods are actually step-by-step calculations for obtaining the closest possible value for different mathematical analyses such as integration, derivatives, and others. The Finite Element Method (FEM), Discrete Element Method (DEM), Boundary Element Method (BEM), with some advanced methods like the Extended Finite Element Method (XFEM), and the Extended Discrete Element Method (XDEM) are used in developing simulators to study hydraulic fracturing in the petroleum industry.

2.2 Modeling Hydraulic Fractures in the Presence of Natural Fractures

The issue of hydraulic and natural fraction interaction has been examined at the laboratory level and numerically using software packages and at the field level. Warpinski and Teufel (1987) found

experimentally that the hydraulic fractures propagated through joints and formed a multi-stranded, non-planar fracture network. The presence of similar networks was also observed in core samples from tight sandstone reservoirs. Warpinski (1993) and Fischer and others (2002) interpreted some of the Barnett shale microseismic data and found that HF propagation and orientation were both affected by existing NF. Lancaster and others (1992) conducted a core study and found that HF can propagate along NF, resulting in propped natural fractures. A recent laboratory study done by Gu and others (2011) examined frictional interfaces in rock samples from various angles and with different stress values and determined their impact on HF propagation, arrest, or diversion on approaching an NF.

Jeffrey and others (2009), Chuprakov and others (2011), and Weng and others (2011) conducted numerical analyses to understand the interaction between HF and cohesion-less, frictionless interfaces. Taleghani and Olson (2014) examined the interaction of HF with cemented NF in two dimensions and found three potential propagation paths. They were the HF propagating through the sealed NF, the HF arresting at the NF, and the HF branching out after intersecting the NF. He and Hutchinson (1989) further extended this work by suggesting different scenarios. They proposed HF to be double branched or single branched on intersecting NF. Taleghani and Olson (2014) studied the debonding and/or shearing of NF during the hydraulic fracturing process. The XFEM was developed by Moes and others (1999) and was applied by Lecampion (2009) to model HF along element edges. Lecampion (2009) did not address fluid flow coupling with HF propagation. The further fluid flow was coupled to this work to make the model more complex and realistic by Taleghani (2009). Taleghani and Olson (2014) showed that when the HF is parallel to the NF, opening of the NF ahead of the hydraulic fracture tip or side will occur. Olson (1993) reached similar conclusions. Offenberger and others (2013) evaluated Schlumberger's Unconventional Fracture Modeling (UFM) module through HF-NF modeling coupled with reservoir simulation. Various UFM simulations were run and hydraulic fracture geometry was observed to be most sensitive to natural fracture density and orientation. Sensitivity analyses were also done to observe the impact of stress orientation, anisotropy, and shadowing on the distribution of fracture networks. However, these studies did not consider the interaction at the micro level. Chuprakov and others (2013) studied the propagation behavior of HF through the natural fractures and accounted for the effects of fluid properties and natural fracture permeability. Kresse and

Weng (2013) further refined the UFM by considering the fluid leak off into existing permeable NFs. According to them, the HF could either propagate through the NF, open the NF, or be arrested at the intersection. Nolte and Smith (1981), Nolte (1991), Warpinski (1993), Barree and Mukherjee (1996), and Mukherjee and others (1991) incorporated the observation that the presence of NF alters the leak off into the formation and that the permeability of NF is both time and pressure dependent. Walsh (1981) investigated the effect of stress and pressure changes on NF permeability.

Aimene and Nairn (2014) modeled the propagation and interaction of multiple HF with NF using the Material Point Method. They considered HF and NF at different angles with respect to maximum horizontal stress and studied the effects of varying stress anisotropy and angle of NF on propagation for a Marcellus shale gas well. Blanton (1982), Warpinski (1987), and Sesetty and Ghassemi (2012) did not consider the stress shadowing effects in their analyses, hence, the mechanical interaction was not completely implemented. Numerical models developed by Koshelev and Ghassemi (2003) considered these interactions but did not consider the fluid flow. Zhang and Jeffrey (2006) included fluid flow and obtained results for a single NF. Weng and others, 2011 modeled HF with multiple NFs and studied the effects of stress shadowing on propagation. Fu and others (2011) simulated HF propagation in a randomly distributed NF network. Sesetty and Ghassemi (2012) developed a numerical model that coupled fluid flow with stress shadowing to simulate complex fracture networks and studied the evolving fracture geometry, fracture aperture, and pressures as a function of injection time to determine possible locations for proppant screen outs and secondary fracture initiation.

Nagel and others (2011) studied natural fracture shear using continuum and 2D Discrete Element Method (DEM) code, varied matrix stiffness, and Poisson's ratio, and observed no changes in NF shear for constant mechanical properties of NF. Nagel and others (2012) developed a fully coupled Discrete Fracture Network (DFN) model to study HF development in the presence of NF. They considered the mechanical properties of NF, such as elastic moduli, strength parameters, and fracture toughness. They studied the same NF shear with 2D DEM code considering matrix properties, DFN effects, and fracture friction angle. They observed that the friction angle had a greater effect on NF shear. They also considered the pressure diffusion during hydraulic fracturing and found that the NF shear strongly depended on the pressure in the NF, which depended on initial fracture aperture. Oussoltsev and others (2013) developed a workflow to simulate HFs in

the Eagle Ford shale using a reservoir-centric stimulation design (RCSD) tool. They presented the natural fractures as 2D discrete fracture networks with no limitation on vertical height and with the ability to model proppant transfer. Nagel and others (2012) coupled DEM and discontinuous deformation analysis (DDA) fluid pipe network models and simulated pressure response during hydraulic fracturing. Gong and others (2011) studied a shale gas reservoir considering NFs by explicitly applying the Discrete Fracture Network (DFN) approach. They considered mechanisms such as gas adsorption/desorption, matrix-fracture transfer, and non-Darcy effects. They conducted history match based on two months' production data and predicted cumulative gas production and gas rate for the next three years.

Shin and Sharma (2014) studied various HF design parameters that influence the resulting HF geometry and its propagation patterns using FEA software. Simulations were conducted with varying parameters, including perforation cluster spacing, number of perforation clusters, fracture height, fracturing fluid viscosity, pumping rate, and Young's Modulus. They considered multiple hydraulic fractures in a target zone with surrounding layers and studied the resulting geometry with respect to job design parameters and some rock properties. Yadav (2011) developed a geomechanical model in FLAC 2D software to study the HF-NF interaction by simulating the path followed by a HF once it intersects a NF. They also studied the extent of the micro-seismic activity cloud when a naturally fractured medium was hydraulically fractured. They conducted a sensitivity analysis to observe the effect of different parameters on the extent of the microseismic cloud.

Abbas and others (2014) modeled HF to investigate the effect of fracture growth and reduction in fracture opening at fracture offset for different combinations of parameters such as formation moduli, far-field stresses, fluid injection rate, the ratio of offset length to the length of straight fractures, and the offset angles. The modeling was done using a code based on the Extended Finite Element Method (XFEM). Their study revealed that the interaction between HF and weak planes resulted in HF propagating through the weak planes, or getting blunted and stopping at the interface, or just propagating in the offset direction. Stress contrast, orientation angle, and interface friction were identified as some of the parameters affecting these interactions. Abbas and others, 2014 discussed the geometry effects of these HF-NF intersection angles when the difference between the vertical confining stress and the minimum principal horizontal stress was kept zero. Meng and De Pater (2011) used Comsol to study HF-NF interaction, observing HF propagation

when it intersects the NF. He obtained fracture width profile, fluid pressure inside the fracture, and leak off rate along the length of the fracture.

Fu and others (2015) studied the specific scenario of the HF propagating through the NF. They mentioned the crossing phenomenon to be unique for the three dimensional case and realistic compared to two dimensional analysis. They used a fully coupled hydraulic fracturing simulation code called "GEOS" and studied HF-NF interaction with NF perpendicular to the HF propagating direction. They conducted laboratory analyses, then simulated and studied a field scale model. One of their key findings was that the HF always crossed the NF if the cementitious filling the NF was very thin. However, their study was restricted to perpendicular natural fractures (with respect to hydraulic propagation direction) and consisted of a single matrix material.

Saurez-Rivera and others (2013) conducted experiments to study the interaction of propagating cracks with discontinuities or planes of weakness. They conducted experiments on outcrops of the Niobrara formation. They measured the fracture conductivity for propped and unpropped cracks at varying stresses. They found out that with increasing stress, the conductivity of the fracture remains higher for longer fractures than shorter ones. They also mention that the distribution of proppants in the fractures is highly influenced by the complexity of the rock matrix or discontinuities in the rock. They describe the fracture system by dividing it into four different segments: 1) wellbore; 2) connection between the wellbore and the fracture system; 3) near-wellbore fracture; and 4) far wellbore fracture. They studied the consequences of every region on hydrocarbon production to determine the most prominent region for production decline. One aspect of their work was to observe the effect of weakness planes on crack propagation in laboratory samples. They tried to study the effect of high, low, and no in-plane stress contrasts on induced fractures approaching weakness planes. These planes of weakness were at different orientations with respect to the direction of maximum horizontal stress. They defined a term called "step-over," which is the shearing of NF due to HF encountering it. The step-over is always said to be present in all of the scenarios considered; however, the step-over effect is clearest in the case of high stress contrast and least apparent in the case of low stress contrast. In the case of no stress contrast, the HF was arrested by the NF and followed the path of least resistance that was supposed to be along the NF.

Gonzalez-Chavez and others (2015) studied two-dimensional HF-NF interactions using commercially available FEA software. They analyzed whether the HF was arrested by the NF, propagated through NF, or followed the path of NF upon intersecting the NF. The resulting geometry depends on the surrounding rock properties, the magnitude and direction of principal horizontal stresses, and the angle between the intersecting fractures. They conducted a semi-circular bending test (SCBT) to determine the cohesive properties to be used in their FEA model. They examined four cases. The angle between the HF and the NF was considered to be either 45° or 90° and for each orientation, they could have either a weak or strong NF, leading to four different scenarios. In the case of an intersection angle of 45° and weaker NF, the HF followed the path of the NF after the intersection with activation of the NF wing. In the case of an intersection angle of 45° and stronger NF, the HF propagated across NF without activating it. For the case of an intersection angle of 90° and weaker NF, the hydraulic fracture followed the path of NF after the intersection with NF and activated one of the NF wing. For the case of an intersection angle of 90° and stronger NF, the HF propagated across NF without activating it. Furthermore, they considered a fifth case, with four NFs perpendicular to the direction of maximum horizontal stress and four NFs parallel to the direction of maximum horizontal stress. It was observed that in the case of the stronger NF, the hydraulic fracture propagated through the NF and sheared it slightly: incomplete activation. In the case of the weaker NF, the HF approaching the NF was directed along the NF.

Until recently, most of the work done considered the HF-NF interaction mainly in 2D. The latest work done by Fu and others (2015) suggests studying this interaction in three dimensions mentioning the limitation or uncertainty in the two-dimensional analysis for HF propagating through NF. As per their study, the results of HF crossing NF differ in 3D and 2D. In 3D, the opening changes with depth and hence the advancing HF tip profile propagating through NF will vary with depth. Their study considers a homogenous single layer of rock and is done using GEOS code.

It was observed from the literature review that the HF-NF interaction is being studied extensively considering its importance in hydraulic fracture job design. This thesis studies the HF-NF interaction in three dimensions using commercially available FEA software. This study demonstrates the successful use of special purpose advanced Cohesive Pore Pressure elements available in FEA software capable of modeling fluid continuity at HF-NF intersection in three

dimensions. These advanced elements are used to define planes that define the direction of HF and represent the NF as a plane of discontinuity.

2.3 General HF-NF Modeling Approaches

Clifton and Abou-Sayed (1981) used an approach similar to FEM and formulated elasticity equations in the form of integral equations. This model was more computationally time consuming. Naceur and others (1990) improved the model by using the boundary integral method for the displacement field and analyzing the effect of the surrounding layers on the fracture, further reducing the computational time. The major drawbacks of the model were its difficulty in modeling simultaneous propagation of multiple fractures and inability to incorporate non-planar fractures. Advani and others (1993) studied propagation of fractures in layered zones, also using FEM. They incorporated non-Newtonian fluid flow in the fracture, but poroelastic effects and non-planar fractures were not considered. The simulator lacked re-meshing techniques, which resulted in a high computational time. This approach was coupled to fluid flow with the elastic opening of the fractures. Choate (1992) developed a 3D fracture propagation model using GEOFRAC. A volume balance criteria was used for modeling. This simulator did not work for complex and heterogeneous formations. Olson (1993) developed a 2D numerical model and studied the joint spacing, lengths, and apertures, taking into account various mechanical properties. Lam and Cleary (1984) studied the effects of bedding planes on a propagation of hydraulic fractures using Displacement Discontinuity Analysis (DDA). Jeffrey and others (1987) also used DDA and studied the effects of bedding or frictional planes on hydraulic fracture propagation, considering the slippage by using Mohr-Coulomb's criteria for failure of rocks. They concluded the treating pressure were high for the cases considered. Beugelsdijk and others (2000), Akulich and Zvyagin, (2008), and Zhao and Young (2009) did similar studies using DEM. Rahman, 2009 did a similar study and observed the effects of poroelasticity using FEM. Olson (2008) developed a numerical code from pseudo-3D displacement discontinuity solutions to study multiple fractures' propagation. As time passed, more advanced numerical techniques were used to model hydraulic fractures. Lecampion (2009) modeled the elasticity equation using XFEM. The main advantage of XFEM was that the fracture was not restricted by the meshes and was allowed to propagate and could cross the elements. Taleghani and Olson (2011) used XFEM in their 2D model and considered the fracture propagation and fluid flow coupling process, which were neglected by

Lecampion (2009). Weng and others (2011) developed a complex fracture network model called the Unconventional Fracture Model (UFM) to study the rock deformation, propagation of fractures, and fluid flow in complex fracture networks using the assumptions and governing equations for pseudo 3D models.

Nagel and others (2014) performed an extensive 2D numerical investigation of zipper frac completion schemes by evaluating the effects of natural fracture orientations, in-situ stresses, and natural fracture friction angles for different lengths and combinations of natural fractures. It was further concluded that the natural fractures strongly affect the completion design for shale. They discussed the numerical study of multi-well completion using DEM. It was portrayed in a fully hydro-mechanical manner that dealt with the ability to enhance natural fracture shear to increase well productivity, considering parameters such as well configuration, in situ stress conditions, in-situ pressure, and mechanical properties for multi-well completions.

Abbas and others (2014) studied hydraulic fracture modeling to investigate the effect of fracture growth and reduction in fracture opening at fracture offset. Different combinations of parameters like formation moduli, far-field stresses, fluid injection rate, ratio of offset length to the length of the straight fractures, and the offset angles were considered. The modeling was done using a code based on XFEM. This code solved for the fluid flow in the fracture and the elastic fracture response by solving for fracture velocity. If the fracture propagates into an unwanted zone, then the fracturing is rendered useless. Hence, fracture growth containment is an active area of research today. Studying the interaction between hydraulic fractures and weak planes, it was said that the HF can cross NF, get blunted and stop at the interface, or just propagate in the offset direction.

Nagel and others (2012), developed a fully coupled 3D discrete fracture network (DFN) model for studying hydraulic fractures in the presence of natural fractures considering the mechanical properties of natural fractures such as elastic properties, strength parameters, dilational properties, fracture toughness, and initial aperture. Nagel and others (2011) and Nagel and others (2012) presented numerical solutions using both 2D and 3D DEM coupled with mechanical behavior of the natural fractures. Nagel and others (2011) studied natural fracture shear using continuum and 2D DEM code and varied matrix stiffness and Poisson's ratio, observing no changes in NF shear when NF mechanical properties were kept constant. Nagel and others (2011) studied the same

shear with 2D DEM code considering matrix properties, DFN effects, and fracture friction angle, and observed that the friction angle had the greatest effect on NF shear.

The XFEM can model fracture growth without taking time for re-mesh (Taleghani and Olson, 2014), which makes it computationally less burdensome than the FEM. The XFEM was developed by Moes and others (1999). Lecampion (2009) applied FEM to model hydraulic fractures assuming a specific pressure distribution or opening profile. Further fluid flow was coupled to this by Taleghani (2009). Crack propagation involved the study of parameters like energy release rate to determine the length, velocity, and orientation of propagated fractures (Taleghani and Olson, 2014).

2.4 Commercial Software Based HF-NF Modeling Approaches

2.4.1 Abaqus

Abaqus is multi-physics software that can be used for modeling HF – NF interaction using different physical phenomena like heat, electricity, low frequency electromagnetic radiation, structural acoustics, and fluid flow through porous media. Computational fluid dynamics (CFD) is one of the capabilities of Abaqus that simulates incompressible fluid flow along with deforming and unstable meshes. It also allows us to couple our own or any other CFD module for studying fluid-structure interaction involving smoothed particle hydrodynamics and a coupled Eulerian-Lagrangian approach. It helps visualize complex models having guts or joining planes. Abaqus was used by Shin and Sharma (2014) to study the various fracturing design parameters that influence the resulting hydraulic fracture dimensions and their propagation patterns. A few other authors have used this type of approach in the field of hydraulic fracturing. However, this section concentrates on Shin and Sharma (2014) to understand the approach used. Simulations were conducted with different parameters, including perforation cluster spacing, number of perforation clusters, fracture height, fracturing fluid viscosity, pumping rate, and Young's Modulus. The problem statement consisted of: 1) preparing a geomechanical model; 2) constructing a horizontal well with perforations; 3) defining planes for hydraulic fracture propagation; 4) simulating the geometry of hydraulic fractures in the presence of other propagating hydraulic fractures at different injection rates and viscosities of injected fluids; and 5) investigating the impact of stress shadowing and fluid distribution on multiple fractures during fracture propagation. The results showed that:

1) there exists an optimum number of perforations for every fracturing stage; 2) slick water has a capability to develop uniform multiple fractures when perforations are closely spaced; 3) high pumping rate is required for propagating fractures through all perforations; and 4) maximum possible small heterogeneities should be considered, as they may alter fracture characteristics to great extent.

2.4.2 Unconventional Fracture Modeling (UFM)

Modeling complex fracture networks using UFM has been studied recently by several authors. The assumptions and governing equations are similar to the pseudo-3D fracture models. The main difference between UFM and conventional modeling is that UFM models the interaction between natural and hydraulic fractures and takes into account the stress shadow effect. Weng and others (2011) refined the UFM, taking into consideration the fluid leak off and shear slippage for existing permeable natural fractures. According to them, the hydraulic fracture can either cross the natural fracture, open the natural fracture, or get arrested at the intersection. These interactions lead to complex fracture networks. These interactions depend on in-situ rock stresses, mechanical properties of rock, properties of natural fractures, and fracturing treatment parameters such as fracturing fluid properties and injection rate. There are various approaches that are time-consuming and the approach by Weng and others (2011) is fast and requires less computation time.

Offenberger and others (2013) evaluated Schlumberger's UFM module through 3D natural and hydraulic fracture modeling coupled with reservoir simulation. It consisted of: 1) geo-cellular Model using 3D seismic data, stratigraphic correlations, whole core, and open hole well log data; 2) discrete Fracture Model (DFM) using seismic data and OBMI interpretation; and 3) recombination of the geo-cellular model and DFM using UFM. Various UFM simulations were run and HF geometry was observed to be most sensitive to natural fracture intensity and orientation. Sensitivity analyses were also done to observe the impact of stress orientation and anisotropy and shadowing on the distribution of HF and NF. DFM allowed evaluation of a potentially fractured matrix's contribution to production. Sensitivity analysis done with UFM showed that: 1) complex networks with shorter half lengths were observed in addition to secondary fractures; 2) NF at higher angles to maximum horizontal stress resulted in increased complexity in fracture networks as the hydraulic fractures most likely crossed the natural fractures; and 3) considering inter and intra-stage shadowing affected both the HF distribution and the placement

of proppant. For validation of the fracturing model, a reservoir model was constructed. HF conductivity was obtained from the Predict K software program. A history match was done, controlled by flowing bottom hole pressure. The main variable changed for history matching was the permeability of the SRV zone, and the value that yielded best match was obtained.

Oussoltsev and others (2013) developed a workflow to simulate hydraulic fractures in the Eagle Ford shale using reservoir-centric stimulation design tool (RCSD). A DFN model was developed using petrophysical data. The model was further conditioned or improvised by seismic data, image log data, and completion data. Fracture geometry was simulated using UFM and the modeled fracture was calibrated using microseismic events considering fluid rheology, fluid loss variables, and stress shadowing effects. The results of the simulator consisted of fracture surface area, fracture propped area, HF geometry for estimating stimulated volume, and reservoir simulator input data for production history matching and forecasting production. Stimulated volume changes with respect to the pumping rate, pumping pressure, and completion parameters could also be obtained using RCSD. Oussoltsev and others (2013) presented natural fractures as a 2D discrete fracture network with no limitation on vertical height limitation in the RCSD tool. RCSD not only had the capability to generate 2D and 3D DFN models, but also to model proppant transfer. This work was a combination of RCSD and UFM. UFM is currently the most effective and precise tool to model HF – NF interaction.

2.4.3 COMSOL

Comsol is a multi-physics software that can be used to study any physics-based system. A predefined set of graphical user interfaces for common commercial problems is available. The geo-mechanics module that is added on to the structural mechanics module contains interfaces that can investigatete deformation, plasticity, creep, and failure of rock and soil and their interaction with supports, piles, and other manufactured structures. Hence, it can be used for modeling hydraulic fractures as well. Apart from the built-in plasticity, model users can also define their own yield functions. Meng and De Pater (2011) used Comsol to: 1) study the interaction of hydraulic and natural fractures by observing the hydraulic fracture propagation once it intersects the natural fracture; 2) obtain the fracture width profile, fluid pressure inside the fracture, and leak off rate along the length of the fracture; and 3) introduce non-linear slip mechanisms apart from simple linear slip mechanisms.

There were two stages involved: 1) preparing a hydraulic propagation model and 2) improvising the HF propagation model to observe and study the HF – NF interaction. The model was built using Matlab scripts for fracture tip and fluid front movements. The finite element routines implemented in Matlab were used for solving a quasi-static problem. A Finite Element Method was used where a 3D elastic model was coupled to a 2D fluid flow field model in order to relate fluid injection to fracture initiation and propagation. Considering the fluid mass balance by observing the fluid injected, fluid in the fracture, and fluid leaked, several iterations were done and, as the fracture propagated, re-meshing was done accordingly.

The fracture width along the fracture length and height were obtained in the form of displacement in the direction of minimal in situ stress for a different cumulative time. Apart from the fracture width, the fluid pressure inside the fracture and the leak-off rate at different times were also obtained. This approach was used by Meng and De Pater (2011) for comparing the simulation results with experiments results. The above model was then improvised for modeling and observing the propagation of a HF when intersected with NF. This was done by defining a fracture propagation criterion at the intersection. This criterion was a breakthrough criterion that suggested if the HF continued through NF, got diverted into NF, or got arrested after the intersection with NF.

2.4.4 FLAC 3D

FLAC 3D is actually Fast Lagrangian Analysis of Continua in three dimensions. It is a finite difference program to study the mechanical behavior of a continuous medium when it reaches equilibrium. Constitutive equations defining the idealized and general principles like strain and laws of motion are used. It is a good tool to solve problems with elastoplastic material behavior resembling high strain scenarios. FLAC 3D models plastic collapse and flow accurately.

Yadav (2011) developed a geomechanical model in FLAC 3D software to study the interaction between HF – NF by simulating the path followed by HF once it intersected a NF. S/he also studied the extent of micro seismic activity cloud when a naturally fractured reservoir was hydraulically fractured. A sensitivity analysis was also done to observe the effect of different parameters on the extent of the microseismic cloud. FLAC 3D can also model single phase fluid flow through porous

media and perform coupled flow and deformation analysis. However, Yadav (2011) did not consider the fluid flow and poroelastic effects in their study.

The built-in programming language called FISH was used to study the fracture width, HF-NF interactions, and failure region around the fracture tip. To validate the model, Yadav (2011) compared the fracture half widths obtained from the numerical method to the analytical ones available in the literature. They observed that higher differential stress and orthogonal weak planes caused the hydraulic fracture to cross the weak planes without changing direction. However, lower strength planes caused slippage and could change the propagation direction of hydraulic fracture. Sensitivity analysis done by changing the fracture spacing indicated that there existed an optimum fracture spacing to obtain dense and complex fracture network, maximizing the microseismicity. The effect of varying several parameters like fracture half-length, formation mechanical properties, fracturing pressure, and strength of weak planes on optimum fracture spacing was conducted. This proved that the strength of weak planes and their Young's Modulus were most sensitive and controlled the fracture spacing window.

2.4.5 Combinational Approaches

The approach used by Aimene and Nairn, 2014 considered a combination of software for a precise HF – NF interaction study and analysis. They modeled the propagation and interaction of multiple HF with NF using a special method called the Material Point Method. OS Particulas software was used with a Crack in the Material Point (CRAMP) algorithm. C++ coding was used with a CRAMP algorithm. The effect on natural fractures of remotely propagating hydraulic fractures was studied for different stress anisotropies and natural fracture orientations. The fault attribute of the mentioned formation was digitized and was an input to FracPredictor that generated an Equivalent Fracture Model (EFM). Then the derived EFM fracture length and angles were exported into the OS Particulas software to create a discrete MPM model. The last step involved OS Particulas simulation for in-situ pre-stress and then the simultaneous increase of pressure. The two focused results of this simulation were a strain map and J integral. Hence, this comparison of microseismic data and MPM results shows similarity, which can help a completion engineer predict which stage will show highest and lowest micro seismicity.

CHAPTER 3 MODELING THE INTERACTION BETWEEN HYDRAULIC AND NATURAL FRACTURES USING THREE DIMENSIONAL FINITE ELEMENT ANALYSIS

3.1 Model Construction

A commercially available FEA software program, ABAQUS, was used for this study. A single HF was modeled with the target and surrounding formations in the presence of a single NF. The actual reservoir case is simplified to a rectangular cuboid shape geomechanical model, as shown in **Figure 3-1.** A vertical HF propagation path is predefined and a single vertical NF is modeled, as shown in **Figure 3-1 and Figure 3-2**. The overburden stress is S_v and the maximum and minimum horizontal stresses are S_{Hmax} and S_{Hmin}, respectively. In **Figure 3-2**, the left figure shows a top view and the right figure shows the side view of the three dimensional geomechanical model.

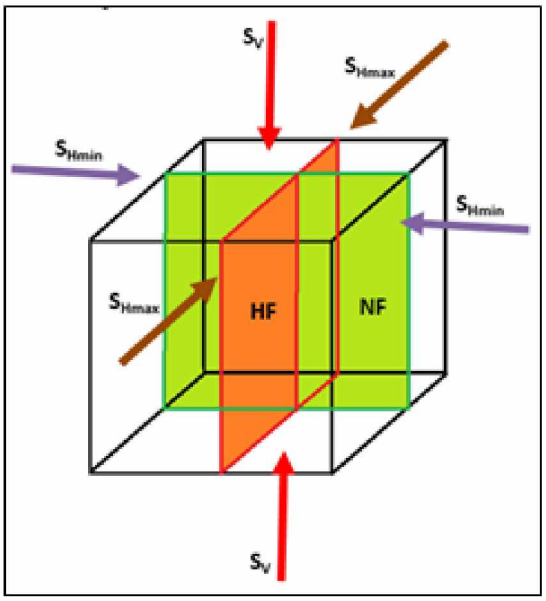

Figure 3-1 Three dimensional geomechanical model representing a single HF in orange and a single NF in green.

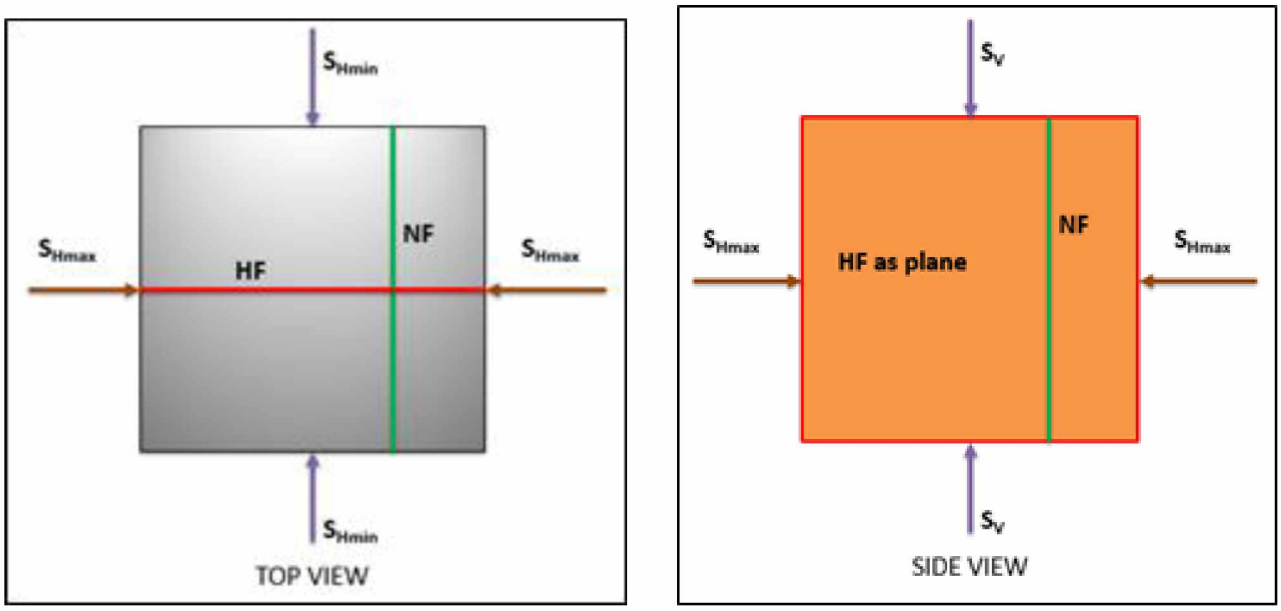

Figure 3-2 Two dimensional planar top and side views of the three dimensional geomechanical model.

The NF and HF planes were constructed using three dimensional advanced Cohesive Pore Pressure Elements-COD3D8P available in the FEA software. The rock matrix was considered a porous elastic medium and was modeled using Reduced Integration Hexahedral Pore Pressure and Stress Elements-C3D8RP. The target layer was surrounded by top and bottom bounding layers to include the effect of surrounding layers. The node defining the HF-NF intersection was kept common to allow fluid flow continuity in all directions. The meshed geomechanical model created using FEA software is shown in **Figure 3-3**. The cohesive planes were embedded in the rock matrix and can be seen in **Figure 3-4**, where the surrounding rock matrix is removed for proper visualization of the planes. The perforation pressure drop is negligible and hence is not considered in this study.

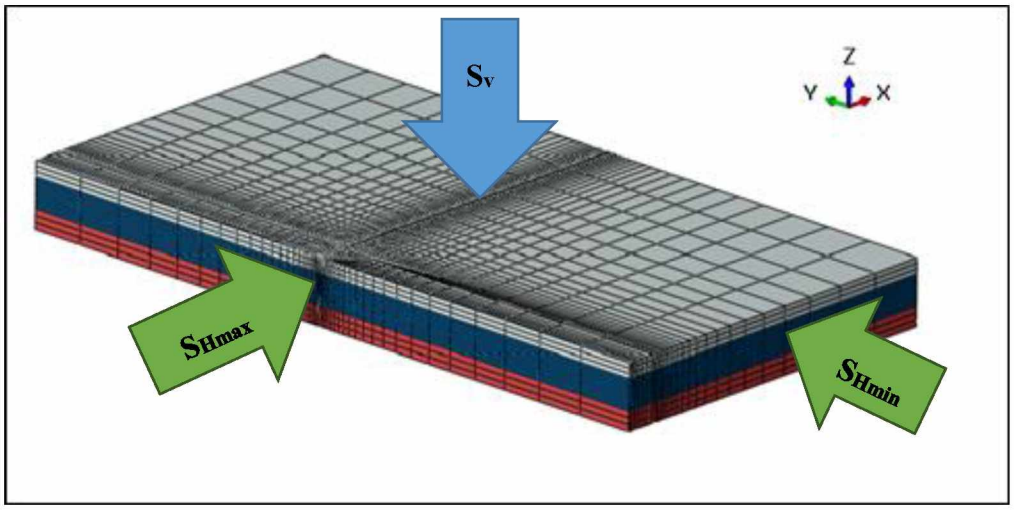

Figure 3-3 Meshed three dimensional geomechanical model with the target and surrounding layers. Distances in X, Y and Z directions are 250 m, 500 m, and 43 m, respectively.

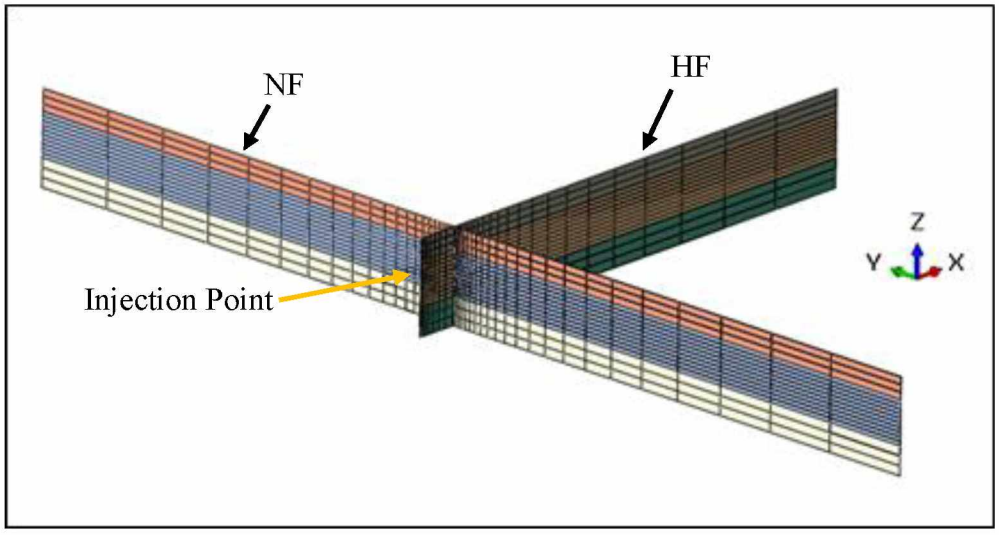

Figure 3-4 HF and NF planes constructed using meshed cohesive element planes.

Two time steps were used in the analysis: a geostatic step required to initialize the model with all initial stress/initial loading conditions and a pumping step representing the actual fracturing process, where fracturing fluid was pumped for a certain period of time and the resulting fracture geometry was observed. The presence or effect of proppants in the fracturing fluid was not considered. The injection rate was applied at the midpoint of target formation at a single node and can be seen as a yellow arrow in **Figure 3-4.** The black arrows in **Figure 3-4** show the HF and NF defining planes, with NF being perpendicular to the defined injection direction or maximum horizontal stress.

It should be noted that the face of the model perpendicular to the injection load and containing the injection load is defined as the inner boundary and other three faces bounding the model are defined as the outer boundary. The remaining two faces are the top and bottom surfaces of the geomechanical model. The displacement and rotation in the X and Y directions were fixed on the outer boundary and the inner boundary was modeled to be symmetric along X-axis. The displacement and rotation of the model bottom were fixed in the Z direction. The lithostatic pressure was applied on the model top. Pore pressure was applied at the top and bottom boundaries for equilibrium and initialization. Gravity effects were also considered in the model. During initialization, the void ratio, stress, and pore pressures were varied with depth. The permeability changed as a function of porosity/void ratio. The NF was considered to be at 5 m distance from the injection point for the base case scenario, which will be discussed in detail later. The length of the model in the HF propagation direction was 250 m, the model length perpendicular to HF propagation direction was 500 m, and the total thickness of all the formations considered was 43 m.

3.2 Theory

3.2.1 Modeling the Rock Matrix

The rock matrix was modeled as porous elastic. A linear Drucker-Prager model was used to determine the failure and/or plastic yielding of the material. This model is a pressure-dependent plasticity model used widely for geotechnical problems. The plot of shear stress σ versus hydrostatic pressure σ_m , as shown in **Figure 3-5,** provides the required relationship.

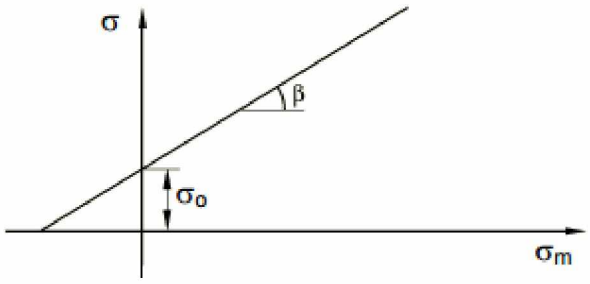

Figure 3-5 Linear Drucker-Prager Model (Abaqus Analysis User Guide, 2016).

Therefore, the governing equation for the Linear Drucker-Prager Model is explained below:

$$\sigma_e = \sigma_o + \sigma_m tan\beta \quad (1)$$

$$\sigma_o = \sqrt{3}\,\sigma_s \quad (2)$$

$$\sigma_m = (1/3)(\sigma_1 + \sigma_2 + \sigma_3) \quad (3)$$

where σ_e is the effective stress; σ_m is a material parameter that is related to shear yield stress; σ_s is shear yield stress; σ_m is hydrostatic stress given in the terms of principal stresses; σ_1, σ_2 and σ_3 are overburden stress, minimum horizontal, stress and maximum horizontal stress, respectively; and β is angle of friction for the material.

3.2.2 Modeling Fluid Flow

The fluid flow in this model can be characterized as 1) fluid flow in the crack and/or in the fracture, 2) fluid leak-off from fracture surfaces, and 3) fluid flow in the porous media. **Figure 3-6** shows the tangential flow in the fractures and the normal flow or leak-off through the fracture surfaces. The fluid flowing in the fracture was considered incompressible Newtonian fluid. Hence, the tangential flow in the fracture was modeled using Reynold's Equation, i.e., **Equations (4) and (5)**. By default in FEA software, there is no initial tangential flow of pore fluid in the cracked elements; hence, an initial gap was defined for initial fluid entry into the cohesive elements/plane that defines the hydraulic fracture.

$$q = -k_t \Delta p \quad (4)$$

$$k_t = \frac{d^3}{12\mu}$$

$$k_t = (d^3/12\mu) \quad (5)$$

where k_t is the tangential permeability and is actually resistance to flow in Reynold's Equation, Δp is the pressure gradient along the cracked element surfaces, d is the cracked element opening, and μ is the viscosity of the fluid being injected.

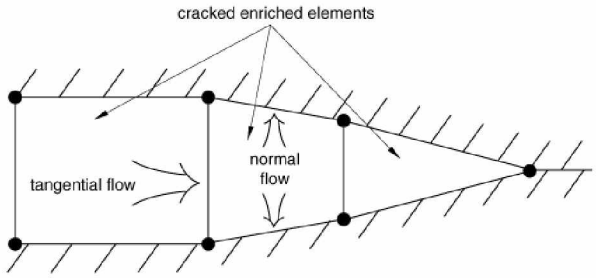

Figure 3-6 Flow in the cracked element (Abaqus Analysis User's Guide, 2016).

The leak-off from the fracture surface to the formation can be modeled considering normal flow through the permeable membrane, as seen in **Figure 3-7 and Equations (6) and (7)**.

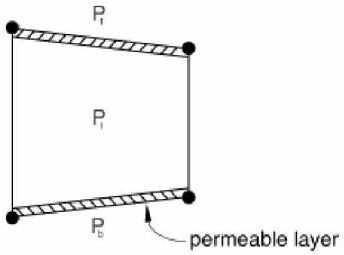

Figure 3-7 Leak-off through permeable layers. (Abaqus Analysis User's Guide, 2016)

$$q_t = c_t(p_i - p_t) \quad (6)$$

$$q_b = c_b(p_i - p_b) \quad (7)$$

where c_t and c_b are the top and bottom fluid leak-off coefficients, respectively, and are kept equal in our study; q_t and q_b are the flow rates into the top and bottom surface of the element being cracked; and are p_i, p_b and p_t the pressures inside the fracture, outside the bottom face of fracture, and outside the top face of fracture, respectively.

The flow in the porous media was modeled by Forchheimer's equation, which reduces to Darcy's law. The wetting fluid saturation was set to 1. The cohesive element used has the ability to ensure fluid continuity at intersecting cohesive planes.

3.2.3 Modeling Deformation and Damage

The damage modeling consisted mainly of two processes: 1) damage initiation and 2) damage evolution. The possible damage propagation path was preset using cohesive elements. The rock matrix was modeled to be porous and elastic. In this study, the damage was modeled using the Bilinear Traction Separation Law, as shown in **Figure 3-8**. According to this law, the cohesive elements are presumed to be intact and stationary, without any movement. When the damage commences, the cohesive elements undergo deformation under the tensile load applied in the form of the injection flow rate. The cohesive traction increases linearly with the crack opening or displacement. The slope of this linear relationship is determined by the stiffness of the elements. The slope is steep when the stiffness is high and gentle when the stiffness is low. The stiffness is a proxy for the Young's modulus of the surrounding formation. When a critical value δ_{crit} corresponds to cohesive traction T_{max}, damage initiation ends and damage evolution commences. Beyond this point, the traction keeps on decreasing until a maximum value of separation or crack opening, δ_{max} , is attained at zero traction value, resulting in complete damage of the elements. The area under this graph represents the critical fracture energy.

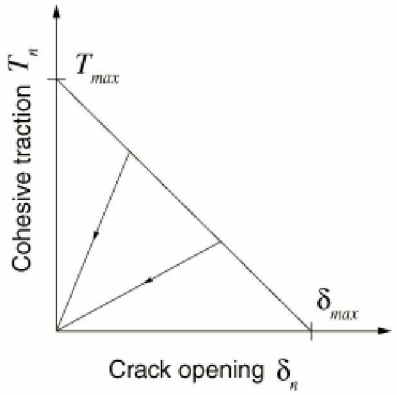

Figure 3-8 Bilinear traction separation law. (Abaqus Analysis User's Guide, 2016)

FEA software has four different criteria used for modeling damage initiation. In this study, the quadratic nominal stress criterion, i.e. **Equation (8)**, was used for modeling damage initiation. According to this criterion, the damage will commence in the cohesive element when the addition of the squares of the ratios of the stresses in the element to ultimate stress or damage initiation stress or nominal stress equals 1.

$$f = (\langle t_n \rangle / t_n^o)^2 + (t_s / t_s^o)^2 + (t_t / t_t^o)^2 \qquad (8)$$

where t_n^o , t_s^o and t_t^o are the damage initiation stresses in the normal, shear, and tangential directions; t_n , t_n and t_t are the stresses in the element in the normal, shear, and tangential directions; and $\langle\rangle$ is a Macaulay bracket indicating that no compressive forces will initiate damage.

The damage evolution law governs the rate at which the stiffness of the cohesive elements is degraded once the damage initiates. The damage factor D has an initial value of 0 when the element is not damaged and has a value of 1 when the element is completely damaged or a fracture is induced. T_n , T_t and T_t are the normal and shear stress components.

$$t_n = (1-D)T_n \, , \, T_n \geq 0 \qquad (9)$$

$$t_s = (1-D)T_s \qquad (10)$$

$$t_t = (1-D)T_t \qquad (11)$$

The mixed mode failure criterion used for damage evolution, are defined using the BK (Benzeggagh and Kenane, 1996) criterion. The equivalent fracture energy release rate G_{equiC} was computed using this law. G_{IC} and G_{IIC} are the critical fracture energies in mode-I and mode-II, respectively. η is the material parameter whose value is 2 for brittle solids and 3 for ductile solids. The critical fracture energy was calculated using Griffith and Irwin's equation (Griffith, 1920).

$$G_{IC} = K_{IC}^2 \frac{(1-\vartheta^2)}{E}$$

$$G_{IC} = K_{IC}^2 \, (1-\nu^2) \, /E \qquad (12)$$

where K_{IC} is the fracture toughness, ν is Poisson's ratio, E is the modulus of elasticity, and G_{IC} is the critical fracture energy. The critical fracture energy in mode-II can be defined in a similar manner:

$$G_{equiC} = G_{IC} + (G_{IIC} - G_{IC}) \, [(G_{II} + G_{III})/(G_I + G_{II} + G_{III})]^{\eta} \qquad (13)$$

where G_{IC} and G_{IIC} are the critical fracture energies in mode-I and mode-11, respectively, and G_I , G_{II} and G_{III} are the fracture energies utilized by the system during damage process.

3.3 Model Validation

A geomechanical model from the literature with radial geometry and a single HF was considered and reconstructed with a rectangular cuboid geometry. It was required to construct the model in the cuboidal form, to simplify the representation of HF and NF, as shown in **Figure 3-3** and **Figure 3-4**. Pumping pressure over the injection time was obtained for the reconstructed model and was matched with the existing radial model, as shown in **Figure 3-9**. A similar type of validation methodology was used by Lu and others, 2015. The profile showed a satisfactory match and the model was validated. The discrepancies in the data observed for first 7 minutes can be attributed to the change in geometry and finer mesh construction for the reconstructed model.

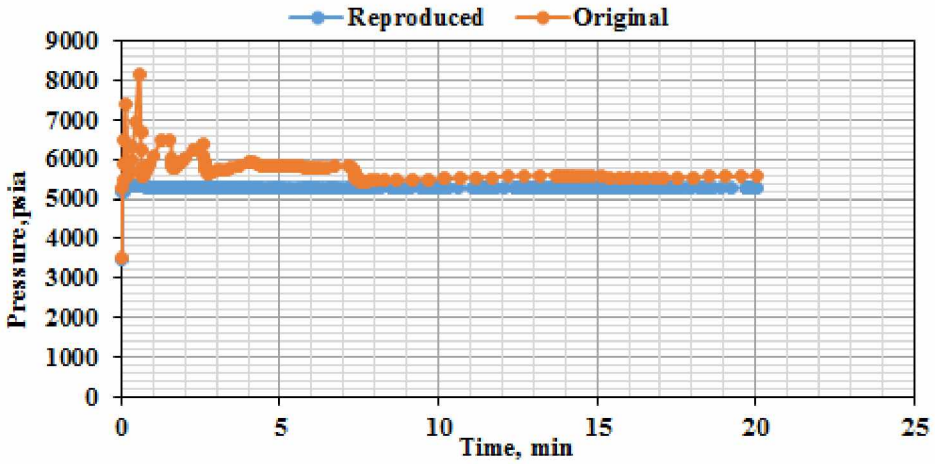

Figure 3-9 Fracture pressure curve for existing radial model and reconstructed model.

3.4 Base Case

The formulation of the Base case was done using guidelines from Gonzalez-Chavez and others (2015). They considered scenarios with "Weaker NF" and "Stronger NF" in a two-dimensional model. The "Weaker NF" and the "Stronger NF" represented the weaker and stronger discontinuity, respectively, with respect to the surroundings. Hence the NF mechanical properties were represented by a factor times the mechanical properties of HF or surrounding medium (Gonzalez-Chavez et al., 2015). A factor of 0.3 was used for weaker NF, with a factor of 1 corresponding to a NF similar to surroundings and a factor of 3 for stronger NF. The main objective of the research was to consider and study the HF-NF interaction, hence, the NF was considered to be weaker than the surrounding formation for the base case. Orthogonal HF-NF intersection was considered in this study. This type of intersection is a good example found in the Barnett shale

(Gonzalez-Chavez et al., 2015) and hence has practical significance. The existing model from the literature with single HF had a low injection rate of ~15 bpm and a low injection fluid viscosity or slick water viscosity of 1 cP. Also, the target formation's Young's Modulus was in the lower range, 1.74E+6 psia. It was decided to increase the base case injection rate to 30 bpm, injection fluid viscosity to 50 cP and target formation Young's Modulus to 3E+6 psia, keeping in mind that the sensitivity analysis range will bracket the base case scenario. Also in accordance with Gonzalez-Chavez and others (2015), in the base case, the NF is situated at a distance of 5 m from the injection point. The input data for the base case and for other sensitivity analysis parameters is summarized in **Table 3-1**.

It should be noted that the HF opening with HF height in this paper is always at the wellbore and the HF opening with HF length refers to a path along the center of the target zone or from injection point straight until the model boundary at 250 m.

Table 3-1 Model input parameters for the base case.

Parameter	Top layer	Target layer	Lower layer
Top Depth, m	2100	2110	2130
Bottom Depth, m	2110	2130	2143
Thickness, m	10	20	13
S_v Total, psia		0.89×Depth(ft)	
S_{Hmin} Total, psia		0.94×S_{Hmax}	
S_{Hmax} Total, psia	0.72×Depth(ft)-399	0.72×Depth(ft)-254	0.72×Depth(ft)-327
Pore Pressure, psia		0.51*Depth(ft)	
Initial Porosity, fraction (average)	0.22	0.27	0.30
Initial Permeability, mD (average)	1.03	5.02	1.13
Poisson's Ratio, fraction	0.15	0.22	0.19
Young's Modulus, psia	6.01E+05	3.00E+06	9.07E+05
Drucker Prager Friction Angle, deg	30	36	28
Drucker Prager Dilation Angle, deg	30	36	28
Formation Density, psia/ft		0.89	
Fracture Toughness, psia-$in^{1/2}$	252	435	312
Damage Initiation Stress, t (psia)	14.5	45	14.5
Injection Rate, bpm		30	
Injection Time, min		20	
Injection Fluid Density, kg/m^3		1000	
Injection Fluid Viscosity, cP		50	
Leak-off Coefficient, bbl/psia.min		1.53E-06	

The HF opening (width) as a function of HF height in the presence of a NF is shown for the base case in **Figure 3-10**. As seen in **Figure 3-10**, the HF opening profile with height was very uneven with a maximum opening at the top, medium at the bottom, and minimum in the target zone. The HF opening as a function of HF length is shown in **Figure 3-11**. The HF opening decreased as a function of length. However, there was a drastic drop in the opening after propagating through the NF at 5 m, as seen in **Figure 3-11.** This agrees with the laboratory findings of Saurez-Rivera and others (2013). In their work, they mentioned that the propagating crack is always restricted by a weak discontinuity initially. This might be the reason for the initially higher HF opening as a function of HF length. Once the HF propagates past the discontinuity, there is a sharp reduction in its opening. The NF did not open in the base case scenario; however, the natural fracture elements were damaged.

Figure 3-12 shows the pressure inside the HF as a function of length. The average opening pressure was observed to be ~5280 psia, with average values of ~6190 psia, ~5334 psia, and ~5014 psia for the vertical principal stress, maximum horizontal principal stress, and minimum horizontal principal stress, respectively. A small spike was observed closer to the boundary of the model and hence was required to be studied, analyzed, and investigated. This was initially thought to be a boundary effect, but for clarification, a bigger model was constructed by increasing the dimension in the direction of HF propagation from 250 m to 500 m. The results for the bigger and smaller model matched, hence, the spike was confidently considered a numerical error or simulation noise and not a boundary effect. The comparisons are shown in **Figure 3-13** through **Figure 3-15.**

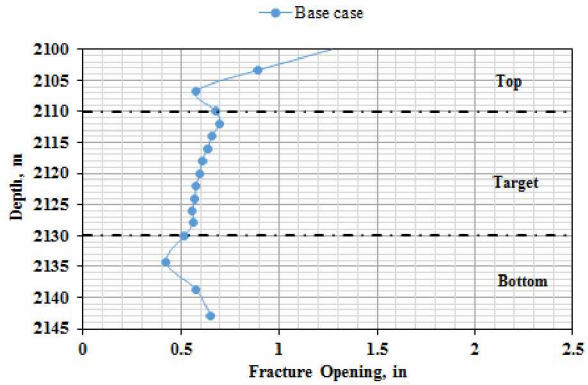

Figure 3-10 HF opening with HF height for base case.

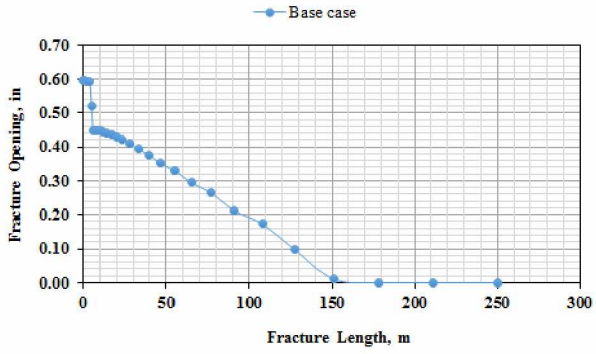

Figure 3-11 HF opening with HF length for base case.

The NF in both the cases did not open; however, NF was activated, as can be seen from the intensity plots for Stiffness Degradation (SDEG) values for cohesive elements representing the natural fractures in **Figure 3-16**. The elements having SDEG values between 0.9-1.0 are damaged, resulting in induced fracture as per the FEA software manual, Gonzalez -Chavez and others (2015), Shin and Sharma (2014), and Haddad and Sepehrnoori (2014). The top and bottom cohesive plane elements were completely damaged. The target zone cohesive elements, however, did not damage completely until the model boundary. This is because the top and bottom formations are mechanically weaker than the target formation. It is to be noted that the NF mechanical properties are based on the mechanical properties of the respective surrounding layers. The HF and NF openings are shown in **Figure 3-17**. As mentioned previously, the NF was activated, but not opened, while the HF opening can be seen clearly in the fracture opening plot in **Figure 3-17**. It should be noted that for all the intensity plots in three dimensions, the deformation is magnified by 200 times for proper visualization of the deformation. The activated NF half-length in the top and bottom zones was 250 m (extended up to the model boundary), while in the target zone, it was ~150 m and was symmetric on both sides. The HF length as a function of depth and various layers is shown in **Figure 3-17**.

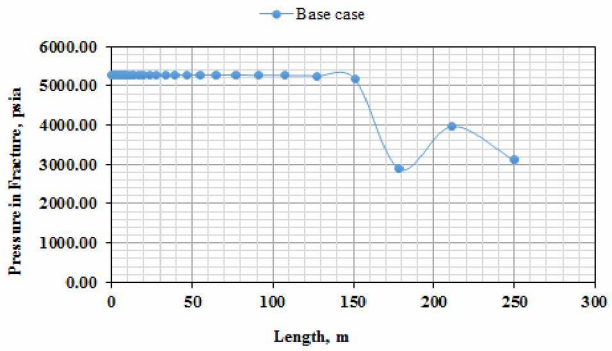

Figure 3-12 HF pressure for base case.

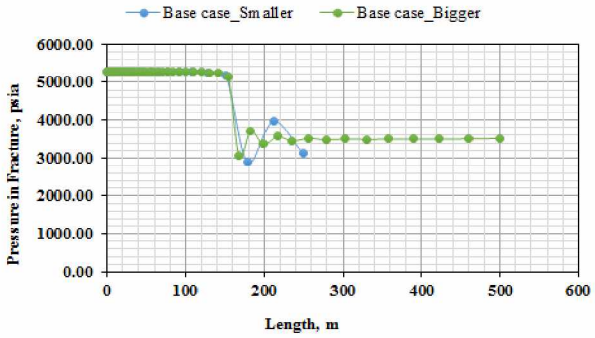

Figure 3-13 HF pressure for dimensionally smaller and bigger base case model.

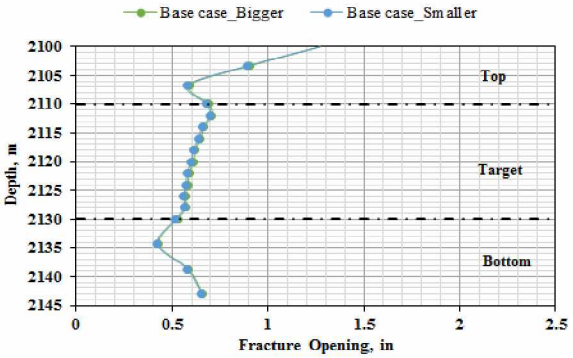

Figure 3-14 HF opening with HF height for dimensionally smaller and bigger base case model.

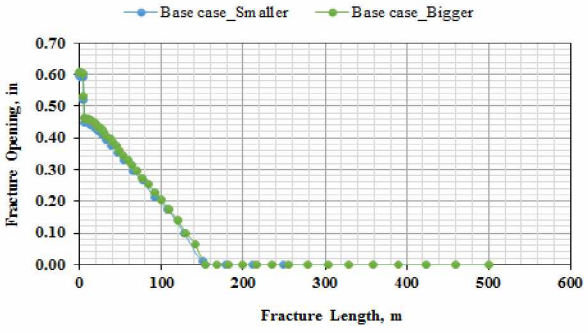

Figure 3-15 HF opening with HF height for dimensionally smaller and bigger base case model.

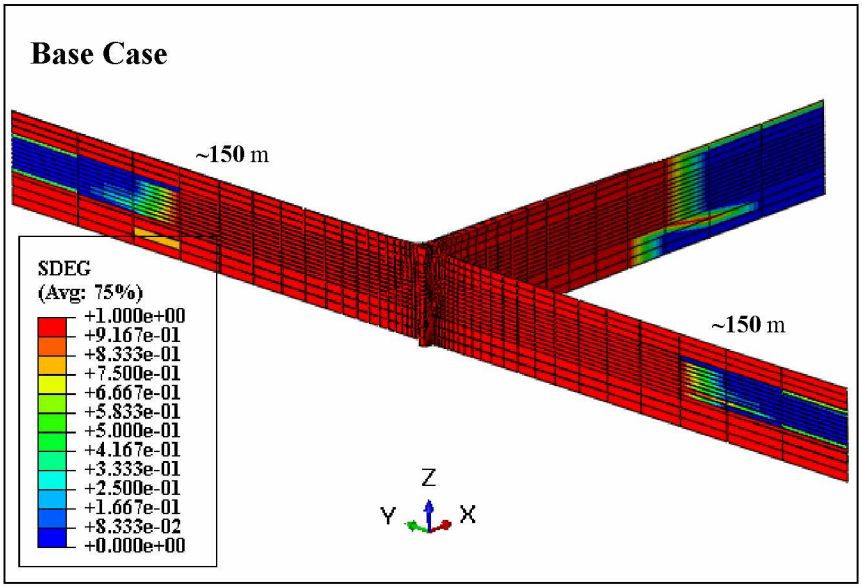

Figure 3-16 Stiffness degradation plot for intersecting HF and NF planes towards the end of pumping time for the base case.

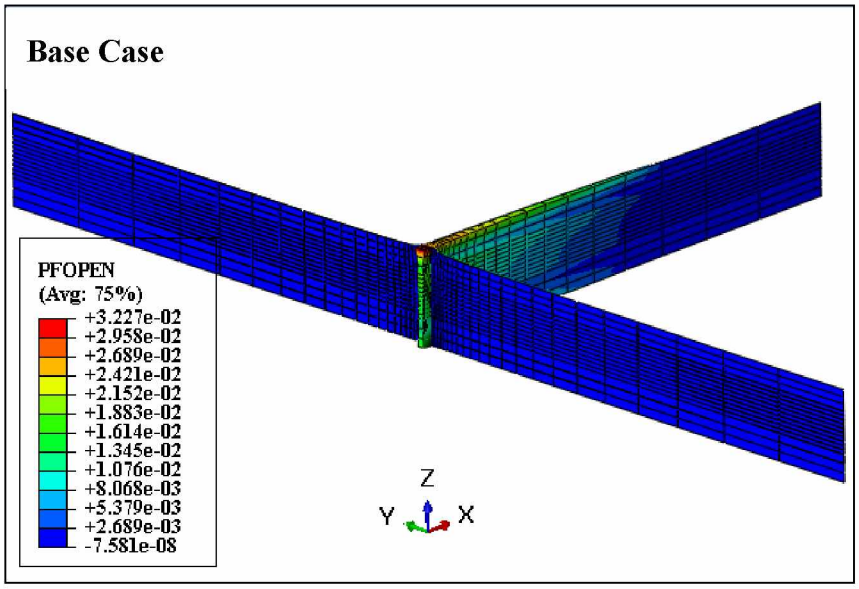

Figure 3-17 Fracture opening for HF and NF planes towards the end of pumping time for the base case.

3.5 Sensitivity Analysis

The hydraulic job design parameters and properties of the surrounding rock affect the behavior of single or multiple propagating hydraulic fractures. Some of the two-dimensional FEA modeling done by Lu and others (2015) and Gonzalez-Chavez and others (2015) also shed some light on some parameters that affect the interaction and geometry of intersecting HF and NF. Apart from the simulation-based studies, laboratory analyses like the one done by Saurez-Rivera and others (2013) also mentioned the influence of some parameters on HF and NF geometry or interaction. We present detailed sensitivity studies of all important parameters of our more realistic and sophisticated three dimensional geomechanical model built using FEA in order to observe their effect on resulting HF-NF geometry and interaction.

The sensitivity analysis in this research mainly considers the effect of job design parameters such as injection fluid rate, injection fluid viscosity, and some of the NF properties, along with stress contrasting effects on the resulting HF-NF interaction and geometry. The various cases considered are summarized in **Table 3-2.**

Table 3-2 Different cases considered for sensitivity analysis.

Categorized Parameters	Case #	Parameter	Explanation
1) Stress Contrast	1	S_{Hmin} = 0.5* S_{Hmax}	High Stress Contrast (base case; S_{Hmin} = 0.94* S_{Hmax})
	2	S_{Hmin} = 0.99* S_{Hmax}	No Stress Contrast (base case; S_{Hmin} = 0.94* S_{Hmax})
	3	Reversed S_{Hmin} and S_{Hmax}	High Stress Contrast and Stresses Reversed
2) Job Design	4	Injection rate = 15 bpm	Half of the base case i.e. 30 bpm
	5	Injection rate = 60 bpm	Twice of the base case i.e. 30 bpm
	6	Injection fluid viscosity = 10 cP	Lower than base case i.e. 50 cP
	7	Injection fluid viscosity = 1 cP	Slick water
	8	Injection fluid viscosity = 100 cP	Higher than base case i.e. 50 cP
3) NF Properties	9	NF same as surroundings	NF strength same as surrounding rock (base case weaker NF, NF strength 0.3 times of surrounding rock)
	10	Stronger NF	NF strength 3 times of surrounding rock (base case weaker NF, NF strength 0.3 times of surrounding rock)
	11	NF distance = 50 m	Higher than base case i.e. 50 m midway as the HF propagated up to 150 m for base case
	12	NF distance = 100 m	Higher than base case i.e. 100 m midway as the HF propagated up to 150 m for base case
	13	NF at 50 m from the injection point, NF=0.6*HF, HF-NF angle=90°	Stronger NF, farther NF than base case. HF-NF angle same as base case
	14	NF at 50 m from the injection point, NF=0.6*HF, HF-NF angle=80°	Stronger NF, farther NF than base case. HF-NF angle lower than base case
	15	NF leak-off = 1.53E-2 bbl/kpsi.min	Higher than base case i.e. 1.53E-3 bbl/kpsia.min
	16	NF leak-off = 1.53E-4 bbl/kpsi.min	Lower than base case i.e. 1.53E-3 bbl/kpsia.min

Table 3-2 continued.

Categorized Parameters	Case #	Parameter	Explanation
4) Formation Properties	17	HF leak-off = 1.53E-2 bbl/kpsi.min	Higher than base case i.e. 1.53E-3 bbl/kpsia.min
	18	HF leak-off = 1.53E-4 bbl/kpsi.min	Lower than base case i.e. 1.53E-3 bbl/kpsia.min
	19	Target thickness = 15 m	Lower than base case i.e. 20 m
	20	Target thickness = 25 m	Higher than base case i.e.20 m
	21	Target E = 1.74E+6 psi	Lower than base case i.e. 3E+6 psia
	22	Target E = 4E+6 psi	Higher than base case i.e. 3E+6 psia
	23	Target ν = 0.16	Lower than base case i.e. 0.22
	24	Target ν = 0.35	Higher than base case i.e. 0.22

3.5.1 Effect of In-Plane Stress Contrast

Saurez-Rivera and others (2013) discussed the effect of in-plane stress contrast, i.e., maximum and minimum horizontal stress contrast, on the HF approaching discontinuities in laboratory samples. They considered experimental square/rectangular blocks having the largest dimension around 3 ft. These blocks had weaker discontinuities perpendicular and parallel to the maximum horizontal stress direction. **Figure 3-18** shows a two-dimensional representation of the laboratory block sample considered by Saurez-Rivera and others (2013). Based on their work, this study simulated similar stress contrast scenarios for a bigger field level geomechanical model and compared the nature of the results to the experiment findings. The following four scenarios were considered and studied: 1) base case: the stress contrast was low, i.e., Minimum Horizontal Stress (S_{Hmin}) was 0.94 times Maximum Horizontal Stress (S_{Hmax}); 2) Case-1: the stress contrast was high, i.e., S_{Hmin} = 0.5* S_{Hmax} ; 3) Case-2: the stresses were almost equal, i.e., S_{Hmin} = 0.99* S_{Hmax} ; and 4) Case-3 with reversed S_{Hmin} and S_{Hmax}: the stress contrast was high, as seen in Case-1, and the principal horizontal stresses were reversed.

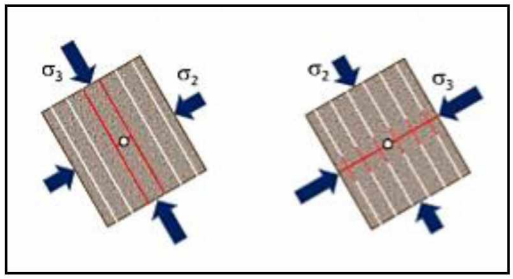

Figure 3-18 Stress contrast scenarios in lab experiments (Saurez-Rivera et al. 2013).

It was observed for the base case that the HF propagated until the NF and then activated the NF but did not open it, as previously seen in **Figure 3-16** and **Figure 3-17**. The same phenomenon was observed for Case-1 and- 2, as shown in **Figure 3-19**. For Case-1, where the stress contrast was high, the length of activated NF in the target zone was smaller compared to the base case and Case-2, as shown in **Figure 3-19.** The activated target NF half-length was observed to be ~105 m in Case-1 versus ~150 m in the Base case and Case-2. This implies that the HF was propagating strongly in a preferential direction because of the high stress contrast.

Furthermore, the HF opened and propagated through NF for Case-1, as observed in **Figure 3-20**. These results show the same behavior as the laboratory results obtained by Saurez-Rivera and others (2013), which says that for high stress contrast scenarios, the propagating crack shears the weaker discontinuity and propagates through it.

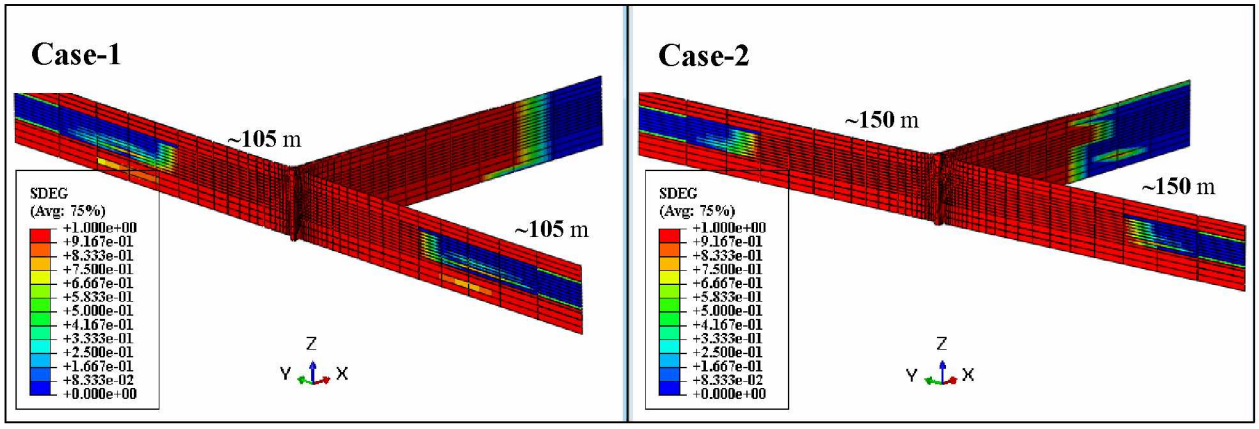

Figure 3-19 Stiffness degradation plot for intersecting HF and NF planes toward the end of pumping time for Case-1 (S_{Hmin}=0.50*S_{Hmax}) and Case-2 (S_{Hmin}=0.99*S_{Hmax}).

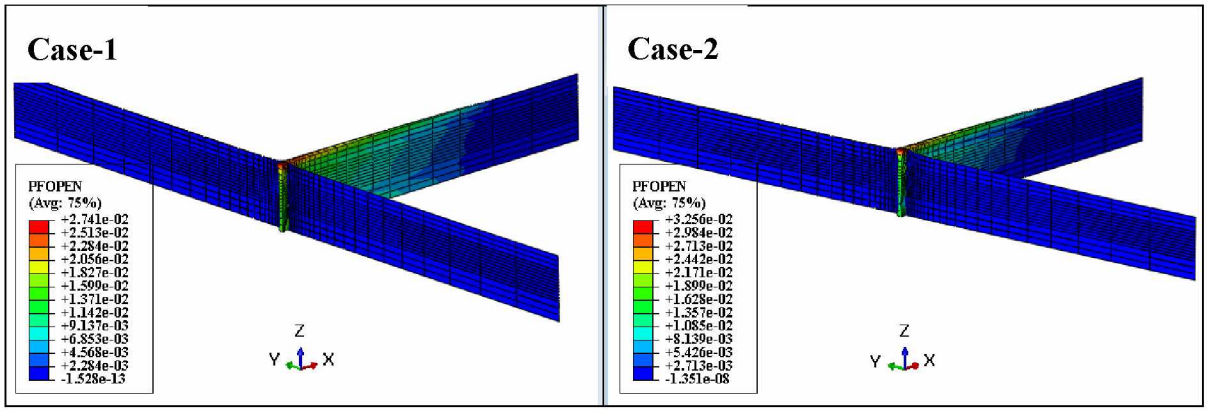

Figure 3-20 Fracture opening for HF and NF planes toward the end of pumping time for Case-1 (S_{Hmin}=0.5*S_{Hmax}) and Case-2 (S_{Hmin}=0.99*S_{Hmax}).

Figure 3-21 shows the HF opening as a function of HF height in the presence of NF for the base case, Case-1, and Case-2. It can be observed that the opening profile is similar for the base case and Case-2, as the contrast is very low and almost same for both cases. For Case-1, where the stress contrast is high, the HF opening profile has higher values than those of the other two cases, except for the target zone where the opening is slightly smaller or almost the same when compared to the other two cases. This can be due to the presence of NF and the NF strength contrast within the layers as the HF tries to propagate through the NF. The NF in the target zone restricts its activation, as observed in the SDEG plots for Case-1, especially when compared to the other two plots for the base case and Case-2. In accordance with our previous explanation, the HF opening should have increased, but it decreased because it found its path of least resistance through the top and the bottom layers. **Figure 3-22** shows the HF opening as a function of length. It can be seen that the trend is the same for both Case-2 and the base case because the stress contrast is very low and similar for both cases.

For Case-1, it should be noted that the opening of HF in the presence of NF was observed to be less than that of the other two cases until the HF reached the NF. Thereafter, it was always higher than the other two cases (**Figure 3-22** and **Figure 3-23**). This agrees completely with the results and the discussion in the above paragraph. The length was also observed to be greater in Case-1 compared to the base case and Case-2. **Figure 3-24** shows the pressure in the HF as a function of length. As expected, it is observed that the opening pressure for the high stress contrast scenario was lower, as opening pressure depends primarily on minimum horizontal principal stress.

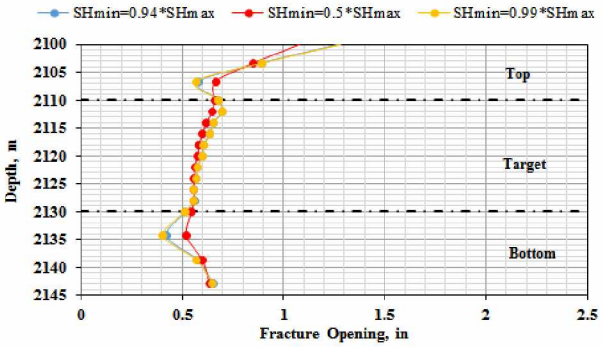

Figure 3-21 Effect of stress contrast on HF opening with HF height.

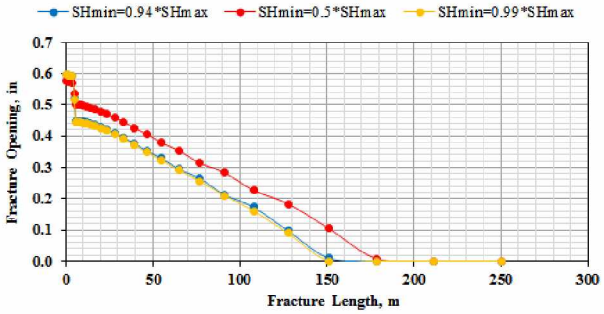

Figure 3-22 Effect of stress contrast on HF opening with HF length.

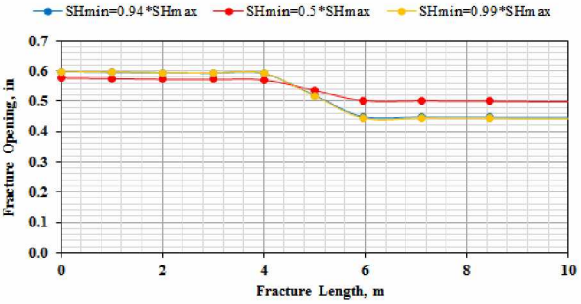

Figure 3-23 Effect of stress contrast on HF opening while crossing NF.

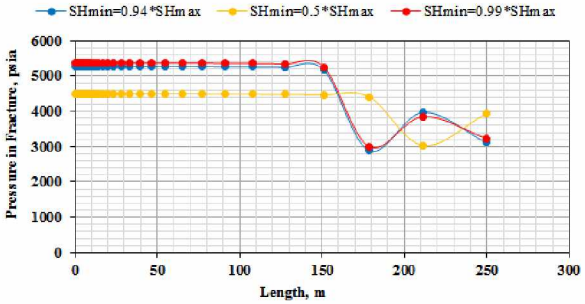

Figure 3-24 Effect of stress contrast on HF pressure.

For the last scenario, Case-3, the stress contrast was high, as seen in Case-1, but the stresses were reversed. This was done to compare the laboratory observations of Saurez-Rivera and others (2013) for a similar scenario. Both HF and NF opened for this scenario and the HF got diverted into NF, as seen in **Figure 3-25**. To reduce the computational time, the simulation time was reduced from 1200 sec to 250 sec. **Figure 3-26** shows the SDEG plot and it can be seen that the NF was activated completely. Our results for this case also agreed with the findings of Saurez-Rivera and others (2013).

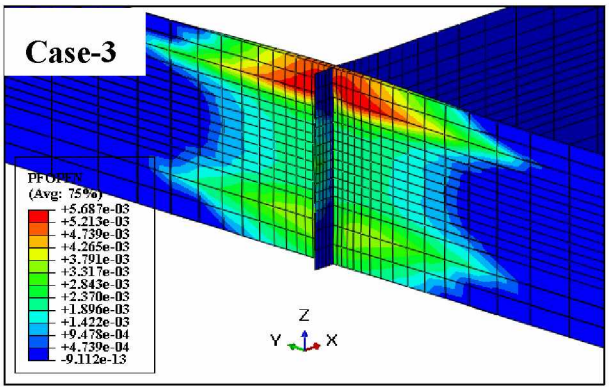

Figure 3-25 Fracture opening for HF and NF planes toward the end of pumping time for Case-3 (Case-1 with the stresses reversed).

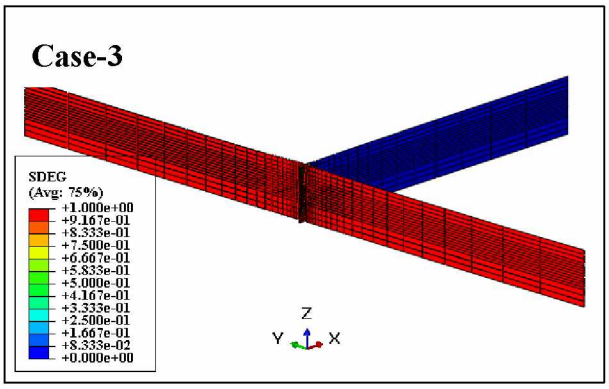

Figure 3-26 Stiffness degradation plot for intersecting HF and NF planes toward the end of pumping time for Case-3 (Case-1 with the stresses reversed).

Figure 3-27 compares the HF opening with height for Case-1 (no stress reversal) and Case-3 (with stress reversal) after 250 sec of injection time. The HF opening in Case-3 is less due to the activated and opened NF. **Figure 3-28** shows the NF opening at the HF-NF intersection with NF height; it follows a similar profile to that observed for HF opening with HF height. **Figure 3-29** shows the HF opening with HF length for both the cases. It is observed that the energy required to open the HF is utilized to open the NF for the reversed stress scenario, resulting in smaller fracture openings. **Figure 3-30** shows the NF opening as a function of NF length. The opened NF length is approximately 35 m. The HF length observed previously was approximately 55 m for Case-1 and 5 m for Case-3. These observations support the assertion that in the reversed stress scenario (Case-3), the HF growth is stunted because of NF growth. This is not the case in the other scenarios.

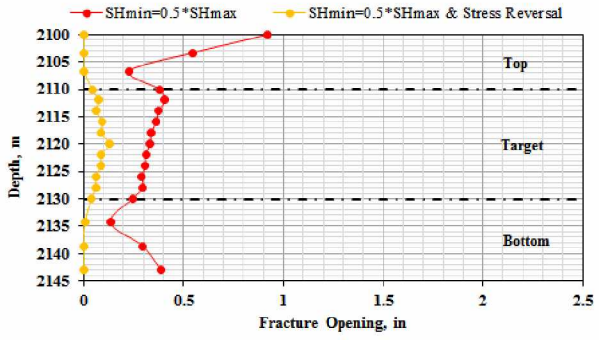

Figure 3-27 Effect of stress reversal on HF opening with height after 250 sec of injection.

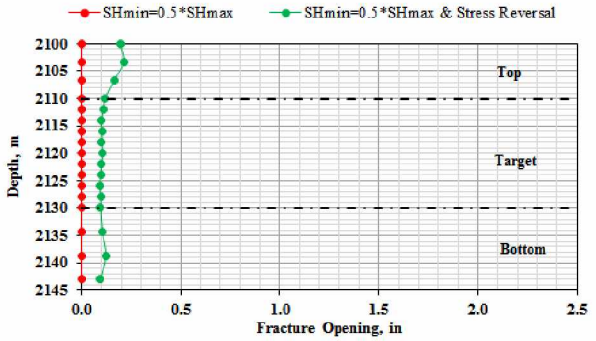

Figure 3-28 Effect of stress reversal on NF opening with length after 250 sec of injection.

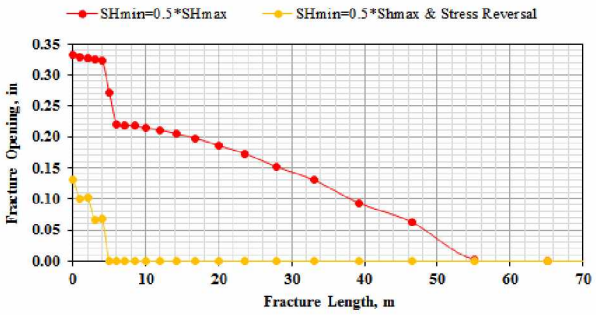

Figure 3-29 Effect of stress reversal on HF opening with height after 250 sec of injection.

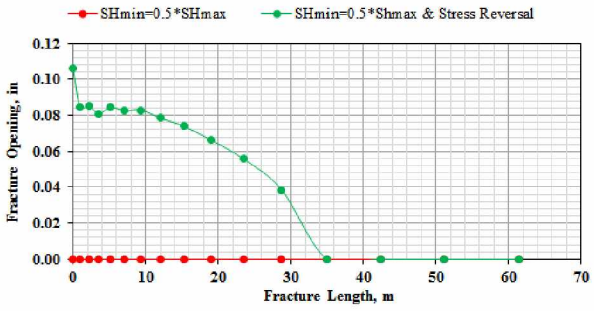

Figure 3-30 Effect of stress reversal on NF opening with length after 250 sec of injection.

3.5.2 Effect of Job Design Parameters

3.5.2.1 Effect of Injection Rate

The HF opening with height in the presence of NF for different injection rates is shown in **Figure 3-31**. As expected, the relationship between the HF opening and injection rate is proportional. **Figure 3-32** shows HF opening with HF length in the presence of NF. Also, the relationship between the HF opening and the injection rate was proportional. However, there was a sudden drop in HF opening after it propagated through NF, as observed in previous cases. **Figure 3-33** gives a closer view of the HF opening while it propagated through the NF at 5 m away from the injection point. The NF was activated for all three cases considered. The NF in the top and the bottom layer was activated throughout to the model boundary for all three cases. The activated NF length reduced in the target zone for the base case, Case-4, and Case-5, as observed in **Figure 3-16** and **Figure 3-34**. Hence, changing injection rate affected the HF geometry but did not affect the NF geometry or activation profile. **Figure 3-35** shows the HF and NF opening in three dimensions, with the activated NF remaining closed for Case-4 and Case-5. The fracture opening path was traced from centre of the target zone into the formation until the model boundary at 250 m. Hence it should be noted that the value of 0 inches opening refers to no opening in the graphs considered in this study.

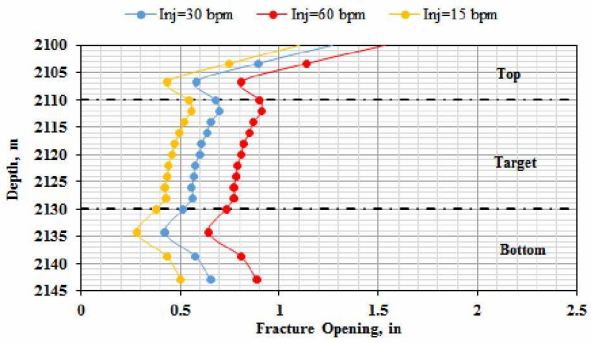

Figure 3-31 Effect of injection rate on HF opening with HF height.

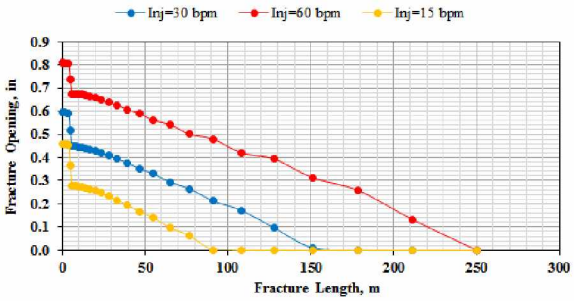

Figure 3-32 Effect of injection rate on HF opening with HF length.

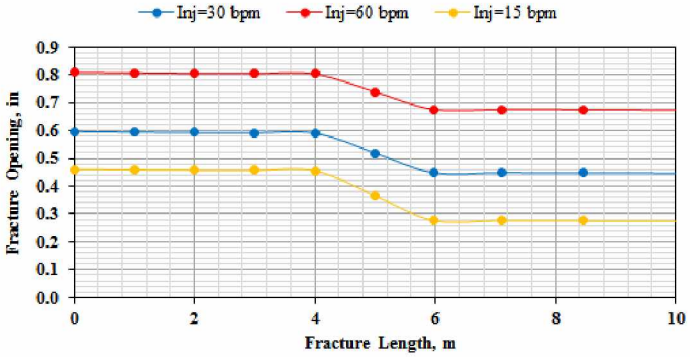

Figure 3-33 Effect of injection rate on HF opening while crossing NF.

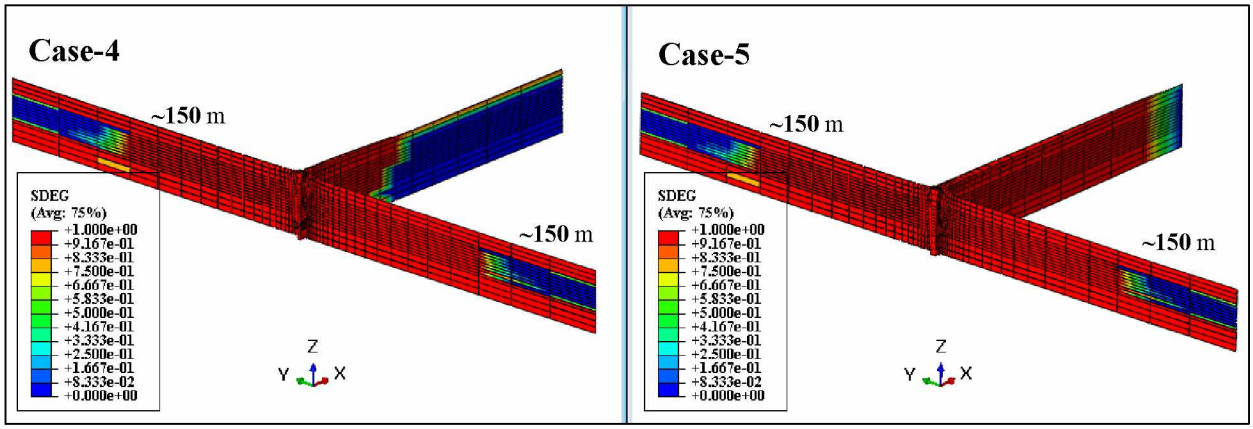

Figure 3-34 Stiffness degradation plot for intersecting HF and NF planes toward the end of pumping time for Case-4 (injection rate= 15 bpm) and Case-5 (injection rate = 60 bpm).

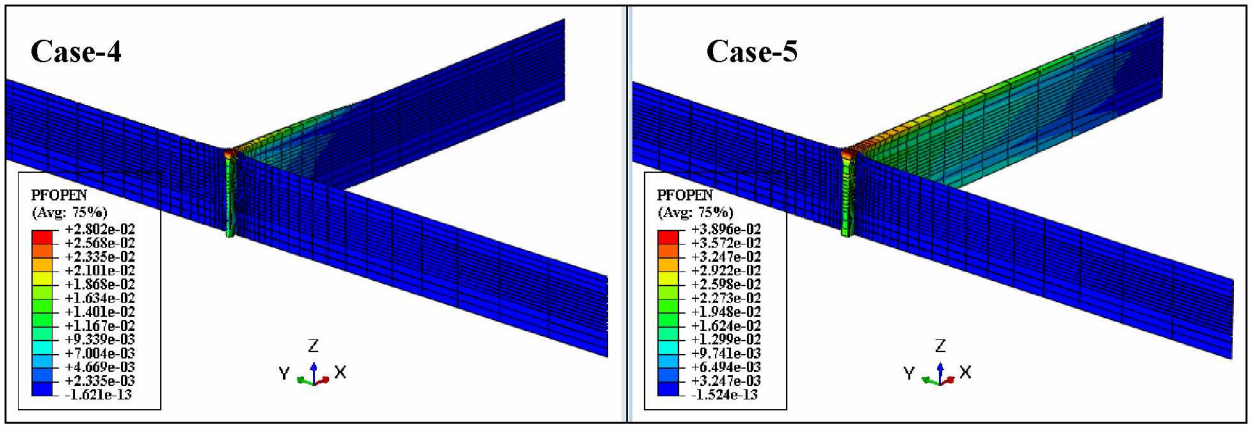

Figure 3-35 Fracture opening for HF and NF planes toward the end of pumping time for Case-4 (injection rate = 15 bpm) and Case-5 (injection rate= 60 bpm).

3.5.2.2 Effect of Injection Fluid Viscosity

Figure 3-36 shows a profile of HF opening as a function of HF height in the presence of NF. The opening decreases with decreasing viscosity. In **Figure 3-37**, the HF opening with HF length in the presence of NF increases with increasing viscosity. However, the fracture length decreases with increasing viscosity. **Figure 3-38** gives a closer look at the HF opening when it propagates through NF at a distance of 5 m from the injection point. A similar sudden drop in the HF opening is seen again after HF propagates through NF. However, the slope of the pressure drops while HF crosses NF, changes, and seems to flatten as the viscosity decreases. It can also be seen from **Figure 3-16** and **Figure 3-39** that the NF activated length in the target zone decreases with decreasing viscosity and is observed to be least in the case of slick water (lowest viscosity). It should be noted that the activation of the NF in the target zone is shorter when the difference in the HF opening before and after propagating through the NF is smaller. Therefore, fracturing fluid viscosity has an inverse relationship with HF length, but a proportional relationship with NF length. This probably happens because the increasing viscosity inhibits the HF propagation but widens the HF, causing longer activated NF length. It was observed that the NF activated length of ~150 m for the base case (50 cP) changed to ~180 m for Case-8 (100 cp) and to ~105 m for slick water (1 cP). **Figure 3-40** shows the HF opening for Case-6 (10 cP) and Case-8 (100 cP). **Figure 3-41** shows the SDEG plot for Case-7 (slick water) and **Figure 3-42** shows the HF opening in the presence of NF in three dimensions. The NF is activated but did not open.

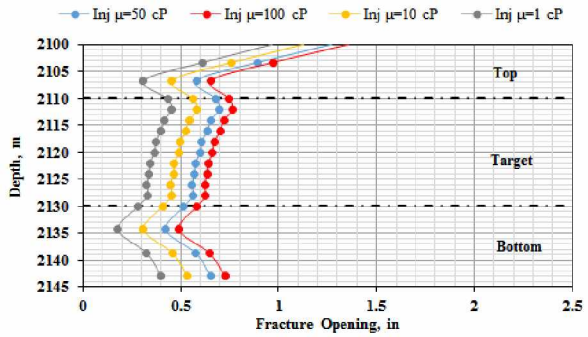

Figure 3-36 Effect of injection fluid viscosity on HF opening with HF height.

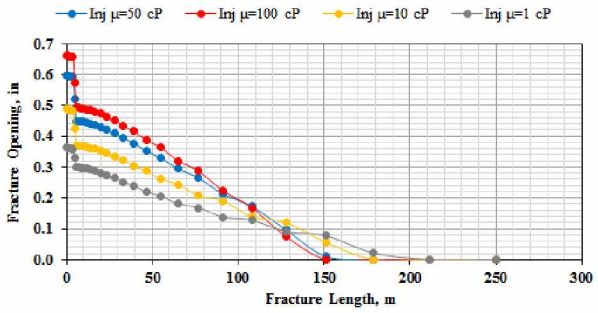

Figure 3-37 Effect of injection fluid viscosity on HF opening with HF length.

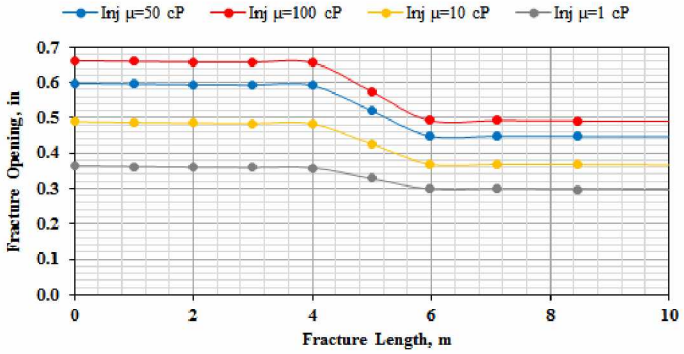

Figure 3-38 Effect of injection fluid viscosity on HF opening while crossing NF.

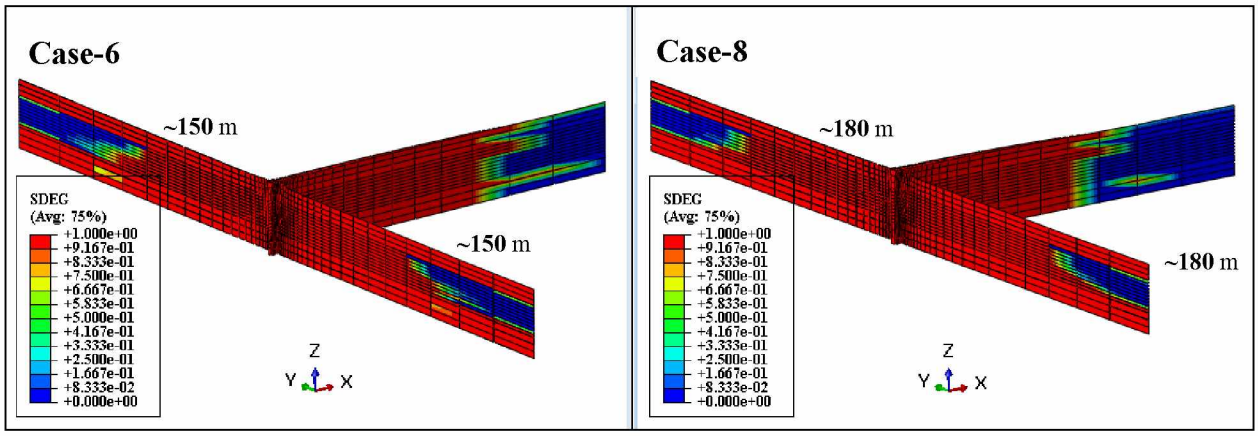

Figure 3-39 Stiffness degradation plot for intersecting HF and NF planes toward the end of pumping time for Case-6 (μ= 10 cP) and Case-8 (μ= 100 cP).

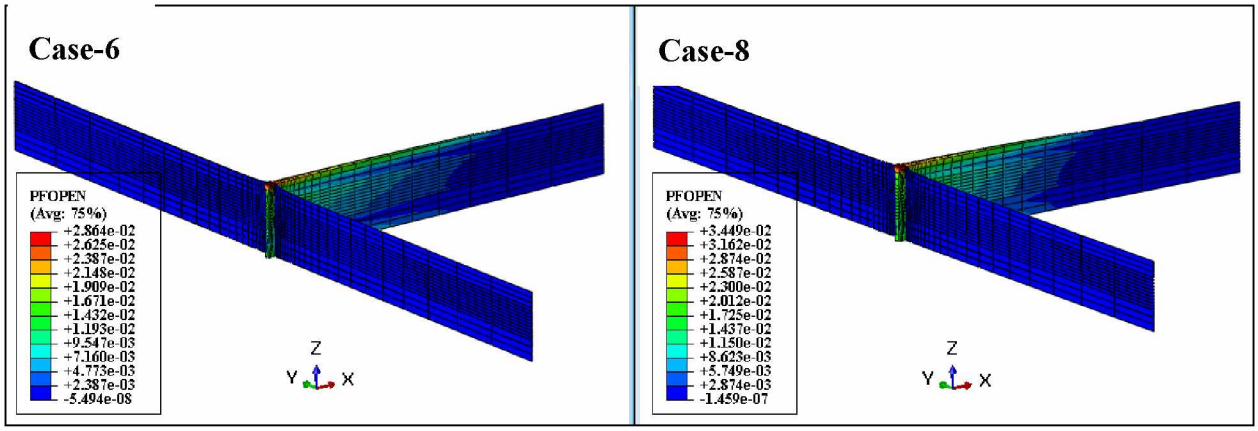

Figure 3-40 Fracture opening for HF and NF planes toward the end of pumping time for Case-6 (μ= 10 cP) and Case-8 (μ= 100 cP).

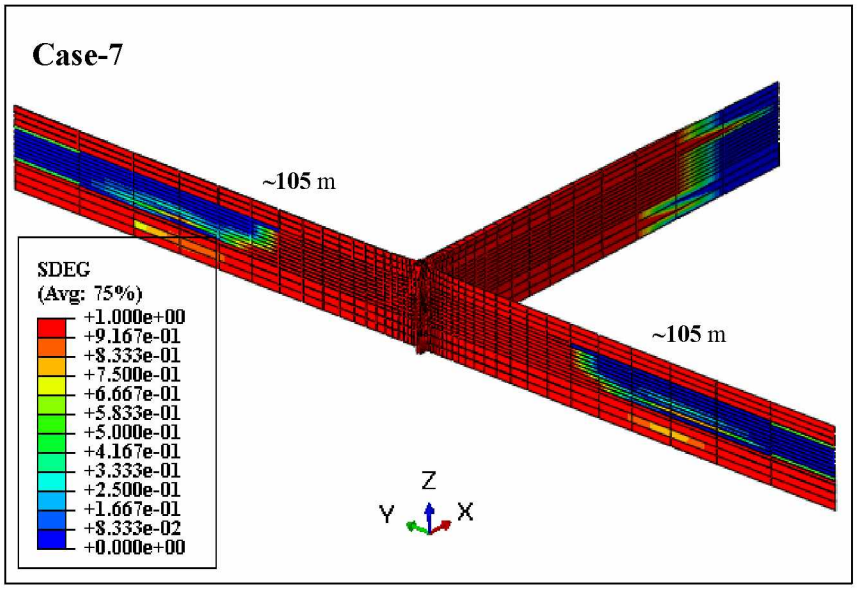

Figure 3-41 Stiffness degradation plot for intersecting HF and NF planes toward the end of pumping time for Case-7 (μ= 1 cP).

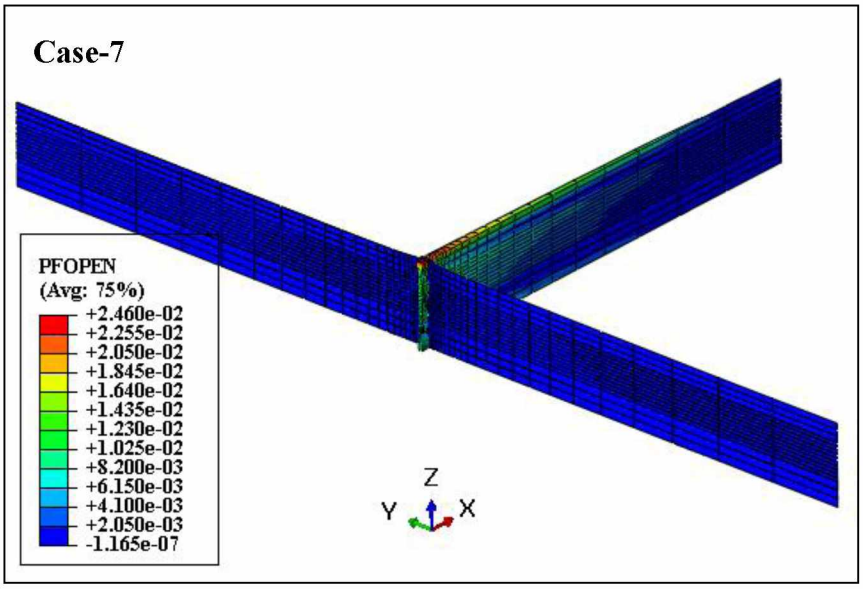

Figure 3-42 Fracture opening for HF and NF planes toward the end of pumping time for Case-7 (μ= 1 cP).

3.5.3 Effect of NF Properties

3.5.3.1 Effect of NF Strength

In Saurez-Rivera and others (2013), laboratory experiments showed that the discontinuities or weakness planes encountered by propagating cracks temporarily restricted the propagating induced crack. **Figure 3-43** shows that the opening of HF encountering weaker NF is high compared to those with stronger discontinuities. This is probably because of the restriction created by the weaker discontinuity. The other two cases in which the NF is stronger or has properties similar to the surroundings are perhaps not seen as planes of weakness. Hence, the increase in HF opening is not seen in these cases. This agrees with the results shown in **Figure 3-44** and **Figure 3-45** (HF opening as a function of HF length in the presence of NF). It can be seen in **Figure 3-44** and **Figure 3-45** that the HF opening, in the presence of a weaker NF, is large until it encounters NF at 5 m. Thereafter, there is a rapid drop in HF opening and then the opening follows the normal HF propagation path. On the other hand, for the stronger NF and for the NF having properties similar to the surroundings, the HF opening with HF length does not show a sudden drop. The discontinuity it encounters is not a weak plane but a stronger one or one similar to the surroundings. The SDEG plots in **Figure 3-16 and Figure 3-46** show clearly the NF was activated in the case of weaker NF and for NF similar to surroundings. The NF is not activated for Case-10. The NF

does not activate or is minimally activated for Case-9 and -10. Furthermore, **Figure 3-17** and **Figure 3-47** show the three dimensional view of opened HF for weaker NF and for stronger NF cases, respectively.

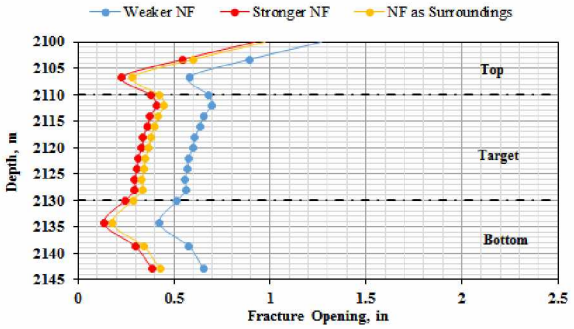

Figure 3-43 Effect of NF strength on HF opening with HF height.

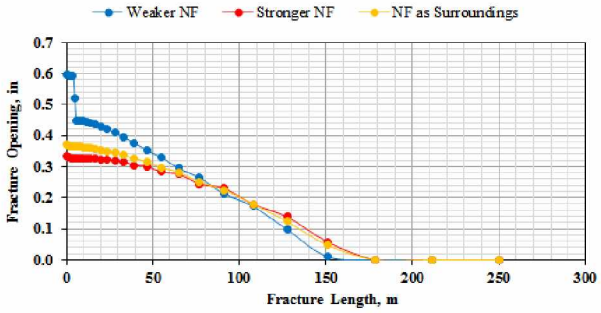

Figure 3-44 Effect of NF strength on HF opening with HF length.

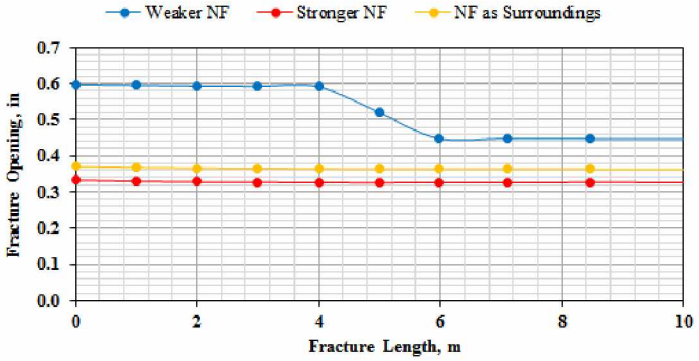

Figure 3-45 Effect of NF strength on HF opening while crossing NF.

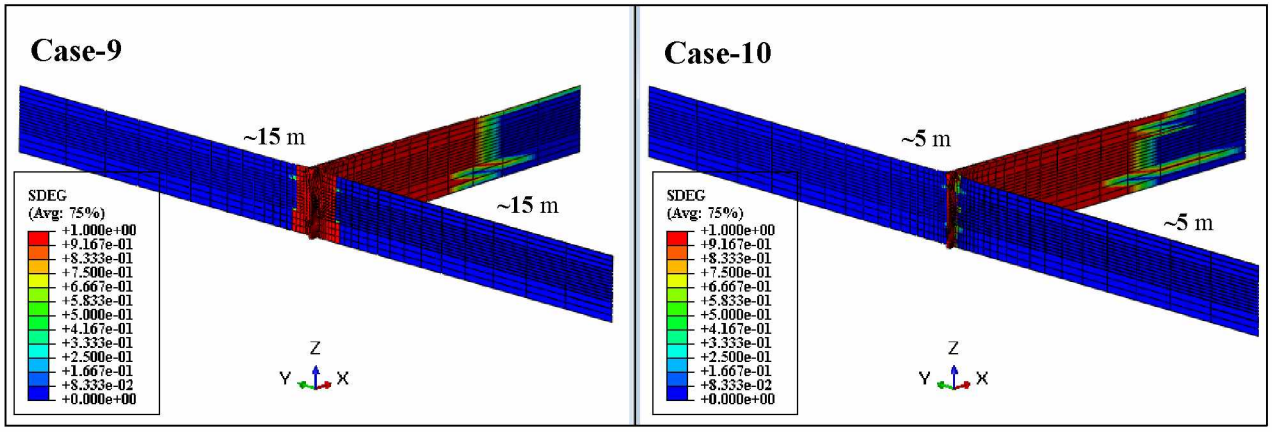

Figure 3-46 Stiffness degradation plot for intersecting HF and NF planes towards the end of pumping time for Case-9 (NF same as surroundings) and Case-10 (NF stronger than surroundings).

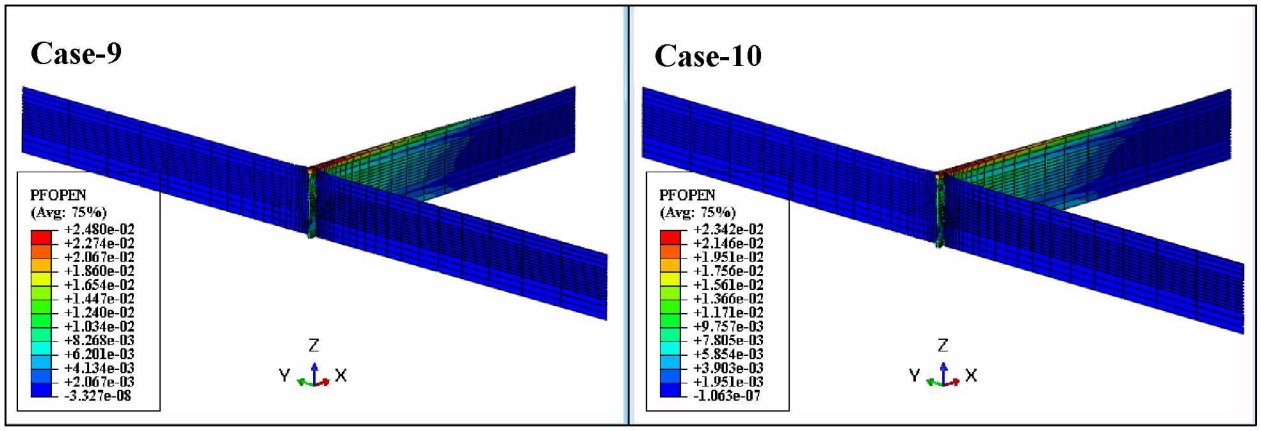

Figure 3-47 Fracture opening for HF and NF planes toward the end of pumping time for Case-9 (NF same as surroundings) and Case-10 (NF stronger than surroundings).

3.5.3.2 Effect of NF Positioning

The NF orthogonally intersecting the HF affected the HF propagation and NF activated length. **Figure 3-48** shows the HF opening with height at the wellbore. It was observed that the HF opening reduced as NF moved away from the injection point. **Figure 3-49** shows that the HF propagated through NF and its length was maximum for the base case. On the other hand, the HF was arrested at 50 m and 100 m for the other two cases considered. The laboratory experiments conducted by Saurez-Rivera and others (2013) showed that the discontinuities or weakness planes encountered by propagating cracks temporarily restricted the propagating induced crack. However, it was observed here that the NF positioning can create enough resistance for the propagating HF to terminate it at NF. The HF opening for NF distance = 50 m and NF distance = 100 m was almost uniform throughout the HF length and was ~1.3 in. and ~0.4 in., respectively. Also, the HF opening with HF length showed a gradual increase in the HF opening for NF distance = 50 m and NF distance = 100 m. This was due to the weaker NF trying to restrict HF propagation. The energy or the pressure at the fracture tip was not enough to propagate the HF through the NF for the two cases. However, this energy was enough to activate the NF completely until the model boundary. **Figure 3-50** shows the completely activated NF for the two cases. It is observed from **Figure 3-51** that the HF was arrested by the NF for the Case-11 and Case-12 and the opening for Case-11 was higher than the opening for Case-12.

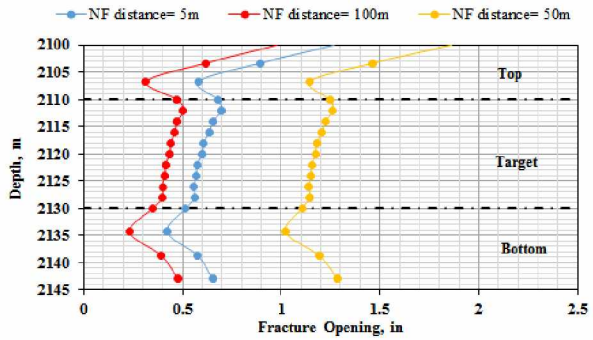

Figure 3-48 Effect of NF positioning on HF opening with HF height.

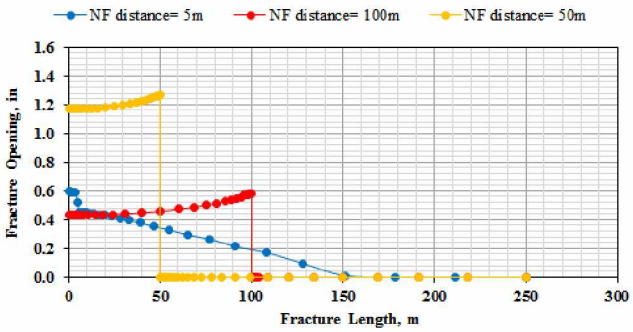

Figure 3-49 Effect of NF positioning on HF opening with HF length.

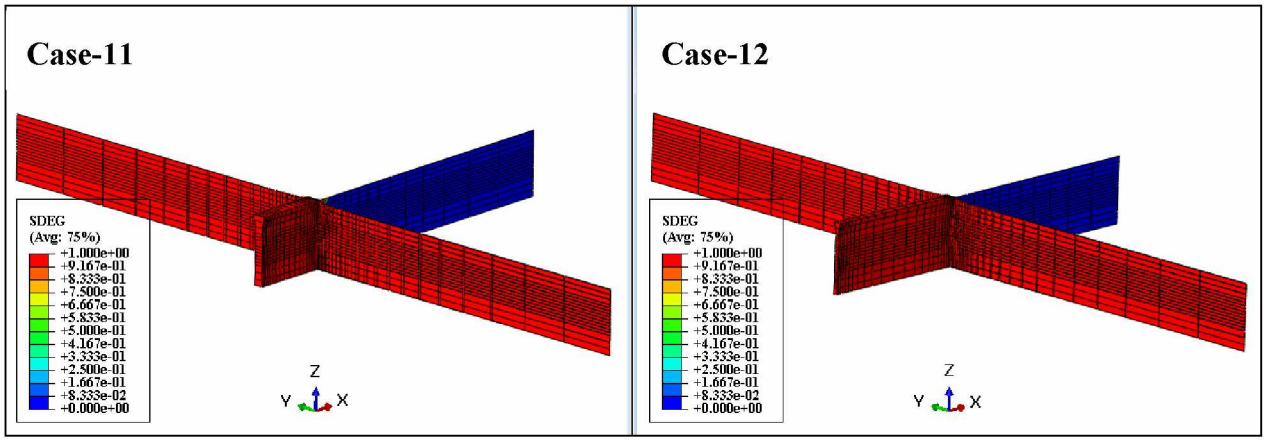

Figure 3-50 Stiffness degradation plot for intersecting HF and NF planes toward the end of pumping time for Case-11 (NF at 50 m from injection point) and Case-12 (NF at 50 m from injection point).

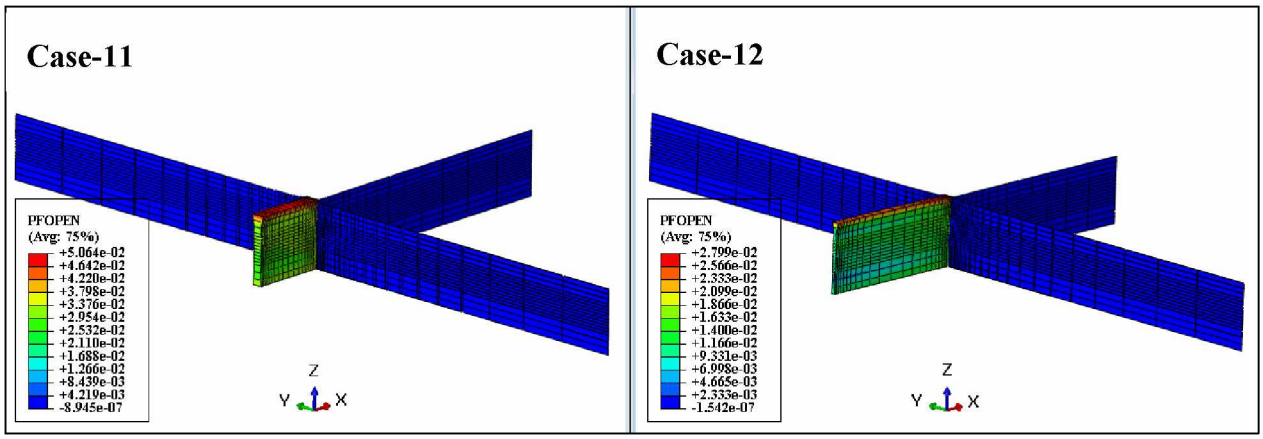

Figure 3-51 Fracture opening for HF and NF planes toward the end of pumping time for Case-11 (NF same as surroundings) and Case-12 (NF at 50 m from injection point).

3.5.3.3 Effect of NF Orientation

Several trials were conducted to consider the effect of NF orientation. To simplify the model construction the HF – NF intersection point was shifted to 50 m away from the injection point. Minimum HF – NF intersection angle of 80 degrees was considered. However, the software was unable to initialize the model. Initialization of model ensures that all the in-situ stresses and initial loads like the gravitational weight of rock formation are applied and the model is stable which then represents the actual formation conditions. Further several attempts were made to run the model with changing HF – NF intersection distance from injection point and HF – NF intersection angle. However, there was no success. The technical literature was again referred. The work done by Haddad and others (2016) was the only one of a similar kind using FEA software. It was observed that they simplified the model by considering 1) constant rock mechanical properties for the all the three layers considered with varying principal stresses or 2) varying rock mechanical properties for all three layers considered with constant principal horizontal stresses. Note: The model considered in this study is more realistic and has varying rock mechanical properties with depth and varying principal horizontal stresses for different layers with depth. Hence, the first approach of Haddad and others (2016) was considered for this sensitivity analysis. The rock mechanical properties were kept constant for all the three layers and incorporated the properties of the target layer. The principal horizontal stresses were varied with depth. However using this approach also the model could not initialize. The decreasing HF – NF intersection angle results in initial non-zero shear stresses along the NF plane (Haddad et al., 2016). In this study, the strength of the NF was considered to be 30% of the surrounding rock strength. The properties defining the strength are the fracture toughness, damage initiation stress and stiffness of the material. Hence, attempts were made to increase the strength of the NF. It was finally observed that for a NF having strength equal to 60% strength of the surrounding formation was able to withstand the shearing forces that helped initialize the model. The attempts made to run lower HF – NF intersection angle models are as shown in **Table 3-3.**

Table 3-3 NF orientation trials.

Multi layer	NF strength	Rock properties	NF properties	HF properties	In-situ stress	Porosity	Permeability	Model runs
√	0.3*HF	varies	varies	varies	varies	varies	varies	x
√	0.3*HF	constant	constant	constant	varies	constant	constant	x
√	0.5*HF	constant	constant	constant	varies	constant	constant	x
√	0.7*HF	constant	constant	constant	varies	constant	constant	√
√	0.6*HF	constant	constant	constant	varies	constant	constant	√
√	**0.6*HF**	**constant**	**constant**	**constant**	**varies**	**varies**	**varies**	√
√	0.6*HF	constant	constant	varies	varies	varies	varies	x
√	0.6*HF	varies	varies	varies	varies	varies	varies	x
√	0.6*HF	constant	varies	varies	varies	varies	varies	x
√	0.6*HF	varies	varies	constant	varies	varies	varies	x
√	0.6*HF	varies	constant	constant	varies	varies	varies	x

Further, a lower intersection angle than 80 degrees was tried. However, there was no success. Different geometries considered for the analysis are as shown in **Figure 3-52**. Hence, another model with HF – NF intersection angle of 90 degrees in conjugation to the successfully run models was constructed and studied. The successfully run combinations along with the base case and NF distance = 50 m were plotted for comparative studies.

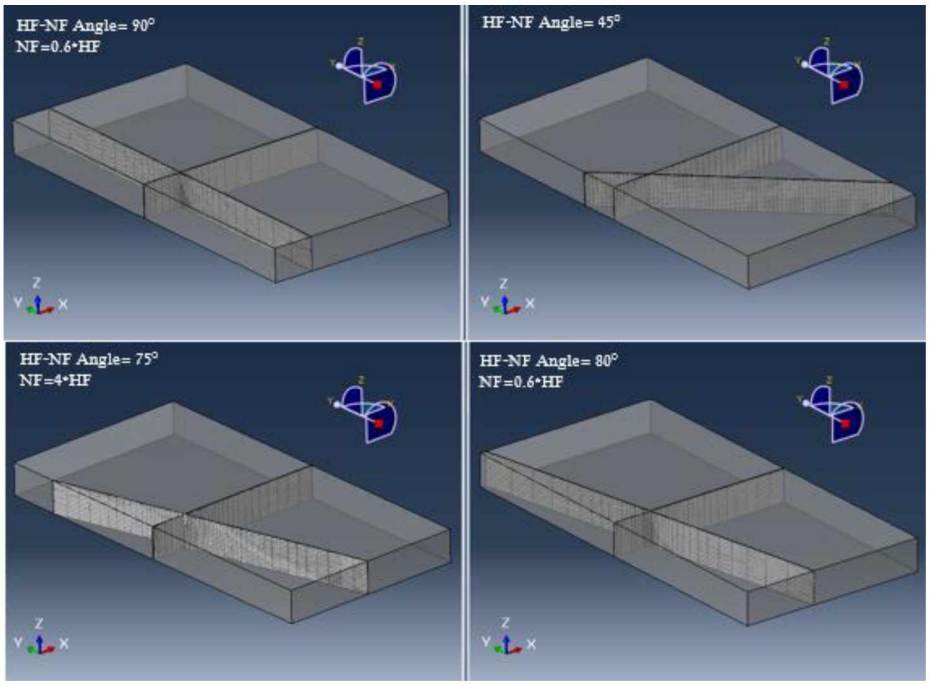

Figure 3-52 Different NF orientation geometries considered.

Figure 3-53 shows the hydraulic fracture opening in the presence of NF. The fracture opening profile with depth was observed to be different for the cases with no contrast in the interlayer rock mechanical properties. The fracture opening at the wellbore was almost same for HF – NF intersection angle of 80 degrees and 90 degrees with same interlayer mechanical properties. However, the openings for these two cases were less than the base case. **Figure 3-54** shows that for orthogonally intersecting HF and NF, the HF propagated through the NF at 50 m for weaker NF (0.6 times surroundings) and same interlayer mechanical properties. However, it should be noted that the NF at 50 m with weaker NF (0.3 times surroundings) and different interlayer mechanical properties arrested the HF. **Figure 3-55** shows that for weaker NF (0.6 times surroundings) and for HF – NF intersection angle of 80 degrees, the opening was less than the one for weaker NF (0.6 times surroundings) and for HF – NF intersection angle of 90 degrees. As seen in **Figure 3-56** the HF – NF intersection angle affected the NF activated length. The NF activated length was observed to be restricted at 175 m for one of the fracture wings and completely activated for the other fracture wing for HF – NF intersection angle of 80 degrees. However, for HF – NF intersection angle of 90 degrees the NF wings got activated until the model boundary. **Figure 3-57** shows the three dimensional fracture opening for the two cases.

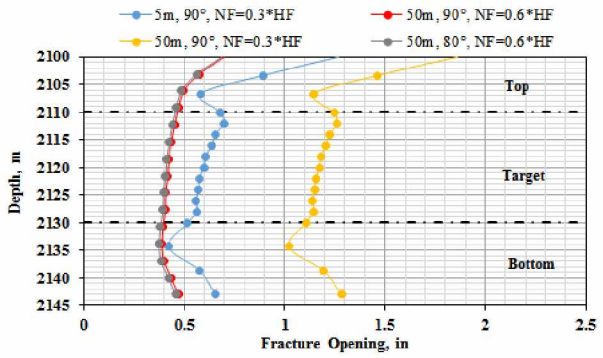

Figure 3-53 - Effect of NF positioning on HF opening with HF height.

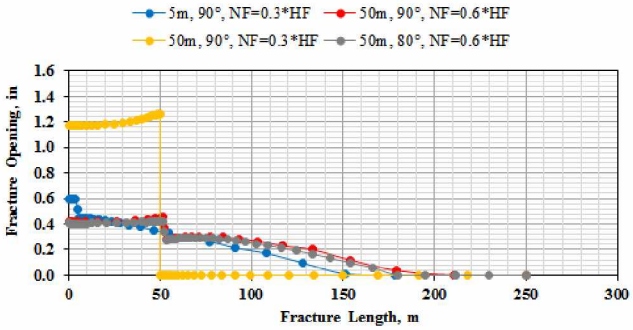

Figure 3-54 - Effect of NF positioning on HF opening with HF length.

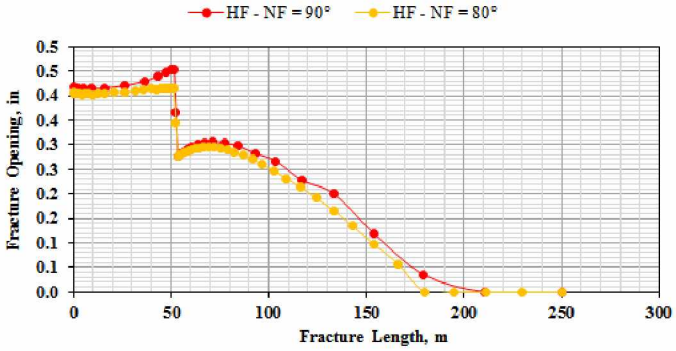

Figure 3-55 - Effect of NF strength on HF opening while crossing NF.

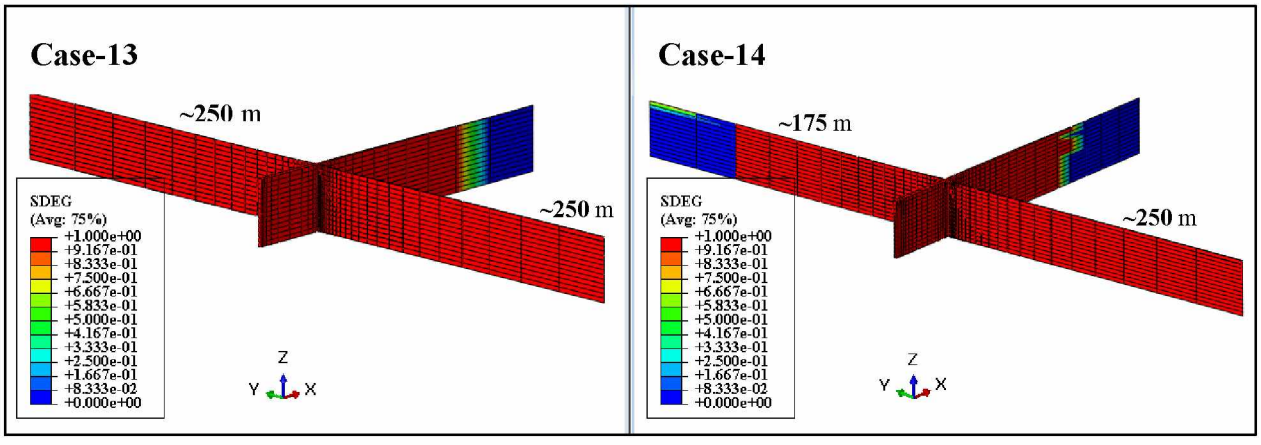

Figure 3-56 - Stiffness degradation plot for intersecting HF and NF planes towards the end of pumping time for Case-13 (NF at 50 m from the injection point, NF=0.6*HF, HF-NF angle=90°) and Case-14 (NF at 50 m from the injection point, NF=0.6*HF, HF-NF angle=80°).

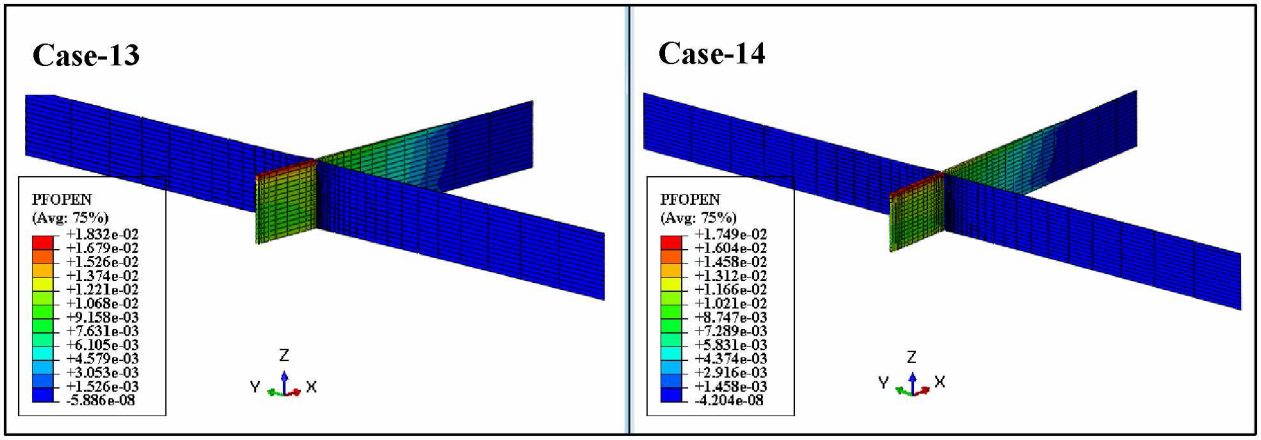

Figure 3-57 - Fracture opening for HF and NF planes towards the end of pumping time for Case-13 (NF at 50 m from the injection point, NF=0.6*HF, HF-NF angle=90°) and Case-14 (NF at 50 m from the injection point, NF=0.6*HF, HF-NF angle=80°).

3.5.3.4 Effect of NF Leak-off Coefficient

This sensitivity parameter does not show a drastic difference in the HF opening pattern, as seen in the case of varying HF leak-off coefficients. This is true because we are altering the NF leak-off coefficient here, while the HF leak-off coefficient remains constant. However, the changing NF leak-off coefficient shows a varying and characteristic HF opening profile and NF activated lengths at the wellbore and HF-NF intersection point. **Figure 3-58** shows that the HF opening decreases with increasing NF leak-off coefficient. However, once the HF crosses the NF, as seen in **Figure 3-59**, the HF opening for the base case and higher NF leak-off coefficient shows wider opening than the one for lower NF leak-off coefficient for some HF length. However, the ultimate opened HF length remains ~150 m for all the three cases. NF takes in more fluid as its leak-off coefficient increases, resulting in a decreasing HF opening for the first 5 m. A momentary increase in the HF opening after the HF-NF intersection point was also observed. This owes to the fact that the fluid rate seems to increase at the intersection point for higher NF leak-off coefficients. This momentary increase can be quantified and observed in **Figure 3-59** and **Figure 3-60**. Also, the NF activated length was found to be inversely proportional to the NF leak-off coefficient (**Figure 3-61**). This is similar to the HF opening relation seen with varying HF leak-off coefficients. **Figure 3-62** shows the 3D presentation of the created fractures.

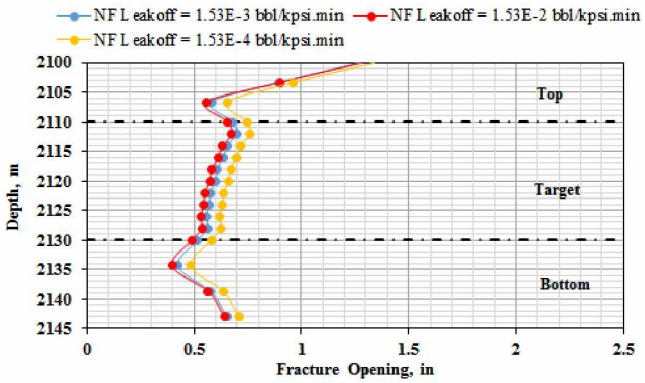

Figure 3-58 Effect of NF leak-off coefficient on HF opening with HF height.

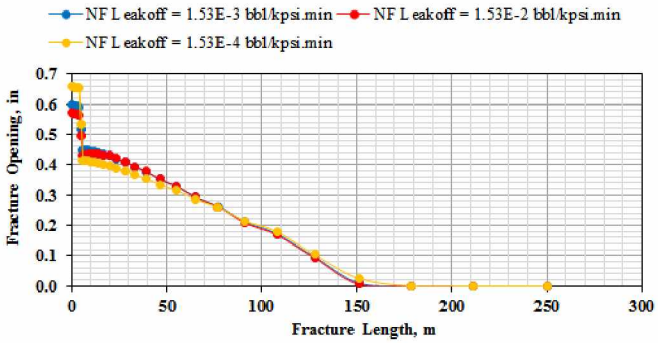

Figure 3-59 Effect of NF leak-off coefficient on HF opening with HF length.

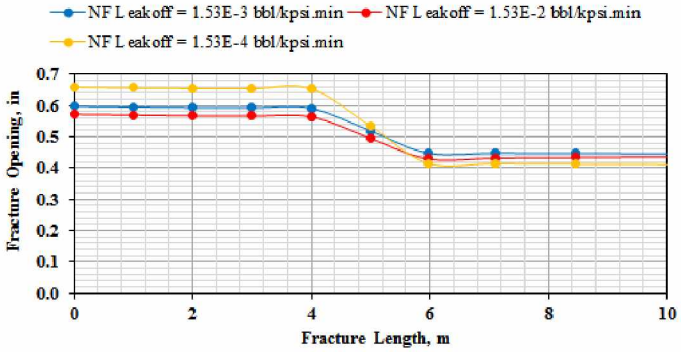

Figure 3-60 Effect of NF leak-off coefficient on HF opening while crossing NF.

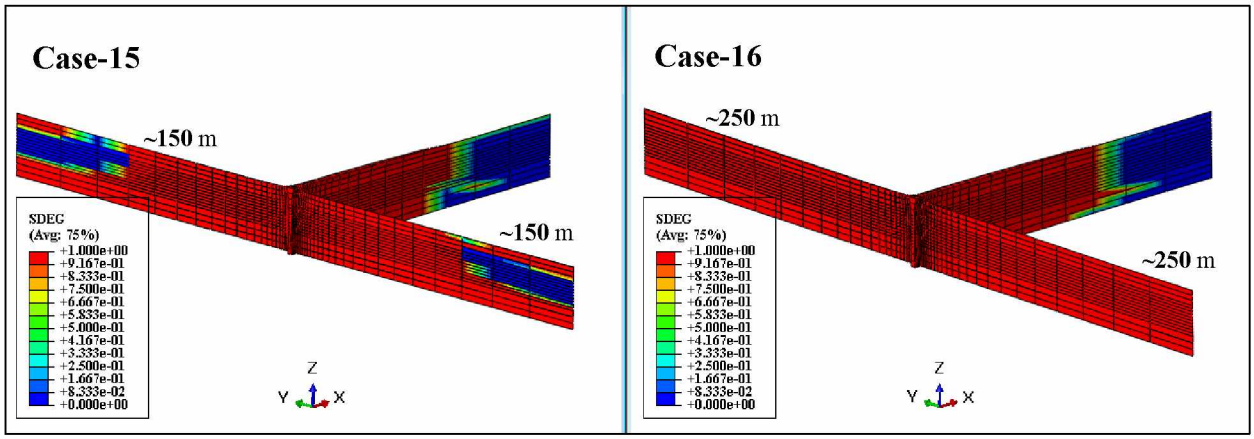

Figure 3-61 Stiffness degradation plot for intersecting HF and NF planes toward the end of pumping time for Case-15 (NF leak-off coefficient = 1.53E-2 bbl/kpsi.min) and Case-16 (NF leak-off coefficient = 1.53E-4 bbl/kpsi.min).

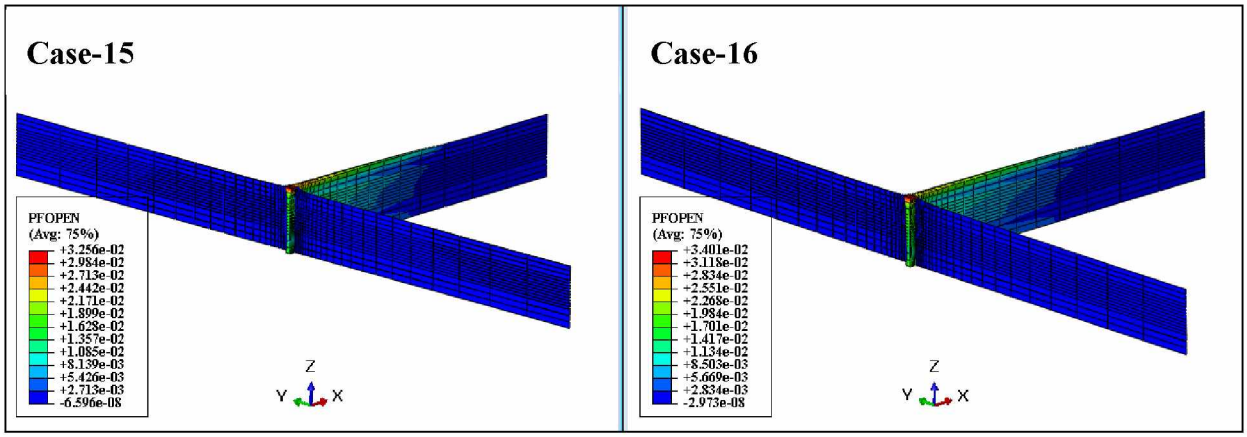

Figure 3-62 Fracture opening for HF and NF planes toward the end of pumping time for Case-15 (NF leak-off coefficient = 1.53E-2 bbl/kpsi.min) and Case-16 (NF leak-off coefficient = 1.53E-4 bbl/kpsi.min).

3.5.4 Effect of Formation Properties

3.5.4.1 Effect of HF Leak-off Coefficient

The fracture propagation is governed by the HF leak-off coefficient if the values are low. However, for higher leak-off coefficient values, the permeability of the formation becomes the governing factor in fracture propagation (Haddad et al., 2014). The results obtained for this sensitivity parameter agreed with the findings of Haddad and others, 2014. **Figure 3-63** shows widest HF for the lowest values of HF leak-off coefficient and narrowest HF for highest HF leak-off coefficients. The permeability in the target zone was higher than the permeability of the surrounding top and bottom layers. However, due to the lower HF leak-off coefficient, the HF opening profile was almost even throughout, as seen in **Figure 3-63.** On the other hand, for higher HF leak-off coefficients, the HF opening was governed by the permeability of the rock medium. This is reflected by the uneven opening profile seen for the higher leak-off coefficients in **Figure 3-63.** **Figure 3-64** shows a wider difference between the HF opening with HF length for lowest and highest HF leak-off coefficients. The highest leak-off coefficient results in narrower and longer HF, while the lowest results in wider and longer HF. Also, there is a significant drop in the HF opening after crossing the NF as the HF leak-off coefficient increases. The weaker NF temporarily restricts HF growth and the HF created surface area is less before it encounters NF. Hence, after crossing NF, the HF opening drops drastically as the surface area of created HF increases, the greatest drop being observed for the highest HF leak-off coefficient case. **Figure 3-65** clearly

represents the described phenomenon. **Figure 3-66** shows that the activated NF length is directly proportional to the HF leak-off coefficient. The activated NF length was maximum for Case-19 and minimum for Case-20. The 3D fracture opening for the three cases considered is shown in **Figure 3-67**.

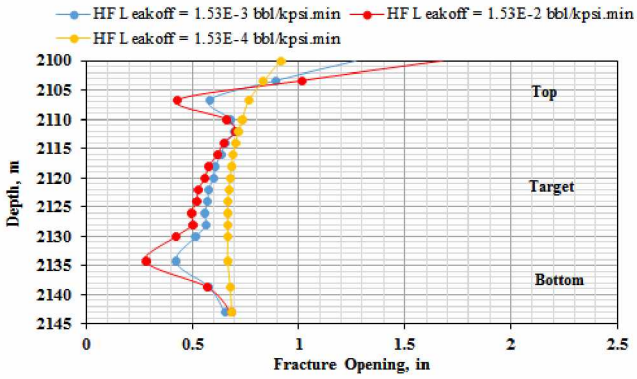

Figure 3-63 Effect of HF leak-off coefficient on HF opening with HF height.

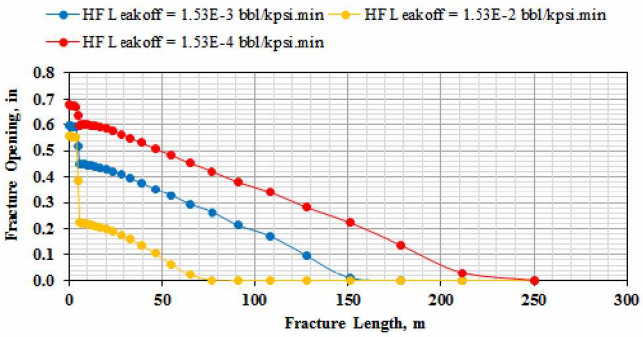

Figure 3-64 Effect of HF leak-off coefficient on HF opening with HF length.

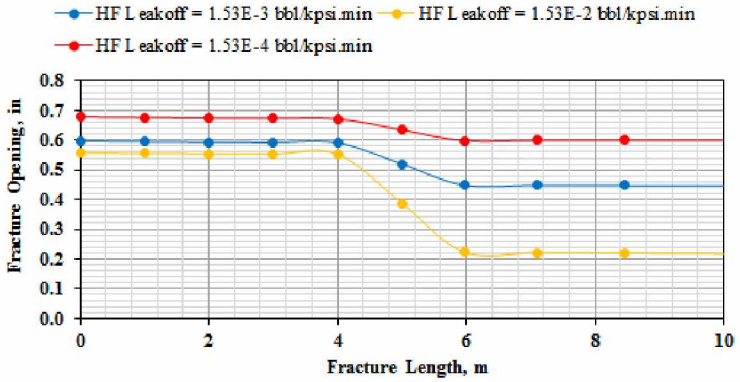

Figure 3-65 Effect of HF leak-off coefficient on HF opening while crossing NF.

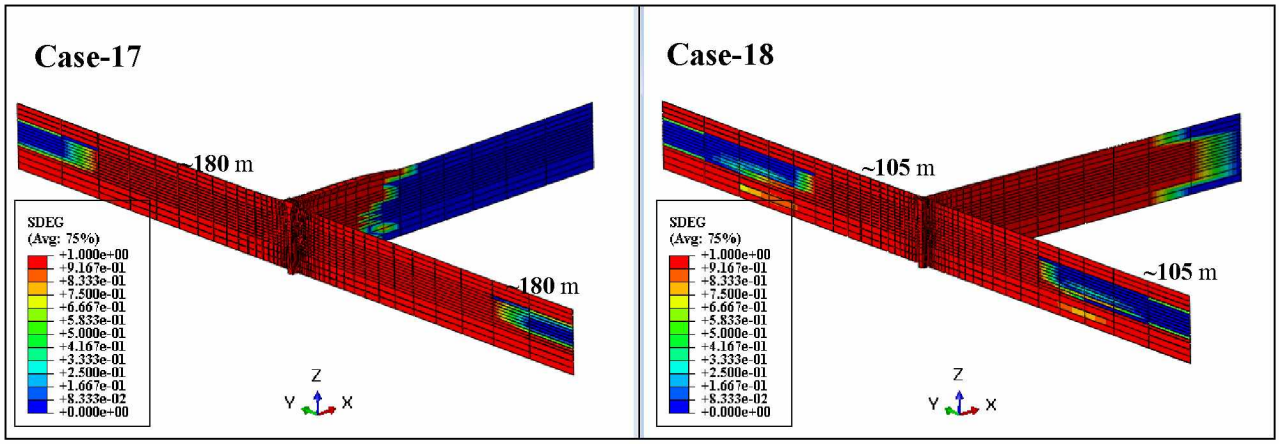

Figure 3-66 Stiffness degradation plot for intersecting HF and NF planes toward the end of pumping time for Case-17 (HF leak-off coefficient = 1.53E-2 bbl/kpsi.min) and Case-18 (HF leak-off coefficient = 1.53E-4 bbl/kpsi.min).

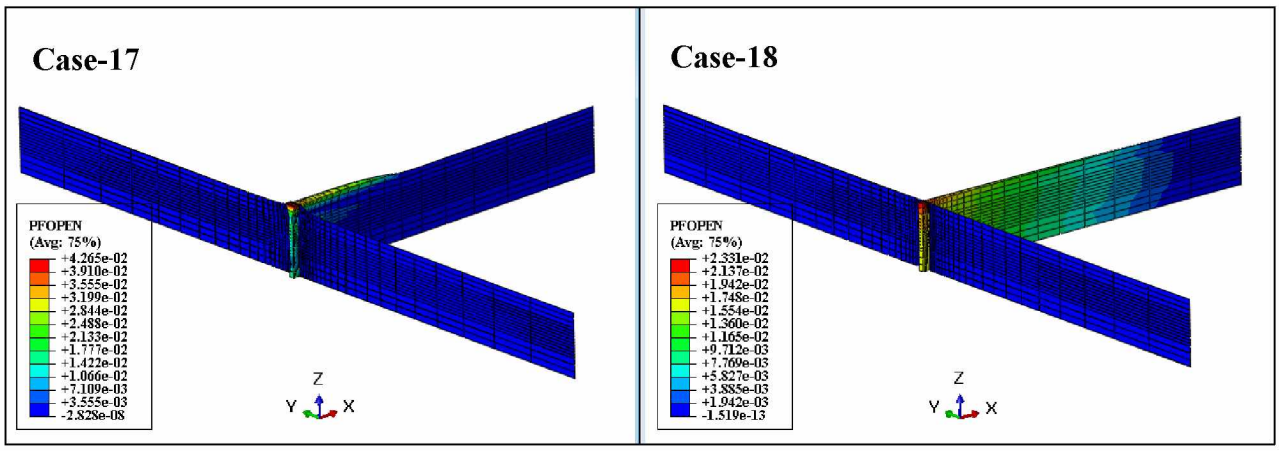

Figure 3-67 Fracture opening for HF and NF planes toward the end of pumping time for Case-17 (HF leak-off coefficient = 1.53E-2 bbl/kpsi.min) and Case-18 (HF leak-off coefficient = 1.53E-4 bbl/kpsi.min).

3.5.4.2 Effect of Target Formation Thickness

The target formation thickness input value was increased and reduced by 25% with respect to the base case to understand the effect of thickness on HF-NF geometry. **Figure 3-68** shows that the HF opening decreased with increasing target formation thickness. A closer look (**Figure 3-69**) clarifies this fact. The HF opening with HF length shows a similar trend and can be seen in **Figure 3-70**. Hence the HF length and HF opening are inversely proportional to the target formation thickness. **Figure 3-71** shows a usual trend when HF propagates through NF, as observed in most

other cases. Reducing the thickness of the target formation results in concavely increasing NF activated length with depth, as seen for Case-17 (**Figure 3-72**). Increasing the thickness of the target formation by 25% showed similar NF activated length as the base case. **Figure 3-73** shows the fracture opening in 3D for the three cases considered.

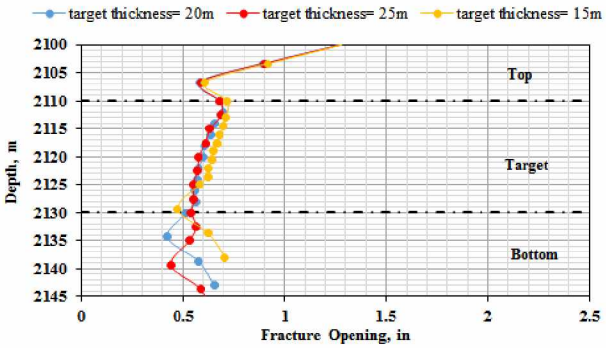

Figure 3-68 Effect of target formation thickness on HF opening with HF height.

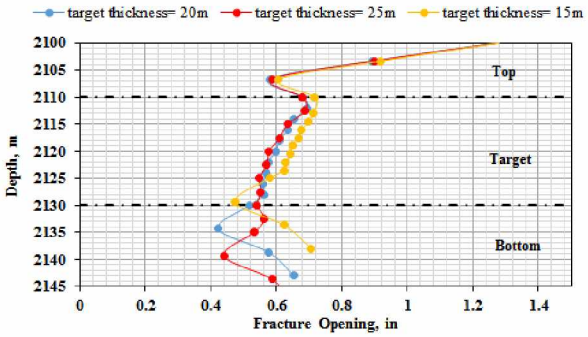

Figure 3-69 Effect of target formation thickness on HF opening with a closer look.

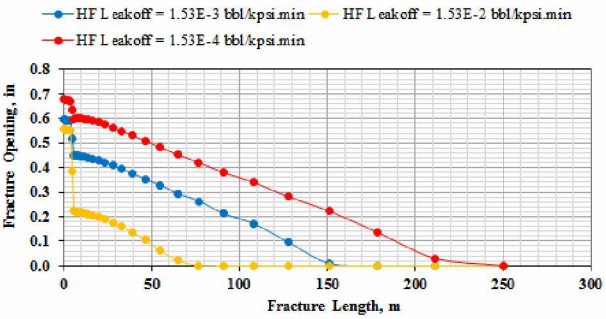

Figure 3-70 Effect of target formation thickness on HF opening with HF length.

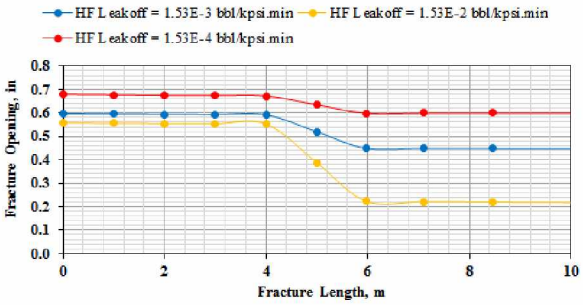

Figure 3-71 Effect of target formation thickness on HF opening while crossing NF.

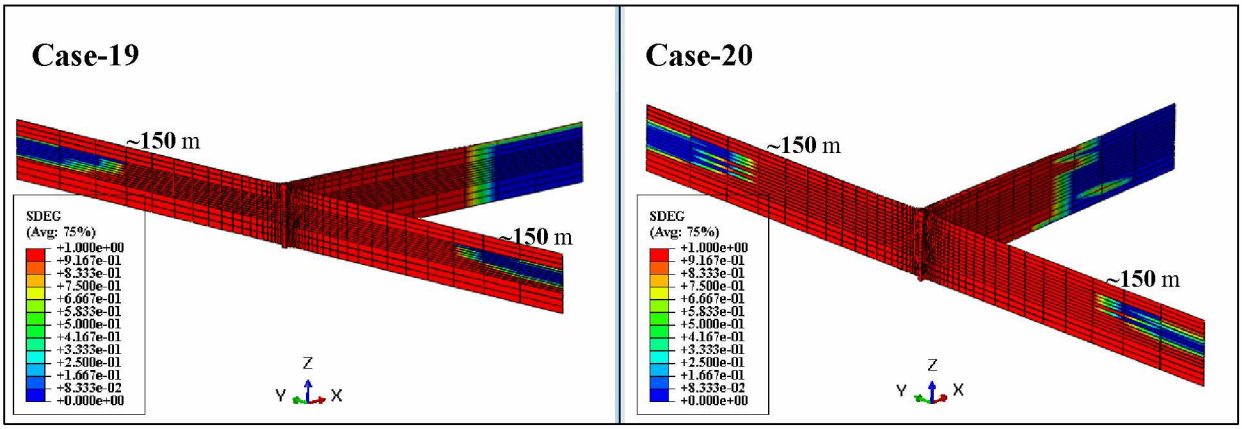

Figure 3-72 Stiffness degradation plot for intersecting HF and NF planes toward the end of pumping time for Case-19 (target formation thickness = 15 m) and Case-20 (target formation thickness = 25 m).

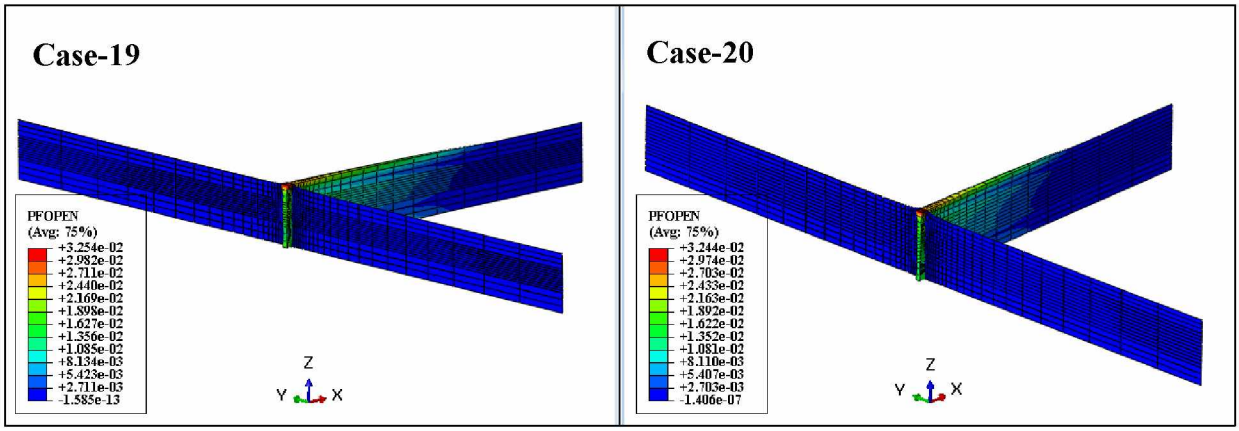

Figure 3-73 Fracture opening for HF and NF planes towards the end of pumping time for Case-19 (target formation thickness = 15 m) and Case-20 (target formation thickness = 25 m.

3.5.4.3 Effect of Target Formation Young's Modulus

The higher the value of Young's modulus, the greater force per unit area required to deform the material. Hence the rigidity or the stiffness of the material increases with increasing value of Young's modulus. This phenomenon was clearly observed in this case. **Figure 3-74** shows higher HF opening for lower Young's modulus. Hence the HF opening varies inversely with the target formation Young's modulus. **Figure 3-75** shows that the HF opening was lowest for the highest Young's modulus, but created the longest HF compared to the other two cases. **Figure 3-76** shows a usual trend observed while HF propagates through the NF. **Figure 3-77** shows the stiffness degradation plots and it can be seen that the NF activated length for Case-13 was same as the base

case. The activated NF length tried to propagate towards the end of the model boundary for higher depths in the target zone, as seen in **Figure 3-77. Figure 3-78** shows the fracture opening for Case-14 and Case-15, with HF length higher with highest Young's modulus for Case-15.

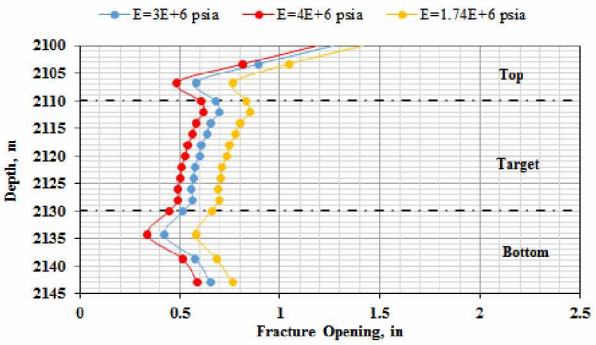

Figure 3-74 Effect of target formation Young's modulus on HF opening with HF height.

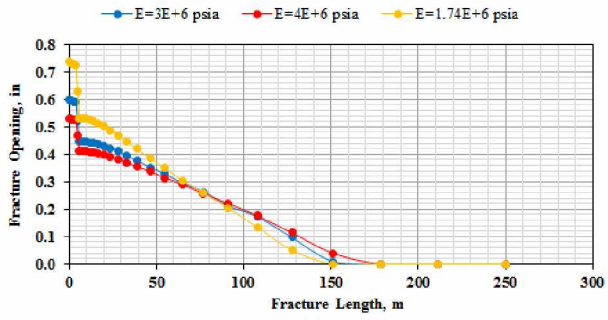

Figure 3-75 Effect of target formation Young's modulus on HF opening with HF length.

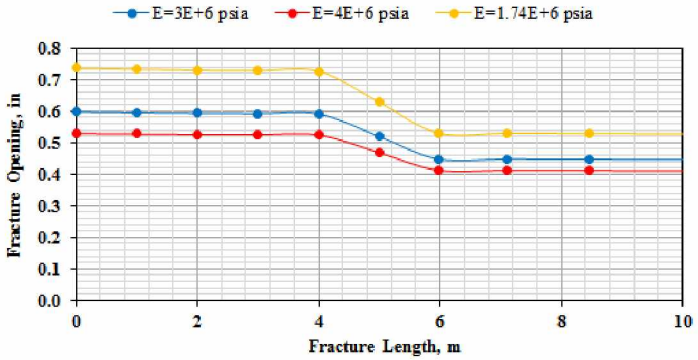

Figure 3-76 Effect of target formation Young's modulus on HF opening while crossing NF.

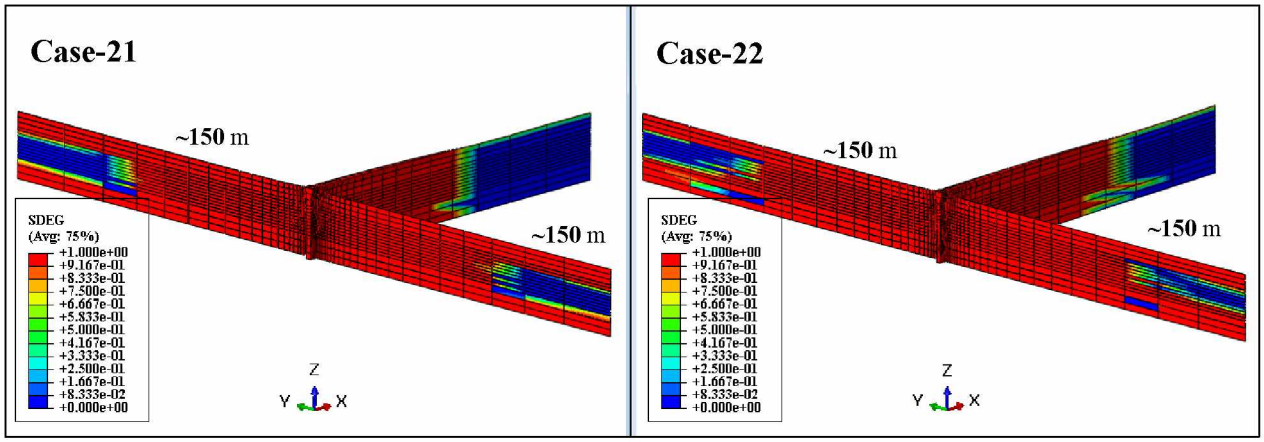

Figure 3-77 Stiffness degradation plot for intersecting HF and NF planes towards the end of pumping time for Case-21 (target formation E = 1.74E+6 psia) and Case-22 (target formation E = 4E+6 psia).

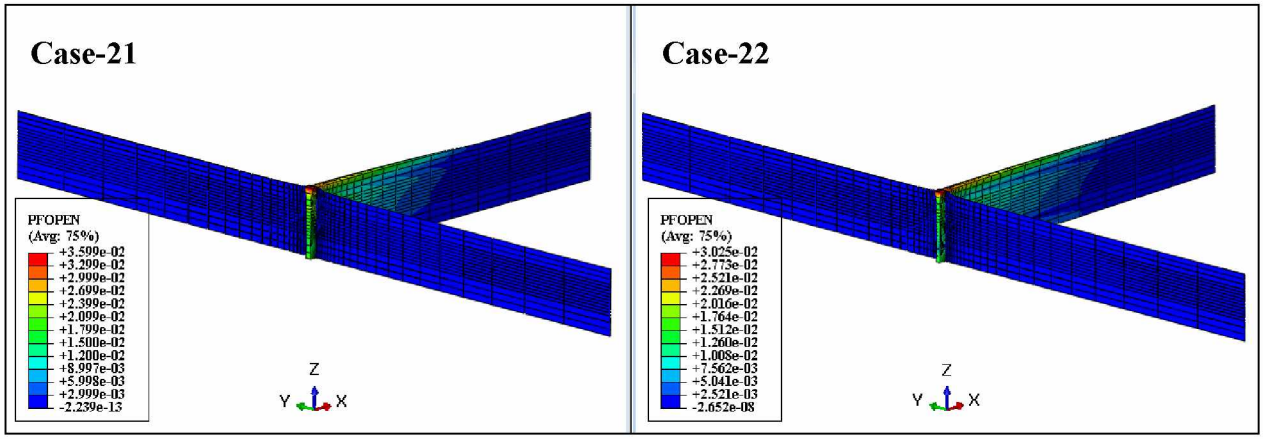

Figure 3-78 Fracture opening for HF and NF planes towards the end of pumping time for Case-21 (target formation E= 1.74E+6 psia) and Case-22 (target formation E= 4E+6 psia).

3.5.4.4 Effect of Target Formation Poisson's Ratio

Poisson's ratio, another property of elastic materials, is the ratio of transverse to axial strain. In a propagating HF, the load applied is the injection rate that tears apart and opens the rock matrix by exerting compressive stress on the fracture faces. If we consider the transverse strain to undergo negligible change for the cases considered, then the HF opening will be inversely proportional to Poisson's ratio. Hence lower values of target formation Poisson's ratio should result in higher fracture opening. **Figure 3-79** shows the highest HF opening for lowest Poisson's ratio value and lowest opening for highest Poisson's ratio value. However, this phenomenon shows a total contrast as we move along the HF length, crossing the NF encountered (**Figure 3-80**). The HF opening

with length was inversely proportional to Poisson's ratio before encountering NF. Conversely, the HF opening now directly varies with Poisson's ratio after crossing NF. The HF opening was observed to drop down to the same value for all three cases, as observed in **Figure 3-81**. The reason for this shift was not understood completely and requires further analysis. However, the changing in-situ stress shadowing effects along with the presence of restricting weaker NF and contrasting interlayer Poisson's ratio might be the reason for such a phenomenon. **Figure 3-82** shows that the NF activated length decreased at the top of the target zone and concavely increased with depth in the target zone for higher target formation Poisson's ratio. The NF activated length at the top of target formation was ~125 m. **Figure 3-83** shows the fracture opening in 3D for the three cases considered.

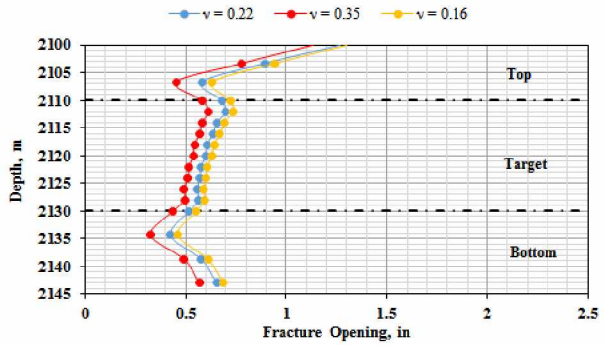

Figure 3-79 Effect of target formation Poisson's ratio on HF opening with HF height.

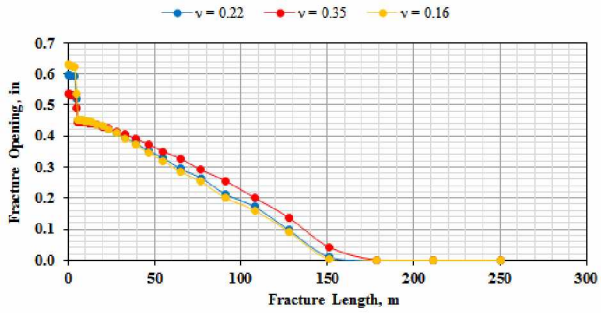

Figure 3-80 Effect of target formation Poisson's ratio on HF opening with HF length.

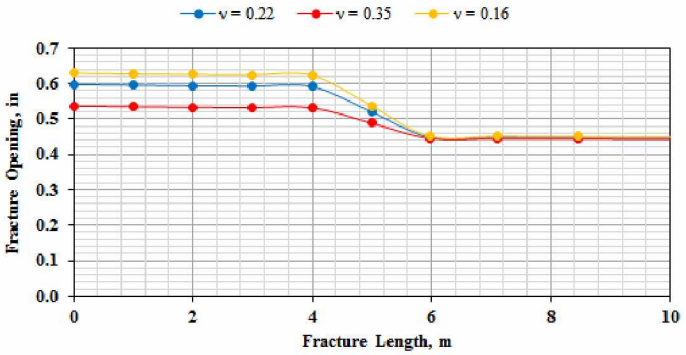

Figure 3-81 Effect of target formation Poisson's ratio on HF opening while crossing NF.

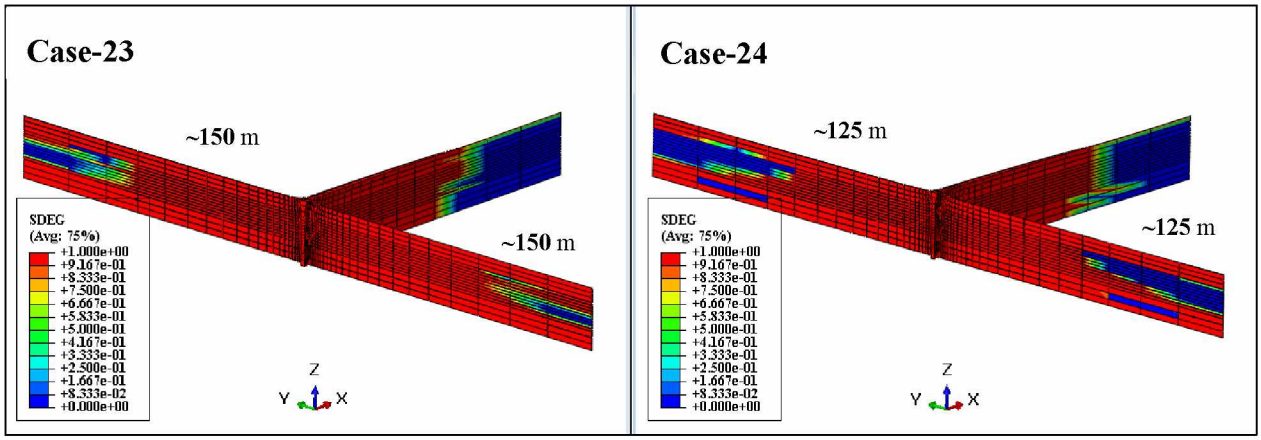

Figure 3-82 Stiffness degradation plot for intersecting HF and NF planes toward the end of pumping time for Case-23 (target formation ν = 0.16) and Case-24 (target formation ν = 0.35).

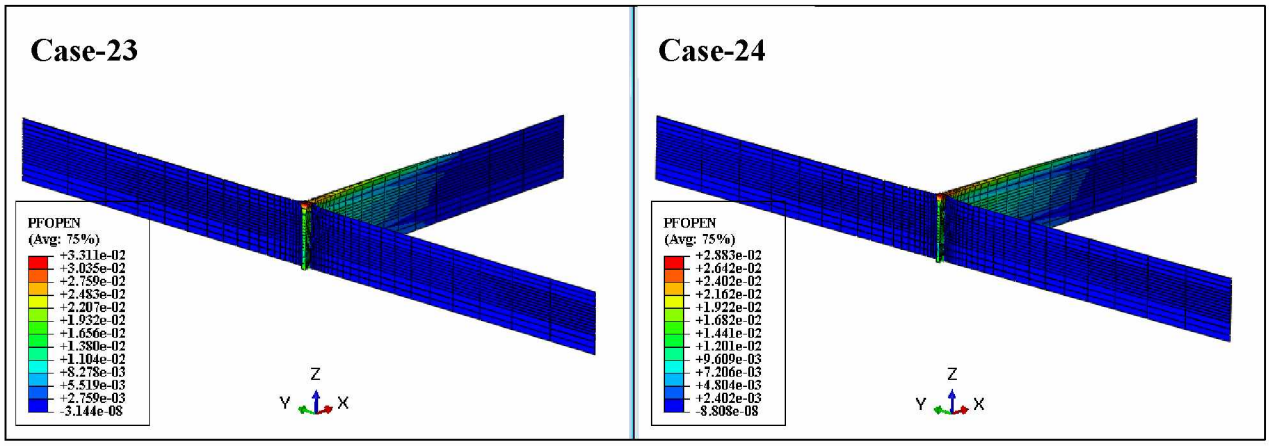

Figure 3-83 Fracture opening for HF and NF planes towards the end of pumping time for Case-23 (target formation ν = 0.16) and Case-24 (target formation ν= 0.35).

3.6 Summarized Observations

The observations for all the cases considered are summarized in **Table 3-4 through Table 3-7.**

Table 3-4 Summarized results for stress contrast category.

Case	Parameter	HF Observations	NF Observations
Base	As mentioned in **Table 3-1**	Propagated through NF. HF opening and half length maximum in top zone and minimum in target zone. Target HF half length ~150 m	Target NF activated half length ~150 m
1	$S_{Hmin} = 0.5 * S_{Hmax}$	Propagated through NF. Maximum HF opening with HF height and length in the categorized parameter. Target HF half length ~180 m	Target NF activated half length ~105 m. Least in categorized parameter
2	$S_{Hmin} = 0.99 * S_{Hmax}$	Propagated through NF. Same HF opening with HF height and length as the base case. Target HF half length ~150 m	Target NF activated half length ~150 m
3	Reversed S_{Hmin} and S_{Hmax}	Propagated along NF after the intersection. HF height contained in the target zone. HF opening less than NF opening. Target HF half length ~5m	Target NF activated half length ~250 m (model boundary). NF opened up to ~35 m in target zone

Table 3-5 Summarized results for job design parameters.

Case	Parameter	HF Observations	NF Observations
Base	As mentioned in **Table 3-1**	Propagated through NF. HF opening and half length maximum in top zone and minimum in target zone. Target HF half length ~150 m	Target NF activated half length ~150 m
4	Injection rate = 15 bpm	Propagated through NF. HF narrower and shorter as compared to the base case. Target HF half length ~90 m	Target NF activated half length ~150 m
5	Injection rate = 60 bpm	Propagated through NF. HF wider and longer as compared to the base case. Target HF half length ~250 m	Target NF activated half length ~150 m
6	Injection fluid viscosity = 10 cP	Propagated through NF. HF narrower and longer as compared to the base case. Target HF half length ~180 m	Target NF activated half length ~150 m
7	Injection fluid viscosity = 1 cP	Propagated through NF. HF narrowest and longest in all viscosity effect scenarios. Target HF half length ~200 m	Target NF activated half length ~105 m
8	Injection fluid viscosity = 100 cP	Propagated through NF. HF widest and shortest in all viscosity effect scenarios. Target HF half length ~150 m	Target NF activated half length ~180 m

Table 3-6 Summarized results for NF properties.

Case	Parameter	HF Observations	NF Observations
Base	As mentioned in **Table 3-1**	Propagated through NF. HF opening and half length maximum in top zone and minimum in target zone. Target HF half length ~150 m	Target NF activated half length ~150 m
9	NF same as surroundings	Propagated through NF. HF length greater base case. HF opening narrower than base case. Target HF half length ~180 m	Target NF activated half length ~15 m
10	Stronger NF	Propagated through NF. HF length greater base case. HF opening narrowest in all NF strength scenarios. Target HF half length ~180 m	Target NF activated half length ~5 m
11	NF distance = 50 m	Arrested at NF. HF wider than base case. HF length same as NF distance = 50 m	Target NF activated half length ~250 m (model boundary)
12	NF distance = 100 m	Arrested at NF. HF wider than a base case but narrower than above case. HF length same as NF distance = 100 m	Target NF activated half length ~250 m (model boundary)
13	NF at 50 m from the injection point, NF=0.6*HF, HF-NF angle=90°	Propagated through NF. HF length greater than base case. HF opening gradually rising until NF and thereafter gradually decreases. HF opening same as the base case. Target HF half-length ~200 m	Target NF activated half length ~250 m (model boundary)
14	NF at 50 m from the injection point, NF=0.6*HF, HF-NF angle=80°	Propagated through NF. HF length greater than base case. HF opening gradually rising until NF and thereafter gradually decreases. HF opening same as the base case. Target HF half-length ~200 m	Target NF activated half-length on left~175 m. Target NF activated half-length on right~250 m (model boundary)

Table 3- 6 continued.

Case	Parameter	HF Observations	NF Observations
15	NF leak-off = 1.53E-2 bbl/kpsi.min	Propagated through NF. HF narrower than the base case before and while crossing NF, thereafter same as the base case. HF length same as the base case. Target HF half length ~150 m	Target NF activated half length ~150 m
16	NF leak-off = 1.53E-4 bbl/kpsi.min	Propagated through NF. HF wider than the base case before and while crossing NF, thereafter same as the base case. HF longer than the base case. Target HF length ~170 m	Target NF activated half length ~250 m (model boundary)

Table 3-7 Summarized results for formation properties.

Case	Parameter	HF Observations	NF Observations
17	HF leak-off = 1.53E-2 bbl/kpsi.min	Propagated through NF. HF narrower and shorter as compared to the base case. Target HF half length ~75 m	Target NF activated half length ~180 m
18	HF leak-off = 1.53E-4 bbl/kpsi.min	Propagated through NF. HF wider and longer as compared to the base case. Target HF half length ~240 m	Target NF activated half length ~105 m
19	Target thickness = 15 m	Propagated through NF. HF wider and longer than base case. Target HF half length ~180 m	Target NF activated half length ~150 m at the top. Tries to activate until model boundary (~250 m) as depth increases
20	Target thickness = 25 m	Propagated through NF. HF narrower and same in length as the base case. Target HF half length ~150 m	Target NF activated half length ~150 m
21	Target E = 1.74E+6 psi	Propagated through NF. HF length same as the base case. HF wider until ~75 m and then same as compared to the base case. Target HF half length ~150 m	Target NF activated half length ~150 m
22	Target E = 4E+6 psi	Propagated through NF. HF narrower as compared to the base case. Target HF half length ~150 m	Target NF activated half length ~150 m at the top. Tries to activate until model boundary (~250 m) as depth increases
23	Target ν = 0.16	Propagated through NF. HF wider than the base case before and while crossing NF, thereafter less than base case. HF length same as the base case. Target HF half length ~150 m	Target NF activated half length ~150 m
24	Target ν = 0.35	Propagated through NF. HF slightly narrower than the base case before and while crossing NF, thereafter greater than base case. HF longer than base case. Target HF half length ~180 m	Target NF activated half length ~125 m

CHAPTER 4 CONCLUSIONS AND RECOMMENDATIONS

4.1 Conclusions

The interaction of orthogonally intersecting single hydraulic fractures (HF) and single natural fractures (NF) was modeled successfully using Finite Element Analysis (FEA). The advanced Cohesive and Pore Pressure Elements in FEA software capable of modeling the fluid continuity at the HF-NF intersection point were used for the fracturing study. Sensitivity parameters were found to affect the NF and HF geometry to greater or lesser extents.

In the case of a HF approaching a NF at a right angle, the HF crossed the NF (activating the NF but not opening it) for the different scenarios considered. The only exception where the NF was opened was the high stress contrast and stress reversal scenario. The HF propagated into the NF and opened it. Hence, for orthogonally intersecting HF and NF, the NF will rarely open. The orthogonal intersection causes the NF to be oriented in the direction perpendicular to maximum horizontal stress. As per the laws of fracture mechanics, a propagating fracture will have the least resistance to opening in the direction of minimum horizontal stress and propagate in the direction of maximum horizontal stress. Hence, the NF will not open for the orthogonal case considered.

For high stress contrast, the NF activated length was greater compared to the low stress contrast. The change in the HF opening after it propagated through the NF was also smaller for the high contrast scenario than the low stress contrast scenario. For high stress contrast with the principle horizontal stresses reversed, it was observed that the HF got diverted into NF. All the stress contrast observations agreed with the laboratory findings of Saurez-Rivera and others (2013). Keeping everything else constant, it can be concluded that higher stress contrasts result in longer HF and shorter activated NF. On the other, low or negligible stress contrast will lead to shorter HF and longer activated NF. Hence, stress contrast and the horizontal principal stresses' directions affected the HF-NF geometry to a greater extent.

Increasing the injection rate resulted in longer and wider HF without significant change in the NF activated length. Hence, it can be concluded that the injection rates in the investigated range (15 bpm to 60 bpm) will lead to similar NF activated length but varying HF geometry for the model under study. Therefore, varying injection rate least affected the NF activation.

It was observed that injection fluid viscosity has an inversely proportional relationship with HF length and a proportional relationship with HF opening. The NF activated length was also directly proportional to injection fluid viscosity. Hence the injection fluid was found to greatly influence the HF-NF geometry and should be carefully studied while designing a fracturing job.

A weak NF plane temporarily restricted the HF propagation. This was not seen in the case of stronger NF planes or NF planes having same properties as the surrounding formation. Therefore, although the weaker NF restricted HF propagation temporarily, it ultimately resulted in a HF with a wider opening and longer activated NF length. Hence, the presence of weaker NF plane has the potential to result in a greater stimulated area compared to stronger NF planes or NF planes with similar or the same strength as the surrounding formation. NF strength can be inferred to significantly affect the NF activated length, which will ultimately affect the stimulated area or volume.

The NF positioning or the NF distance from the injection point affected the propagating HF geometry and NF activated length. A NF far away from the injection point arrests the HF once it reaches the NF. On the other hand, a NF closer to the injection point allows the fracture to propagate through it. This NF positioning also affects the NF activated lengths. A NF away from the injection point arrests the HF but results in completely activated NF length. However, a NF closer to the injection point does not activate completely, as mentioned in the previous case. To conclude, the NF farther away from the injection point does not get activated completely but results in shorter and wider HF compared to the HF for the case with NF closer to the injection point. NF positioning significantly affects the HF-NF geometry: it governs the change in HF propagation paths, i.e. from HF crossing NF to HF being arrested at NF.

The HF opening was inversely proportional to the target formation Young's modulus, however, the NF activated length was not much affected by changing the target formation Young's modulus. Hence the softer the surrounding formation, the wider the HF with minimal effect on NF activated length. To infer, a softer target formation all other parameters remaining constant will result in wider but shorter HF and almost the same NF activated length. Young's modulus was observed to affect the HF geometry slightly but not affect the NF activated length.

The target formation Poisson's ratio was also inversely related to the HF opening prior to encountering NF. After crossing the NF, the HF opening showed a direct relationship with the target formation Poisson's ratio. An exact reason for this behavior was not found, however, it is thought to be due to the overall resulting in-situ stresses, stress shadowing effects, and the presence of NF. More investigation and studies need to be done in this direction. Also, the NF activated length was observed to be inversely proportional to the target formation Poisson's ratio. Hence a target formation with lower Poisson's ratio value will have wider HF length until it encounters NF. However, the HF opening with HF length will show an opposite change in the relationship after crossing the NF. The HF opening will be directly proportional to the target formation Poisson's ratio after crossing NF. Hence Poisson's ratio can be a significant and critical parameter to be considered and studied in HF – NF interaction.

The HF length and width were observed to be inversely proportional to target formation thickness. However, the NF activated length was only affected by lower/equal target formation thickness compared to surrounding formations. Hence target formation thickness definitely affects the HF geometry, but only affects the NF if it is equal to or less than surrounding formation thickness. Target formation thickness may affect the HF-NF geometry to a greater or lesser extent and should be concluded for individual cases.

Lower HF and/or NF leak-off coefficients govern the HF and/or NF geometry. However, for higher values of leak-off coefficients, the permeability of the surrounding medium plays an important role in HF and/or NF geometry.

The opening and the length of the HF were directly proportional to the HF leak-off coefficient, the NF leak-off coefficient being constant. The NF activated length was also directly proportional to the HF leak-off coefficient, the NF leak-off coefficient being constant. Hence higher HF leak-off coefficients will result in shorter and narrower HF and longer activated NF lengths. On the other hand, lower HF leak-off coefficients will result in longer and wider HF but restricted activated NF lengths. Therefore, HF leak-off coefficient significantly affects the HF and NF geometry.

The NF leak-off coefficient, the HF leak-off coefficient being constant, does not affect the HF opening pattern to the extent observed while varying HF leak-off coefficient. However, it does affect the HF opening with depth and HF length. Higher NF leak-off coefficients result in narrower

HF until HF encounters the NF; thereafter, it does not show any effect on HF geometry. Also, NF leak-off coefficient, HF leak-off coefficient being constant, is directly proportional to the NF activated length.

The final objective of the sensitivity analysis was to screen out the most and least sensitive parameters affecting the HF-NF interaction. The sensitivity analysis can be broadly classified as the effect of 1) in-situ stress contrast, 2) job design parameters, 3) NF properties, and 4) formation properties. A color coded conclusion table was constructed to easily understand and visualize the impact of these parameters on HF, NF and HF-NF geometry and interaction**. Figure 4-1** shows the legends for subsequent conclusion tables. Various geometrical HF-NF parameters will be considered in subsequent tables to come to conclusions. The term "# same" and "# different" means the number of these considered geometrical HF-NF parameters to be "same as base case" and "different from base case" results, respectively. Dark green represents the most sensitive parameter as it corresponds to a maximum number of resultant geometrical HF-NF parameters different from the base case. On the other hand, bright red represents the least important parameter.

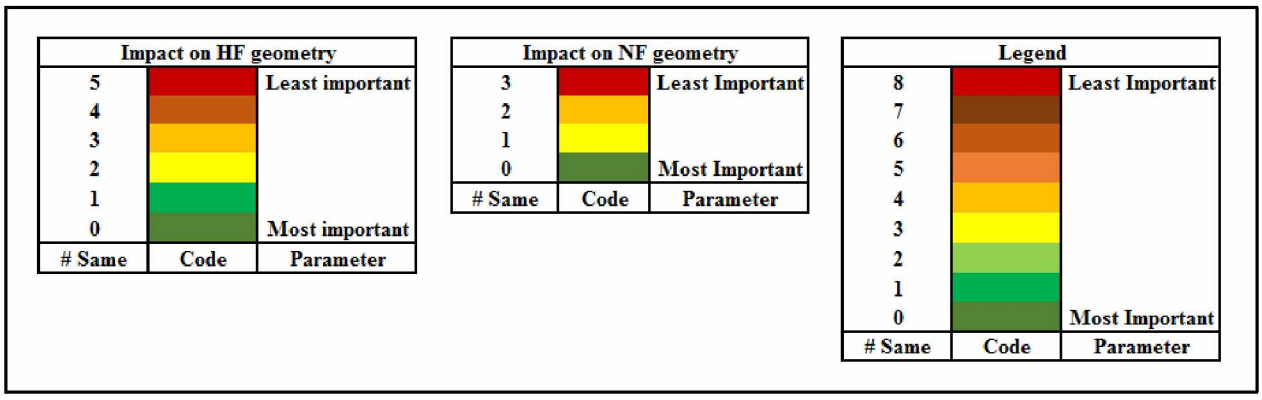

Figure 4-1 Legend for HF-NF interaction conclusions

Table 4-1 shows the impact of various parameters on HF geometrical parameters like the width of HF at wellbore, HF opening with HF length before and after crossing NF, and HF length. The words same, greater, and less correspond to the value of these parameters compared to the base case. The last three columns talk about the thought process for final conclusions and are based on the "# same" and "# different" definitions mentioned previously. The most important parameters are observed to be a high stress contrast with stress reversal, highest injection rate, and farther NF distance from the injection point. The least important case was the one with horizontal stresses

almost equal. This was obvious as it was very close to the base case. However, it is practically feasible to say that high stress contrast, highest injection viscosity, highest and lowest NF leak-off coefficients, thicker target formation, lowest target formation Young's modulus, and target formation Poisson's ratio affect the HF geometry moderately. Similarly, it is fair to say that high stress contrast with stress reversal, injection rate, lower injection viscosities, NF strengths, farther NF distance from the injection point, HF leak-off coefficients, thinner target formation, and highest Young's modulus affect the HF geometry greatly. Ultimately, the remaining yellow shades can be concluded to affect the HF geometry moderately.

Table 4-1 Impact of sensitivity parameters on HF geometry

Categorized parameter	Case	Parameter	HF (compared to base case)					Results variance from base case		Conclusions
			Width @ Wellbore	Width w/ Length		Length m	Interaction with NF	# Same	# Different	
				Before NF	After NF					
1) Stress Contrast	1	$S_{Hmin} = 0.5^* S_{Hmax}$	Same	Same	Greater	180	Propagated Through	3	2	
	2	$S_{Hmin} = 0.99^* S_{Hmax}$	Same	Same	Same	150	Propagated Through	4	1	
	3	Reversed S_{Hmin} and S_{Hmax}	Less	Less	Zero	5	Diverted	0	5	
2) Job Design	4	Injection rate = 15 bpm	Less	Less	Less	90	Propagated Through	1	4	
	5	Injection rate = 60 bpm	Greater	Greater	Greater	250	Propagated Through	0	5	
	6	Injection fluid viscosity = 10 cP	Less	Less	Less	180	Propagated Through	1	4	
	7	Injection fluid viscosity = 1 cP	Less	Less	Less	200	Propagated Through	1	4	
	8	Injection fluid viscosity = 100 cP	Greater	Greater	Greater	150	Propagated Through	2	3	
3) NF Properties	9	NF same as surroundings	Less	Less	Less	180	Propagated Through	1	4	
	10	Stronger NF	Less	Less	Less	180	Propagated Through	1	4	
	11	NF distance = 50 m	Greater	Greater	Zero	50	Arrested	0	5	
	12	NF distance = 100 m	Less	Greater	Zero	100	Arrested	0	5	
	13	HF-NF angle= 90°	Less	Less	Greater	200	Propagated Through	0	5	
	14	*HF-NF angle= 80°	Same	Less	Less	180	Propagated Through	1	4	
	15	NF leak-off = 1.53E-2 bbl/kpsi.min	Less	Less	Same	150	Propagated Through	3	2	
	16	NF leak-off = 1.53E-4 bbl/kpsi.min	Greater	Greater	Same	170	Propagated Through	2	3	
4) Formation Properties	17	HF leak-off = 1.53E-2 bbl/kpsi.min	Less	Less	Less	75	Propagated Through	1	4	
	18	HF leak-off = 1.53E-4 bbl/kpsi.min	Greater	Greater	Greater	240	Propagated Through	1	4	
	19	Target thickness = 15 m	Greater	Greater	Greater	180	Propagated Through	1	4	
	20	Target thickness = 25 m	Less	Less	Less	150	Propagated Through	2	3	
	21	Target E = 1.74E+6 psi	Greater	Greater	Same	150	Propagated Through	3	2	
	22	Target E = 4E+6 psi	Less	Less	Less	180	Propagated Through	1	4	
	23	Target ν = 0.16	Greater	Greater	Same	150	Propagated Through	3	2	
	24	Target ν = 0.35	Less	Less	Same	180	Propagated Through	2	3	

* Compared to Case-13 as base case

Table 4-2 shows the impact of various parameters on NF geometrical parameters like width at HF-NF intersection, NF opening with NF length, and activated NF length. The approach and the terms used are similar to the ones explained for the HF impact parameters. It was observed that the most important parameter in this context was the high stress contrast with stress reversal. Conversely, the least important parameters are the injection rate, lower injection viscosity (10 cP), higher NF leak-off coefficient, target formation thickness and Young's modulus and lowest value of target formation Poisson's ratio. The remaining parameters, in yellow, were thus the moderately important parameters.

Table 4-2 Impact of sensitivity parameters on NF geometry

Categorized parameter	Case	Parameter	NF (compared to base case)			Results variance from base case		
			Width @ intersection	Width w/ Length	Activated Length m	# Same	# Different	Conclusions
1) Stress Contrast	1	S_{Hmin} = 0.5* S_{Hmax}	Same	Same	105	2	1	
	2	S_{Hmin} = 0.99* S_{Hmax}	Same	Same	150	2	1	
	3	Reversed S_{Hmin} and S_{Hmax}	Greater	Greater	~250 m (Opened = 35m)	0	3	
2) Job Design	4	Injection rate = 15 bpm	Same	Same	150	3	0	
	5	Injection rate = 60 bpm	Same	Same	150	3	0	
	6	Injection fluid viscosity = 10 cP	Same	Same	150	3	0	
	7	Injection fluid viscosity = 1 cP	Same	Same	105	2	1	
	8	Injection fluid viscosity = 100 cP	Same	Same	180	2	1	
3) NF Properties	9	NF same as surroundings	Same	Same	15	2	1	
	10	Stronger NF	Same	Same	5	2	1	
	11	NF distance = 50 m	Same	Same	250	2	1	
	12	NF distance = 100 m	Same	Same	250	2	1	
	13	*HF-NF angle= 90°	Same	Same	250	2	1	
	14	**HF-NF angle= 80°	Same	Same	250, 175	2	1	
	15	NF leak-off = 1.53E-2 bbl/kpsi.min	Same	Same	150	3	0	
	16	NF leak-off = 1.53E-4 bbl/kpsi.min	Same	Same	250	2	1	
4) Formation Properties	17	HF leak-off = 1.53E-2 bbl/kpsi.min	Same	Same	180	2	1	
	18	HF leak-off = 1.53E-4 bbl/kpsi.min	Same	Same	105	2	1	
	19	Target thickness = 15 m	Same	Same	150	3	0	
	20	Target thickness = 25 m	Same	Same	150	3	0	
	21	Target E = 1.74E+6 psi	Same	Same	150	3	0	
	22	Target E = 4E+6 psi	Same	Same	150	3	0	
	23	Target ν = 0.16	Same	Same	150	3	0	
	24	Target ν = 0.35	Same	Same	125	2	1	

* Compared to base case ** Compared to Case-13

The final part of the conclusion was to collectively study the effect of sensitivity parameters on HF-NF interaction and geometry. The only parameter added to the ones explained in the individual impact analysis of HF and NF is the interaction of HF with NF. This parameter basically indicates if the HF was propagated through NF, arrested by NF, or diverted into NF. The observations for each of these parameters are seen in the **Table 4-3** and **Table 4-4**

This study will help an engineer to understand the mechanical behavior of rock with respect to the HF-NF interaction at a single HF and single NF level. It will quantify the effect of the sensitivity parameters on the HF-NF geometry. This will help an engineer to understand the pros and cons of a particular project involving hydraulic fracturing in the presence of NF and the scale the significance of various parameters affecting the HF-NF interaction. This will ultimately help to design an optimum hydraulic fracture job.

Table 4-3. For the purpose of proper visualization and presentation, the conclusions were separated as seen in Table 4-4. The terms and definitions used here are again same as explained in the case of HF. Precisely, the most important parameter and the least important parameter were observed to be a high stress contrast with stress reversal and high stress contrast respectively. However, the most important parameters can be reasonably concluded to be a high stress contrast with stress reversal, and farther NF distance from the injection point. The least important parameters were found to be almost equal horizontal stresses case, higher NF leak-off coefficient, lower target formation Young's modulus and Poisson's ratio and high stress contrast. The remaining parameters marked yellow moderately affected the HF – NF interaction and geometry.

This study definitely quantifies the effect of the parameters on the studied HF – NF geometry. However, most of them cannot be manually controlled. The uncontrollable parameters still provide us a guideline and idea of the HF – NF interaction for practical existing scenarios. The only broadly categorized parameters that are controllable are the job design parameters. Hence these parameters should be closely examined and then executed in the field. Special care should be taken while deciding the viscosity of the injection fluid.

This study will help an engineer to understand the mechanical behavior of rock with respect to the HF-NF interaction at a single HF and single NF level. It will quantify the effect of the sensitivity

parameters on the HF-NF geometry. This will help an engineer to understand the pros and cons of a particular project involving hydraulic fracturing in the presence of NF and the scale the significance of various parameters affecting the HF-NF interaction. This will ultimately help to design an optimum hydraulic fracture job.

Table 4-3 HF-NF collective observations for impact analysis

Categorized parameter	Case	Parameter	HF (compared to base case)					NF (compared to base case)		
			Width @ Wellbore	Width w/ Length		Length m	Interaction with NF	Width @ intersection	Width w/ Length	Activated Length m
				Before NF	After NF					
1) Stress Contrast	1	S_{Hmin} = 0.5* S_{Hmax}	Same	Same	Greater	180	Propagated Through	Same	Same	105
	2	S_{Hmin} = 0.99* S_{Hmax}	Same	Same	Same	150	Propagated Through	Same	Same	150
	3	Reversed S_{Hmin} and S_{Hmax}	Less	Less	Zero	5	Diverted	Greater	Greater	~250 m (Opened = 35m)
2) Job Design	4	Injection rate = 15 bpm	Less	Less	Less	90	Propagated Through	Same	Same	150
	5	Injection rate = 60 bpm	Greater	Greater	Greater	250	Propagated Through	Same	Same	150
	6	Injection fluid viscosity = 10 cP	Less	Less	Less	180	Propagated Through	Same	Same	150
	7	Injection fluid viscosity = 1 cP	Less	Less	Less	200	Propagated Through	Same	Same	105
	8	Injection fluid viscosity = 100 cP	Greater	Greater	Greater	150	Propagated Through	Same	Same	180
3) NF Properties	9	NF same as surroundings	Less	Less	Less	180	Propagated Through	Same	Same	15
	10	Stronger NF	Less	Less	Less	180	Propagated Through	Same	Same	5
	11	NF distance = 50 m	Greater	Greater	Zero	50	Arrested	Same	Same	250
	12	NF distance = 100 m	Less	Greater	Zero	100	Arrested	Same	Same	250
	13	*HF-NF angle= 90°	Less	Less	Greater	200	Propagated Through	Same	Same	250
	14	**HF-NF angle= 80°	Same	Less	Less	180	Propagated Through	Same	Same	250, 175
	15	NF leak-off = 1.53E-2 bbl/kpsi.min	Less	Less	Same	150	Propagated Through	Same	Same	150
	16	NF leak-off = 1.53E-4 bbl/kpsi.min	Greater	Greater	Same	170	Propagated Through	Same	Same	250
4) Formation Properties	17	HF leak-off = 1.53E-2 bbl/kpsi.min	Less	Less	Less	75	Propagated Through	Same	Same	180
	18	HF leak-off = 1.53E-4 bbl/kpsi.min	Greater	Greater	Greater	240	Propagated Through	Same	Same	105
	19	Target thickness = 15 m	Greater	Greater	Greater	180	Propagated Through	Same	Same	150
	20	Target thickness = 25 m	Less	Less	Less	150	Propagated Through	Same	Same	150
	21	Target E = 1.74E+6 psi	Greater	Greater	Same	150	Propagated Through	Same	Same	150
	22	Target E = 4E+6 psi	Less	Less	Less	180	Propagated Through	Same	Same	150
	23	Target ν = 0.16	Greater	Greater	Same	150	Propagated Through	Same	Same	150
	24	Target ν = 0.35	Less	Less	Same	180	Propagated Through	Same	Same	125

* Compared to base case ** Compared to Case-13

Table 4-4 Impact of sensitivity parameters collectively on HF - NF geometry

Categorized parameter	Case	Parameter	Results variance from base case		
			# Same	# Different	Conclusions
1) Stress Contrast	1	S_{Hmin} = 0.5* S_{Hmax}	5	3	
	2	S_{Hmin} = 0.99* S_{Hmax}	8	0	
	3	Reversed S_{Hmin} and S_{Hmax}	0	8	
2) Job Design	4	Injection rate = 15 bpm	4	4	
	5	Injection rate = 60 bpm	4	4	
	6	Injection fluid viscosity = 10 cP	4	4	
	7	Injection fluid viscosity = 1 cP	3	5	
	8	Injection fluid viscosity = 100 cP	4	4	
3) NF Properties	9	NF same as surroundings	3	5	
	10	Stronger NF	3	5	
	11	NF distance = 50 m	2	6	
	12	NF distance = 100 m	2	6	
	13	*HF-NF angle= 90°	2	6	
	14	**HF-NF angle= 80°	3	5	
	15	NF leak-off = 1.53E-2 bbl/kpsi.min	6	2	
	16	NF leak-off = 1.53E-4 bbl/kpsi.min	4	4	
4) Formation Properties	17	HF leak-off = 1.53E-2 bbl/kpsi.min	3	5	
	18	HF leak-off = 1.53E-4 bbl/kpsi.min	3	5	
	19	Target thickness = 15 m	4	4	
	20	Target thickness = 25 m	4	4	
	21	Target E = 1.74E+6 psi	6	2	
	22	Target E = 4E+6 psi	4	4	
	23	Target ν = 0.16	6	2	
	24	Target ν = 0.35	4	4	

* Compared to base case ** Compared to Case-13

4.2 Recommendations

The considered scenario of orthogonal HF-NF intersection is realistic and represents a scenario seen in the Barnett shale. However, the chances of a NF opening in this type of situation are almost impossible. Considering a non-orthogonal intersection might show different and interesting behavior and results.

The base data set used for the multilayer three dimensional geomechanical model causes the HF height to extend throughout the three layers considered. It would be interesting to study the scenarios where the NF and/or HF are contained in the "interest zone," which is usually the target zone.

There is a limitation of using this FEA software to solve a geotechnical problem related to the petroleum industry. Most hydraulic fracturing is carried out in tight or unconventional formations with ultra low permeability. Low permeability requires fine meshing in the used FEA software to avoid spurious oscillations and run the model successfully. However, fine meshing a three dimensional model increases the computational cost and sometimes makes a simple problem time-consuming and impractical to solve. An approach or technique to address this issue will definitely add greatly to the study and analysis.

Studying and analyzing the interaction of a single HF and multiple NF and/or multiple HF and single NF will definitely be interesting. This study does not consider the effect of proppants in the fracturing fluid. Hence considering such effects will make the model more realistic and practical.

The methodology and results from this study will be applicable if hydraulic fracturing treatments become logistically possible and economic in the Shublik Shale of Alaska. However, to properly apply this technique, an understanding of the natural fracture distribution and a knowledge of Shublik shale mechanical properties, principal in-situ stress directions and magnitudes is required.

REFERENCES

Abaqus Analysis User's Manual. 2016. Dassault Systemes Simulia Corporation, Providence, RI

Abbas, S., Gordeliy, E., Peirce, A., Lecampion, B., Chuprakov, D., and Prioul, R. (2014, February 4). Limited Height Growth and Reduced Opening of Hydraulic Fractures due to Fracture Offsets: An XFEM Application. Presented at SPE Hydraulic Fracturing Technology Conference, 4-6 February, The Woodlands, Texas, USA. SPE-168622-MS. http://dx.doi.org/10.2118/168622-MS

Advani, S. H., Lee, T. S., Dean, R. H., Pak, C. K., and Avasthi, J. M. (1993, January 1). Consequences of Fracturing Fluid Lag in Three-Dimensional Hydraulic Fractures. Presented at Low Permeability Reservoirs Symposium, 26-28 April, Denver, Colorado, USA. SPE-25888-MS. http://dx.doi.org/10.2118/25888-MS

Aimene, Y. E., and Nairn, J. A. (2014, February 25). Modeling Multiple Hydraulic Fractures Interacting with Natural Fractures Using the Material Point Method. Presented at SPE/EAGE European Unconventional Resources Conference and Exhibition, 25-27 February 2014, Vienna, Austria. SPE-167801-MS.http://dx.doi.org/10.2118/167801-MS

Akulich A. V. and Zvyagin, A. V. (2008). Interaction Between Hydraulic and Natural fractures. *Fluid Dynamics*. 43(03): 428 – 435

Alaska Department of revenue. 2015. Alaska's oil and gas competitiveness report 2015. Alaska Department of revenue, 27 February 2015, http://dor.alaska.gov/Portals/5/Alaska's%20Oil%20and%20Gas%20Competitiveness%20Report%202015.pdf (assessed 25 April 2016)

Barenblatt G. I. (1946). On Equilibrium Cracks formed in Brittle Fracture. Soviet Physics – *Doklady*

Barree, R. D., and Mukherjee, H. (1996, January 1). Determination of Pressure Dependent Leak off and Its Effect on Fracture Geometry. Presented at SPE Annual Technical Conference and Exhibition, 6-9 October 1996, Denver, Colorado. SPE-36424-MS. http://dx.doi.org/10.2118/36424-MS

Benzeggagh, M.L., Kenane, M. (1996). Measurement of Mixed-Mode Delamination Fracture Toughness of Unidirectional Glass/Epoxy Composites with Mixed-Mode Bending Apparatus. *Composite Science and Technology.* 55: 439-449

Beugelsdijk, L. J. L., de Pater, C. J., and Sato, K. (2000, January 1). Experimental Hydraulic Fracture Propagation in a Multi-Fractured Medium. Presented at SPE Asia Pacific Conference on Integrated Modelling for Asset Management, 25-26 April, Yokohama, Japan. SPE-/59419-MS. http://dx.doi.org/10.2118/59419-MS

Blanton, T. L. (1982, January 1). An Experimental Study of Interaction between Hydraulically Induced and Pre-Existing Fractures. Presented at SPE Unconventional Gas Recovery Symposium, 16-18 May 1982, Pittsburgh, Pennsylvania. SPE-10847-MS. http://dx.doi.org/10.2118/10847-MS

Choate, P. R. (1992, January 1). A New 3D Hydraulic Fracture Simulator That Implicitly Computes the Fracture Boundary Movements. Presented at European Petroleum Conference, 16-18 November, Cannes, France, Europe. SPE-24989-MS.http://dx.doi.org/10.2118/24989-MS

Chuprakov, D. A., Akulich, A. V., Siebrits, E., and Thiercelin, M. (2011, February 1). Hydraulic-Fracture Propagation in a Naturally Fractured Reservoir. *SPE Prod and Oper* 26(1):88 – 97. SPE-128715-PA. http://dx.doi.org/10.2118/128715-PA

Chuprakov, D., Melchaeva, O., and Prioul, R. (2013, May 20). Hydraulic Fracture Propagation across a Weak Discontinuity Controlled by Fluid Injection. Presented at ISRM International Conference for Effective and Sustainable Hydraulic Fracturing, 20-22 May, Brisbane, Australia. ISRM-ICHF-2013-008

Clifton, R. J., and Abou-Sayed, A. S. (1981, January 1). A Variational Approach To The Prediction Of The Three-Dimensional Geometry Of Hydraulic Fractures. Presented at SPE/DOE Low Permeability Gas Reservoirs Symposium, 27-29 May, Denver, Colorado, USA. SPE-9879-MS. http://dx.doi.org/10.2118/9879-MS

E and E Publishing, LLC. 2013. Fracking trade secrets would get no protection under draft Alaska rule. E and E Publishing, LLC, 3 January 2013, http://www.eenews.net/stories/1059974249 (assessed 25 April 2015)

Fu, P., Cruz, L., Moos, D., Settgast, R. R., and Ryerson, F. J. (2015, July 1). Numerical Investigation of a Hydraulic Fracture Bypassing a Natural Fracture in 3D. Presented at 49th U.S. Rock Mechanics/Geotechnics Symposium, 28 June-1 July 2015, San Francisco, California American Rock Mechanics Association. ARMA-2015-671.

Fu, P., Johnson, S. M., and Carrigan, C. R. (2011, June 26). Simulating Complex Fracture Systems in Geothermal Reservoirs Using an Explicitly Coupled Hydro-Geomechanical Model. Presented at 45th U.S. Rock Mechanics / Geomechanics Symposium, 26-29 June 2011, San Francisco, California American ARMA-11-244.

Geertsma, J., and De Klerk, F. (1969, December 1). A Rapid Method of Predicting Width and Extent of Hydraulically Induced Fractures. *J Pet Technol*. 21(12). 1571-1581. SPE-2458-PA. http://dx.doi.org/10.2118/2458-PA

Gong, B., Qin, G., Towler, B. F., and Wang, H. (2011, November 1). Discrete Modeling of Natural and Hydraulic Fractures in Shale-Gas Reservoirs. Presented at SPE Annual Technical Conference and Exhibition, 30 October-2 November 2011, Denver, Colorado, USA. SPE-146842-MS. http://dx.doi.org/10.2118/146842-MS

Gonzalez-Chavez, M., Puyang, P., and Taleghani, A. D. (2015, July 20). From Semi-Circular Bending Test to Microseismic Maps: An Integrated Modeling Approach to Incorporate Natural Fracture Effects on Hydraulic Fracturing. Presented at Unconventional Resources Technology Conference, 20-22 July 2015, San Antonio, Texas, USA. SPE-178544-MS. http://dx.doi.org/10.2118/178544-MS

Griffith A. A. (1920). The phenomena of rupture and flow in solids. *Phil. Trans. Roy Soc of London* 221(A): 163-198. http://dx.doi.org/10.1098/rsta.1921.0006.

Gu, H., Weng, X., Lund, J. B., Mack, M. G., Ganguly, U., and Suarez-Rivera, R. (2011, January 1). Hydraulic Fracture Crossing Natural Fracture at Non-Orthogonal Angles, A Criterion, Its Validation, and Applications. Presented at SPE Hydraulic Fracturing Technology Conference, 24-26 January 2011, The Woodlands, Texas, USA SPE-139984-MS. http://dx.doi.org/10.2118/139984-MS

Haddad, M., and Sepehrnoori, K. (2014, August 28). Simulation of Multiple-Stage Fracturing in Quasibrittle Shale Formations Using Pore Pressure Cohesive Zone Model. Presented at The Unconventional Resources Technology Conference, 25-27 August 2014, Denver, Colorado, USA. URTeC-1922219. http://dx.doi.org/10.15530/urtec-2014-1922219

Haddad, M., Du, J., and Vidal-Gilbert, S. (2016, February 1). Integration of Dynamic Microseismic Data with a True 3D Modeling of Hydraulic Fracture Propagation in Vaca Muerta Shale. Presented at SPE Hydraulic Fracturing Technology Conference, 9-11 February, The Woodlands, Texas, USA. http://dx.doi.org/10.2118/179164-MS

He, M.Y. and Hutchinson, J.W. (1989). Crack Deflection at an Interface between Dissimilar Elastic Materials. *Int. J. Solids Struct.* 25(9):1053-1067. http://dx.doi.org/10.1016/0020-7683(89)90021-8

Howard, G. C., and Fast, C. R. (1957, January 1). Optimum Fluid Characteristics for Fracture Extension. Presented at Drilling and Production Practice, 1 January, New York, New York, United States. API-57-261.

Hubbert, M. K., and Willis, D. G. (1957, January 1). Mechanics of Hydraulic Fracturing. Society of Petroleum Engineers. SPE-686-G

Irwin G. R. (1957). Analysis of Stresses and Strain near the End of a Crack Traversing a Plate. J. of App. Mech. 24: 361-364

Jeffrey, R. G., Vandamme, L., and Roegiers, J.-C. (1987, January 1). Mechanical Interactions in Branched or Subparallel Hydraulic Fractures. Presented at Low Permeability Reservoirs Symposium, 18-19 May, Denver, Colorado, USA. SPE-16422-MS. http://dx.doi.org/10.2118/16422-MS

Jeffrey, R. G., Zhang, X., and Thiercelin, M. J. (2009, January 1). Hydraulic Fracture Offsetting in Naturally Fractures Reservoirs: Quantifying a Long-Recognized Process. Presented at SPE Hydraulic Fracturing Technology Conference, 19-21 January, The Woodlands, Texas. SPE-119351-MS. http://dx.doi.org/10.2118/119351-MS

Koshelev, V. and A. Ghassemi, (2003). Numerical Modeling of Stress Distribution and Crack Trajectory near a fault or a Natural Fracture. Soil-Rock America Symp. Boston

Kresse, O., and Weng, X. (2013, May 20). Hydraulic Fracturing in Formations with Permeable Natural Fractures. Presented at ISRM International Conference for Effective and Sustainable Hydraulic Fracturing, 20-22 May 2013, Brisbane, Australia. ISRM-ICHF-2013-028

Lam K. Y. and Cleary M. P. (1984). Slippage and Re-Initiation of Fractures (Hydraulic) at Frictional Interfaces. International Journal for Numerical and Analytical Methods in Geomechanics. 08(06): 589-604

Lancaster, D. E., McKetta, S. F., Hill, R. E., Guidry, F. K., and Jochen, J. E. (1992, January 1). Reservoir Evaluation, Completion Techniques, and Recent Results from Barnett Shale Development in the Fort Worth Basin. Presented at Offshore Technology Conference-Asia, 25-28 March 2014, Kuala Lumpur, Malaysia SPE-24884-MS. http://dx.doi.org/10.2118/24884-MS

Lecampion B. (2009). An Extended Finite Element Method for Hydraulic Fracture Problems. Communications in Numerical Methods in Engineering. 25(02): 121 – 133

Lecampion, B. (2009). An Extended Finite Element for Hydraulic Fracture Problems. *Int. J. Numer. Meth. In Engng*. 25 (2): 212-133. http://dx.doi.org/10.1002/cnm.1111

Lu, Cong; Li, Mei; Guo, Jian-Chun; Tang, Xu-Hai; Zhu, Hai-Yan; Yong-Hui, Wang; Liang, Hao (2015, June). Engineering geological characteristics and the hydraulic fracture propagation mechanism of the sand-shale interbedded formation in the Xu5 reservoir. Journal of Geophysics and Engineering 321(3). http://dx.doi.org/10.1088/1742-2132/12/3/321

Meng, C., and De Pater, H. J. (2011, January 1). Hydraulic Fracture Propagation in Pre-Fractured Natural Rocks. Presented at SPE Hydraulic Fracturing Technology Conference, 24-26 January, The Woodlands, Texas, USA SPE-140429-MS. http://dx.doi.org/10.2118/140429-MS

Moes, N., Dolbow, J., and Belytschko, T. (1999). A finite element method for crack growth without remeshing. *Int J. Numer. Meth. in Engng.* 46(1):131-150.

Mukherjee, H., Larkin, S., and Kordziel, W. (1991, January 1). Extension of Fracture Pressure Decline Curve Analysis to Fissured Formations. SPE-21872-MS. http://dx.doi.org/10.2118/21872-MS

Naceur, K. B., Thiercelin, M., and Touboul, E. (1990, May 1). Simulation of Fluid Flow in Hydraulic Fracturing: Implications for 3D Propagation. SPE Production Engineering. 05(02): 133 - 141. SPE-16032-PA. http://dx.doi.org/10.2118/16032-PA

Nagel, N. B., Gil, I., Sanchez-Nagel, M., and Damjanac, B. (2011, January 24). Simulating Hydraulic Fracturing in Real Fractured Rocks - Overcoming the Limits of Pseudo3D Models. Presented at SPE Hydraulic Fracturing Technology Conference, 24-26 January 2011, The Woodlands, Texas, USA SPE-140480-MS. http://dx.doi.org/10.2118/140480-MS

Nagel, N. B., Sanchez-Nagel, M., Lee, B., and Garcia, X. (2012, November 1). Hydraulic Fracturing Optimization for Unconventional Reservoirs - The Critical Role of the Mechanical Properties of the Natural Fracture Network. Presented at SPE Canadian Unconventional Resources Conference, 30 October-1 November 2012, Calgary, Alberta, Canada SPE-161934-MS. http://dx.doi.org/10.2118/161934-MS

Nagel, N., Sheibani, F., Lee, B., Agharazi, A., and Zhang, F. (2014, February 4). Fully-Coupled Numerical Evaluations of Multiwell Completion Schemes: The Critical Role of In-Situ Pressure Changes and Well Configuration. Presented at SPE Hydraulic Fracturing Technology Conference, 4-6 February 2014, The Woodlands, Texas, USA. SPE-168581-MS. http://dx.doi.org/10.2118/168581-MS

Narr, W., Schechter, D. and Thompson, L., 2006, Naturally Fractured Reservoir Characterization, Richardson, TX: Society of Petroleum Engineers

Nolte, K. G. (1991, February 1). Fracturing-Pressure Analysis for Nonideal Behavior. *J Pet Technol* 43(2): 210-218. SPE-20704-PA. http://dx.doi.org/10.2118/20704-PA

Nolte, K. G., and Smith, M. B. (1981, September 1). Interpretation of Fracturing Pressures. *J Pet Technol* 33(9): 1767-1775. SPE-8297-PA. http://dx.doi.org/10.2118/8297-PA

Nordgren, R. P. (1972, August 1). Propagation of a Vertical Hydraulic Fracture. SPE-3009-PA. *SPE J.* 12(4): 306 – 314. http://dx.doi.org/10.2118/3009-PA

Offenberger, R., Ball, N., Kanneganti, K., and Oussoltsev, D. (2013, August 12). Integration of Natural and Hydraulic Fracture Network Modeling with Reservoir Simulation for an Eagle Ford Well. Presented at Unconventional Resources Technology Conference, 12-14 August 2013, Denver, Colorado. URTEC2013-049. http://dx.doi.org/10.1190/URTEC2013-049

Olson J. E. (1993). Joint Pattern Development: Effects of Subcritical Crack Growth and Mechanical Crack Interaction. Journal of Geophysical Research. 98(07): 12251 – 12265

Olson, J. E. (2008, January 1). Multi-fracture propagation modeling: Applications to hydraulic fracturing in shales and tight gas sands. Presented at The 42nd U.S. Rock Mechanics Symposium (USRMS), 29 June-2 July, San Francisco, California, USA. ARMA-08-327.

Olson, J. E., Bahorich, B., and Holder, J. (2012, January 1). Examining Hydraulic Fracture: Natural Fracture Interaction in Hydrostone Block Experiments. Presented at SPE Hydraulic Fracturing Technology Conference, 6-8 February 2012, The Woodlands, Texas, USA. SPE-152618-MS. http://dx.doi.org/10.2118/152618-MS

Olson, J.E. and Pollard, D.D. 1991. The initiation and Growth of En Echelon Viens. J. Struct. Geol. 13 (5): 595-608. http://dx.doi.org/10.1016/0191-8141(91)90046-L

Oussoltsev, D., Offenberger, R. M., Kanneganti, K. T., Ball, N., and Grant, D. (2013, April 10). Application of Reservoir-Centric Stimulation Design Tool in Completion Optimization for Eagle Ford Shale. Presented at SPE Unconventional Resources Conference-USA, 10-12 April 2013, The Woodlands, Texas, USA SPE-164526-MS. http://dx.doi.org/10.2118/164526-MS

Pattillo, P. D. (1975, January 1). A Modification of Carter's Equation for Fracture Area. Presented at Fall Meeting of the Society of Petroleum Engineers of AIME, 28 September-1 October, Dallas, Texas, United States. SPE-5630-MS. http://dx.doi.org/10.2118/5630-MS

Perkins, T. K., and Kern, L. R. (1961, September 1). Widths of Hydraulic Fractures. *J Pet Technol* 13(9): 937-949. SPE-89-PA. http://dx.doi.org/10.2118/89-PA

Rahman, M. M. (2009, January 1). A Fully Coupled Numerical Poroelastic Model to Investigate Interaction between Induced Hydraulic Fracture and Preexisting Natural Fracture in a Naturally Fractured Reservoir: Potential Application in Tight Gas and Geothermal Reservoirs. Presented at SPE Annual Technical Conference and Exhibition, 4-7 October, New Orleans, Louisiana, USA. SPE-124269-MS. http://dx.doi.org/10.2118/124269-MS

Sack, R. A. (1946). Extension of Griffith Theory of Rupture to Three Dimensions. Proc. Phys. Soc. 58: 729

Sauuarez-Rivera, R., Burghardt, J., Edelman, E., Stanchits, S., and Surdi, A. (2013, June 23). Geomechanics Considerations for Hydraulic Fracture Productivity. Presented at 47th U.S. Rock Mechanics/Geomechanics Symposium, 23-26 June 2013, San Francisco, California American Rock Mechanics Association. ARMA-2013-666.

Sesetty, V., and Ghassemi, A. (2012, January 1). Simulation of Hydraulic Fractures and Their Interactions with Natural Fractures. Presented at 46th U.S. Rock Mechanics/Geomechanics Symposium, 24-27 June 2012, Chicago, Illinois. ARMA-2012-331.

Shin, D. H., and Sharma, M. M. (2014, February 4). Factors Controlling the Simultaneous Propagation of Multiple Competing Fractures in a Horizontal Well. Presented at SPE Hydraulic Fracturing Technology Conference, 4-6 February 2014, The Woodlands, Texas, USA. SPE-168599-MS. http://dx.doi.org/10.2118/168599-MS

Simonson, E. R., Abou-Sayed, A. S., and Clifton, R. J. (1978, February 1). Containment of Massive Hydraulic Fractures. *SPE J.* 18(01): 27 – 32. SPE-6089-PA. http://dx.doi.org/10.2118/6089-PA

Smith M. B. and Montgomery C. T. 2015. *Hydraulic Fracturing*, first edition. Florida: Taylor and Francis Group.

Sneddon, I. N. and Elliott, H. A. (1946). The opening of a Griffith cracks under internal pressure. Quarterly of Appl. Math. 4: 262

Taleghani, A.D. 2009. Analysis of Hydraulic Fracture Propagation in Fractured Reservoirs: An Improved Model for Interaction Between Induced and Natural Fractures. Ph.D. Dissertation. The University of Texas at Austin, USA

Taleghani, A.D., and Olson, J. E. (2011, September 1). Numerical Modeling of Multistranded-Hydraulic-Fracture Propagation: Accounting for the Interaction between Induced and Natural Fractures. *SPE J* 16(3):575-581. SPE-124884-PA. http://dx.doi.org/10.2118/124884-PA

Taleghani, A.D., and Olson, J. E. (2014, February 1). How Natural Fractures Could Affect Hydraulic-Fracture Geometry? *SPE J.* SPE-167608-PA. http://dx.doi.org/10.2118/167608-PA

Teufel, L.W. 1979. An Experimental Study of Hydraulic Fracture Propagation in Layered Rock. Ph.D. Dissertation. Texas A & M University, College Station. Texas.

U.S. Energy Information Administration. 2016. Hydraulic fracturing accounts for about half of current U.S. crude oil production. U.S. Energy Information Administration, 15 March 2016, https://www.eia.gov/todayinenergy/detail.cfm?id=25372 (accessed 25 April 2016)

U.S. Geological Survey. 2012. Assessment of potential oil and gas resources in source rocks (shale) of the Alaska North Slope - overview of geology and results. U.S. Geological Survey, March 2012, http://energy.usgs.gov/Portals/0/Rooms/audiovisual/AK_ShaleResourcesRelease_pdfweb_mar2012.pdf (assessed 25 April 2016)

U.S. Geological Survey. 2012. Assessment of potential oil and gas resources in source rocks of the Alaska North Slope, 2012. U.S. Geological Survey, 1 February 2012, http://pubs.usgs.gov/fs/2012/3013/pdf/fs2012-3013.pdf (assessed 25 April 2016)

U.S. Geological Survey. 2015. Water use for fracking. U.S. Geological Survey, 30 June 2015, http://www.usgs.gov/newsroom/images/2015_06_30/water_use_for_fracking.jpg (accessed 25 April 2016)

Walsh, J.B. (1981). Effect of Pore Pressure and Confining Pressure on Fracture Permeability. *Int. J. Rock Mech. and Min. Sci. and Geomech. Abstr.* 18(5): 429-435. http://dx.doi.org/10.1016/0148-9062(81)90006-1

Warpinski, N. R. (1993, February 1). Hydraulic Fracturing in Tight, Fissured Media. *J Pet Technol* 43(2): 146-209. SPE-20154-PA. http://dx.doi.org/10.2118/20154-PA

Warpinski, N. R., and Branagan, P. T. (1989, September 1). Altered-Stress Fracturing. *J Pet Technol* 41(9): 990-997. SPE-17533-PA. http://dx.doi.org/10.2118/17533-PA

Warpinski, N. R., and Teufel, L. W. (1987, February 1). Influence of Geologic Discontinuities on Hydraulic Fracture Propagation. *J Pet Technol* 39(2): 209-220. SPE-13224-PA. http://dx.doi.org/10.2118/13224-PA

Weng, X., Kresse, O., Cohen, C.-E., Wu, R., and Gu, H. (2011, November 1). Modeling of Hydraulic-Fracture-Network Propagation in a Naturally Fractured Formation. *SPE Prod and Oper* 26(1): 368 - 380. SPE-140253-PA. http://dx.doi.org/10.2118/140253-PA

Wick, T., Singh, G., and Wheeler, M. F. (2014, February 4). Pressurized-fracture Propagation Using a Phase-field Approach coupled to a Reservoir Simulator. Presented at SPE Hydraulic Fracturing Technology Conference, 4-6 February, The Woodlands, Texas, USA. SPE-168597-MS. http://dx.doi.org/10.2118/168597-MS

Yadav, H. (2011). Hydraulic Fracturing in Naturally Fractured Reservoirs and the Impact of Geomechanics on Microseismicity. Master's Thesis. The university of Texas at Austin. Texas.

Zhang, X. and Jeffrey, R. G. (2006, July 25). The role of friction and secondary flaws on deflection and re-initiation of hydraulic fractures at orthogonal pre-existing fractures. Geophysical Journal International 166(3): 1454–1465. http://dx.doi.org/10.1111/j.1365-246X.2006.03062.x

Zhao, X. P., and Young, R. P. (2009, January 1). Numerical Simulation of Seismicity Induced by Hydraulic Fracturing in Naturally Fractured Reservoirs. Presented at SPE Annual Technical Conference and Exhibition, 4-7 October, New Orleans, Louisiana, USA. SPE-124690-MS. http://dx.doi.org/10.2118/124690-MS

Zheltov, A. K. (1955, January 1). Formation of Vertical Fractures by Means of Highly Viscous Liquid. Presented at 4th World Petroleum Congress, 6-15 June, Rome, Italy. WPC-6132.